# Synaptic Connectivity in the Mushroom Body

## Calyx of *Drosophila melanogaster*

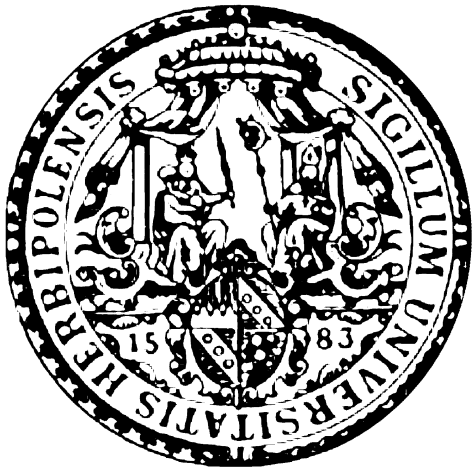


Dissertation zur Erlangung des
naturwissenschaftlichen Doktorgrades
der Julius-Maximilians-Universität Würzburg

vorgelegt von
Frauke Engelhardt, geb. Christiansen
aus Berlin

Würzburg 2013

Eingereicht am:.....

Mitglieder der Promotionskommission:

Vorsitzender:.....

Gutachter:.....

Gutachter:.....

Tag des Promotionskolloquiums:.....

Doktorurkunde ausgehändigt am:.....

Erklärung

gemäß § 4 Absatz 3 der Promotionsordnung der Fakultät für Biologie der Julius-Maximilians-Universität zu Würzburg vom 15. März 1999:

Die vorgelegte Dissertation mit dem Titel „Synaptic Connectivity in the Mushroom Body Calyx of Drosophila melanogaster" besteht aus drei Publikationen und zusätzlich einer Zusammenfassung, einer allgemeinen Einführung, einer allgemeinen Diskussion und den methodischen Details. Die Darstellung meines eigenständig geleisteten Anteils an den Publikationen folgt im Anschluss an diese Seite.

Die vorliegende Arbeit wurde weder in gleicher noch in ähnlicher Form bereits in einem anderen Prüfungsverfahren vorgelegt. Außer dem Diplom in Biologie an der Freien Universität Berlin habe ich zuvor keine akademischen Grade erworben oder versucht zu erwerben.

Berlin,

_____ _____

Date Frauke Engelhardt

This thesis is based on the following manuscripts

I. Owald, D.*, Fouquet, W.*, Schmidt, M., Wichmann, C., Mertel, S., Depner, H., Christiansen, F., Zube, C., Quentin, C., Korner, J., Urlaub, H., Mechtler, K., and Sigrist, S.J. (2010). A Syd-1 homologue regulates pre- and postsynaptic maturation in *Drosophila*. J Cell Biol 188, 565-579.

*equal contribution

FC performed the experiments presented in Fig. 2D; CZ and FC performed the experiment shown in Fig. 2B,C.

II. Kremer, M.C.*, Christiansen, F.*, Leiss, F.*, Paehler, M., Knapek, S., Andlauer, T.F.M., Förstner, F., Kloppenburg, P., Sigrist, S.J., Tavosanis, G. (2010) Structural Long-Term Changes at Mushroom Body Input Synapses. Curr Biol. 20, 1938-44

*equal contribution

MCK, FC, FL, SJS and GT designed the research. FC performed the experiments presented in Fig. 4 and analyzed the corresponding data. The data analysis protocol for the presynaptic analysis used throughout the paper was designed by FC. FC did fly genetics and the cloning. FC, TFMA and SJS wrote the parts of the paper concerning the presynaptic analysis.

III. Christiansen, F.*, Zube, C.*, Andlauer, T.F.M., Wichmann, C., Fouquet, W., Owald, D., Mertel, S., Leiss, F., Tavosanis, G., Farca Luna, A.J., Fiala, A., Sigrist ,S.J. (2011) Presynapses in Kenyon cell dendrites in the mushroom body calyx of *Drosophila*. J Neurosci 31, 9696-9707

*equal contribution

FC and SJS designed the research. FC performed the experiments presented in Figs. 1-4, 6 and 7 and analyzed all data except for the data presented in Fig. 3 and Fig. 5. FC did all the fly genetics and the cloning. FC, CZ and SJS wrote the paper.

# TABLE OF CONTENTS

# 1. SUMMARY

Learning and memory is considered to require synaptic plasticity at presynaptic specializations of neurons. Kenyon cells are the intrinsic neurons of the primary olfactory learning center in the brain of arthropods – the mushroom body neuropils. An olfactory mushroom body memory trace is supposed to be located at the presynapses of Kenyon cells. In the calyx, a sub-compartment of the mushroom bodies, Kenyon cell dendrites receive olfactory input provided via projection neurons. Their output synapses, however, were thought to reside exclusively along their axonal projections outside the calyx, in the mushroom body lobes. By means of high-resolution imaging and with novel transgenic tools, we showed that the calyx of the fruit fly *Drosophila melanogaster* also comprised Kenyon cell presynapses. At these presynapses, synaptic vesicles were present, which were capable of neurotransmitter release upon stimulation. In addition, the newly identified Kenyon cell presynapses shared similarities with most other presynapses: their active zones, the sites of vesicle fusion, contained the proteins Bruchpilot and Syd-1. These proteins are part of the cytomatrix at the active zone, a scaffold controlling synaptic vesicle endo- and exocytosis. Kenyon cell presynapses were present in γ- and α/β-type KCs but not in α′/β′-type Kenyon cells.

The newly identified Kenyon cell derived presynapses in the calyx are candidate sites for an olfactory associative memory trace. We hypothesize that, as in mammals, recurrent neuronal activity might operate for memory retrieval in the fly olfactory system.

Moreover, we present evidence for structural synaptic plasticity in the mushroom body calyx. This is the first demonstration of synaptic plasticity in the central nervous system of *Drosophila melanogaster*. The volume of the mushroom body calyx can change according to changes in the environment. Also size and numbers of microglomeruli- sub-structures of the calyx, at which projection neurons contact Kenyon cells – can change. We investigated the synapses within the microglomeruli in detail by using new transgenic tools for visualizing presynaptic active zones and postsynaptic densities. Here, we could show, by disruption of the projection neuron - Kenyon cell circuit, that synapses of microglomeruli were subject to activity-dependent synaptic plasticity. Projection neurons that could not generate action potentials compensated their functional limitation by increasing the number of active zones per microglomerulus. Moreover, they built more and enlarged microglomeruli. Our data provide clear evidence for an activity-induced, structural synaptic plasticity as well as for the activity-induced reorganization of the olfactory circuitry in the mushroom body calyx.

# 1.1 Zusammenfassung

Synaptische Plastizität an den präsynaptischen Spezialisierungen von Neuronen sind nach allgemeinem Verständnis die Grundlage für Lern- und Gedächtnisprozesse. Kenyon Zellen sind die intrinsischen Zellen des Zentrums für olfaktorisches Lernen im Gehirn von Arthropoden – den Pilzkörper Neuropilen. An den Präsynapsen der Kenyon Zellen wird eine olfaktorische Gedächtnisspur vermutet. Im Kalyx, einer Substruktur der Pilzkörper, erhalten die Kenyon Zell Dendriten ihren olfaktorischen Input durch Projektionsneurone. Ihre Präsynapsen wiederum befinden sich ausschließlich in ihren axonalen Kompartimenten außerhalb des Kalyx, nämlich in den Loben der Pilzkörper. Mit Hilfe von hochauflösenden bildgebenden Techniken und neuen transgenen Methoden, ist es uns in der Fruchtfliege *Drosophila melanogaster* gelungen, Kenyon Zell Präsynapsen im Kalyx zu identifizieren. Diese Präsynapsen enthalten synaptische Vesikel, die nach Stimulation ihren Inhalt freisetzen können. Sie weisen noch weitere Gemeinsamkeiten mit den meisten anderen Präsynapsen auf: Ihre Aktiven Zonen, die Orte der Transmitterfreisetzung, enthalten die Proteine Bruchpilot und Syd-1. Diese sind Teil der Zytomatrix an der Aktiven Zone, ein Proteingerüst das Endo- und Exozytose der synaptischen Vesikel kontrolliert. Die Präsynapsen im Kalyx wurden in γ- und α/β-Typ Kenyon Zellen aber nicht in α′/β′-Typ Kenyon Zellen gefunden.

Die neu identifizierten Kenyon Zell Präsynapsen beherbergen potentiell eine Gedächtnisspur für olfaktorisch assoziatives Lernen. Möglicherweise wird im olfaktorischen Nervensystem von Fruchtfliegen rücklaufende neuronale Aktivität benötigt, um Gedächtnis abzurufen, so wie es auch für Säuger beschrieben ist.

Darüber hinaus zeigen wir synaptische Plastizität im Kalyx. Dies ist die erste Beschreibung überhaupt von synaptischer Plastizität im zentralen Nervensystem von *Drosophila melanogaster*. Das Volumen des Kalyx kann sich als Antwort auf äußere Einflüsse verändern. Genauso auch Größe und Anzahl der Mikroglomeruli, Substrukturen des Kalyx, in denen Projektionsneurone und Kenyon Zellen aufeinander treffen. Wir untersuchten die Synapsen in Mikroglomeruli detailliert, mithilfe von neuen transgenen Methoden, die es erlauben, präsynaptische Aktive Zonen sowie Postsynaptische Spezialisierungen zu visualisieren. Mittels Beeinträchtigung der Kommunikation zwischen Projektionsneuronen und Kenyon Zellen, konnten wir synaptische Plastizität in Mikroglomeruli zeigen. Projektionsneurone, die nicht in der Lage waren, Aktionspotentiale zu erzeugen, kompensierten ihre funktionelle Einschränkung durch den vermehrten Einbau von Aktiven Zonen in Mikroglomeruli. Außerdem produzierten sie mehr und vergrößerte Mikroglomeruli. Unsere Daten zeigen deutlich eine aktivitätsinduzierte Veränderung des olfaktorischen neuronalen Netzes, sowie strukturelle synaptische Plastizität im Kalyx.

# 2. INTRODUCTION

The study of animal behavior is certainly one of the oldest disciplines of biology. Observing the habits of other animals already helped early humans to survive, as it helped getting to know predators and prey better.

The term behavior refers to all actions carried out by an organism including motor activity as well as transmission of acoustic and olfactory signals. The physical substrate of behavior is the nervous system. It receives sensory information through sensory receptors and conducts signals via nerves to the central nervous system (CNS). In the CNS, sensory information is integrated, which means that it is interpreted and associated with suitable responses of the body. The signals from the CNS are then transmitted to effector cells, for example muscle cells, which carry out the behavior. Many behaviors rely on a given set of neurons, acting together as a neuronal circuit.

I take special interest in elucidating the circuit mechanisms that underlie behavior. Yet given the enormous complexity of the human brain (~120 billion neurons (Herculano-Houzel, 2009)) and the diversity of synaptic contacts, it currently appears as an impossible mission to unravel neuronal circuits underlying behavior. Fortunately, nerve cells in all animals are highly similar in terms of cell biology. Therefore, smaller brains in smaller animals, with less neurons and less synapses, may contribute to our understanding of brain function. The biggest differences between animals from distant phylogenetic branches lie in the architecture of the nervous system. However, for example the architecture of the olfactory circuit, is remarkably similar among insects and mammals (Hildebrand and Shepherd, 1997). In this work, I focus on the mushroom bodies (MBs), a paired neuropil in the brain of arthropods, involved in higher olfactory processing, as well as in learning and memory (introduced in 2.6.3).

## 2.1 *Drosophila melanogaster*

In terms of numbers, the olfactory system of *Drosophila melanogaster* is far less complex than the mammalian olfactory system. For example, in the mouse, millions of olfactory receptor neurons (ORNs) target almost 2000 glomeruli in each of the olfactory bulbs, the first olfactory neuropils in the brain (Mori et al., 1999; Zhang and Firestein, 2002). In

contrast, *Drosophila*, whose brain consists of only about 100'000 neurons (Ito et al., 2013), has merely about 1200 ORNs per antenna (Vosshall and Stocker, 2007), targeting 43 glomeruli in each antennal lobe (AL, introduced in 2.6.2; Vosshall and Stocker, 2007).

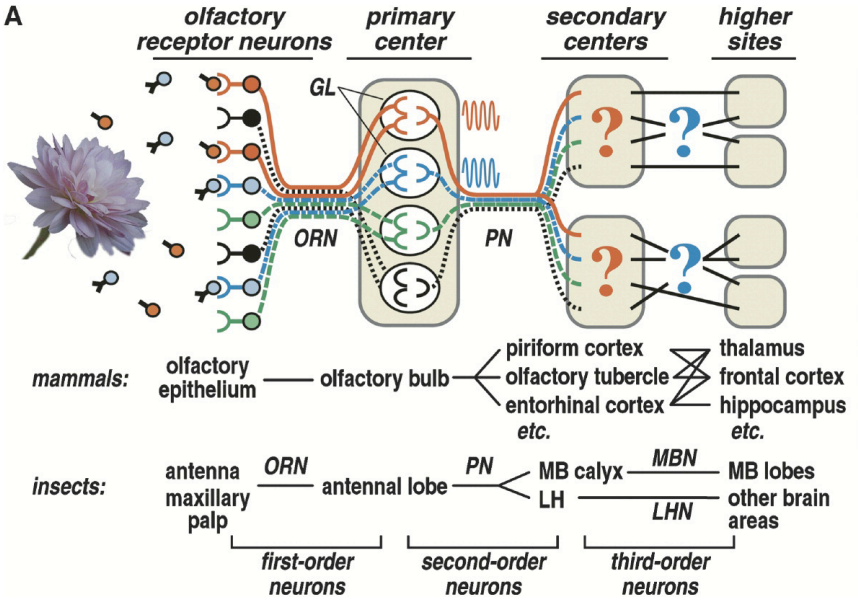


Fig. 1: Parallels in olfactory processing between mammals and insects.

The odorants emitted from a stimulus activate distinct subsets of ORNs (here in red and blue), which converge on specific glomeruli (GL) in either the olfactory bulbs or the ALs. The information about the active glomeruli is relayed to multiple secondary centers via projection neurons (PNs, second-order neurons). They terminate in the secondary centers in a stereotypic manner, but their spatial localizations are only partially understood. Almost no data are available about the connection patterns of the third-order neurons (question marks).
From Tanaka et al., 2004. Reprinted with permission from Elsevier.

Thomas Hunt Morgan introduced the fruit fly *Drosophila melanogaster* as a model organism early in the 20th century, transferring genetic research to experimental animals (Squire and Kandel, 1999). He appreciated that *Drosophila* had only four pairs of chromosomes. In addition, the animals can be reared by the thousands in the laboratory, as they are small and a female fly lays up to 100 eggs per day. It is possible to produce mutations in single genes using chemical techniques and, because of the fruit fly's relatively short generation cycle of 12 days (at 25 °C), to quickly breed many flies carrying a certain mutation. Since its introduction by Morgan, *Drosophila* has proven very valuable in developmental biology. In 1967, Seymour Benzer took the next step for studying the genetics of behavior, and addressed learning and memory in *Drosophila*

(Benzer, 1967; Squire and Kandel, 1999). He produced mutations in single genes and examined their effects on behavior. Genes identified to play a role in *Drosophila* olfactory learning have conserved roles in mammalian organisms, which highlights the value of *Drosophila* for learning and memory research.

Furthermore, over the last decades, many genetic tools have been invented to ease the work with *Drosophila* even more, for instance, balancer chromosomes: they keep genetic variants stable by suppressing recombination, because they contain multiple inversions (Muller, 1927; Thompson, 1977). In addition, p-element based genetics have made the fly widely accessible to transgenesis (Rubin and Spradling, 1982). Moreover, the invention of the GAL4/UAS expression system revolutionized the field, as it was the key step that made targeting of gene products to specific sets of neurons possible (Brand and Perrimon, 1993). This technique was used for many experiments in the context of this thesis and will therefore be introduced in more detail.

GAL4 is a transcription factor from the budding yeast *Saccharomyces cerevisiae*. It triggers the transcription of the *gal* family of genes, which are involved in galactose metabolism, by binding to the upstream activating sequence (UAS) upstream of their promoters. The sequence coding for GAL4 can be introduced to the *Drosophila* genome via p-element based insertion. Depending on the endogenous promoter or enhancer in the vicinity of the integration site, the expression of *gal4* is spatially and temporally defined. Therefore, this procedure is also conferred to as enhancer trapping. Nowadays a large variety of enhancer trap lines is available, with GAL4 expression in many different tissues. P-element based insertion also allows for the generation of transgenic flies carrying a gene of interest fused to UAS sequences. If a GAL4 expressing fruit fly is mated with a fly containing a UAS-controlled gene of interest, their offspring will express the gene downstream the UAS sequence in the GAL4-expressing tissue. In summary, this technique allows for the expression of a gene of interest in a defined group of neurons in a certain time window.

The protein GAL80 is another central regulator in galactose utilization in *S. cerevisiae*, and it is also used as a genetic tool in *Drosophila*. It binds to GAL4 and thereby prevents recruitment of polymerase to the UAS. GAL80 was added to the *Drosophila* GAL4/UAS toolset to label single cells within a GAL4 expressing tissue. This technique is called *mosaic analysis with a repressible cell marker* (MARCM; Lee and Luo, 2001).

# 2.2 The synapse

The cellular building blocks of the nervous system are neurons and glia. Neurons are interconnected, highly active secretory cells. With their long extended axons and elaborate dendritic arbors, neurons are the basic building blocks for the circuitries that detect, store, and transmit information in the nervous system. They communicate at specialized points of contact, synapses. However, neurons can also form synapses with muscles as postsynaptic partners. These neurons are referred to as motoneurons and the respective synapses are termed neuromuscular junctions (NMJs).

Information in neurons is coded as electrical activity. At electrical or fast synapses, also termed gap junctions, direct and fast conductance of signals in the form of ions or small second messenger molecules is mediated through intercellular channels, allowing for direct cell-to-cell coupling. At chemical synapses, the electrical activity that arrives at the presynaptic terminal is converted into a chemical signal, which, in turn, is released from the presynaptic neuron. The chemical signal eventually triggers electrical activity in the postsynaptic neuron. The chemical synapse consists of a presynaptic and a postsynaptic membrane, both of which are closely and precisely aligned, leaving only a small synaptic cleft in between them. From now on, I will focus on the description of chemical synapses.

## 2.2.1 The presynapse with the presynaptic active zone and relevant proteins

Fast chemical transmission is mediated by precisely regulated neurotransmitter release by fusion of synaptic vesicles (SVs) with the presynaptic membranes upon $Ca^{2+}$ influx. The site of SV clustering, tethering and fusion at the presynaptic membrane is a highly specialized compartment called active zone (AZ; Couteaux and Pecot-Dechavassine, 1970; Heuser and Reese, 1973). After tethering at the AZ the SVs become fusion-competent, a mechanism called priming. The pool of tethered and primed SVs is termed readily-releasable pool. In brief, an action potential (AP) that arrives at the presynapse triggers the opening of voltage-gated $Ca^{2+}$ channels that are clustered at the active zone. $Ca^{2+}$ ions enter and bind to the protein Synaptotagmin, which leads to the fusion of SVs in the readily-releasable pool with the AZ membrane (Südhof and Rothman, 2009). The readily-releasable pool contains about 1% of the SVs in a nerve terminal. Many more SVs are clustered in recycling (~15%) and reserve pools (~85%), which can be mobilized by stronger stimulation (Rizzoli and Betz, 2005; Ho et al., 2011).

The AZ comprises a unique set of proteins (Schoch and Gundelfinger, 2006). These proteins are either attached to the AZ membrane (e.g. Syntaxin) or to SVs (e.g.

Synaptotagmin). They are arranged in a highly ordered architecture and form an electron-dense structure called cytomatrix (Cytomatrix at the AZ, CAZ). The CAZ docks and primes SVs, it clusters $Ca^{2+}$ channels and is responsible for the close alignment of pre- and postsynaptic membranes via transsynaptic cell-adhesion molecules (Südhof, 2012). The core constituents of the CAZ are RIM, MUNC13, RIM-BP, liprinα and ELKS proteins (Südhof, 2012). Ultrastructural studies of the AZ have revealed that the CAZ differs in morphology between animals and synapse types (Fig. 2A-D). However, all of these electron-dense projections extend from the cytomatrix into the cytoplasm and tether SVs (Zhai and Bellen, 2004). In dipterous insects such as *Drosophila*, the dense projection is typically T-shaped (Trujillo-Cenoz and Melamed, 1973) and is referred to as T-bar.

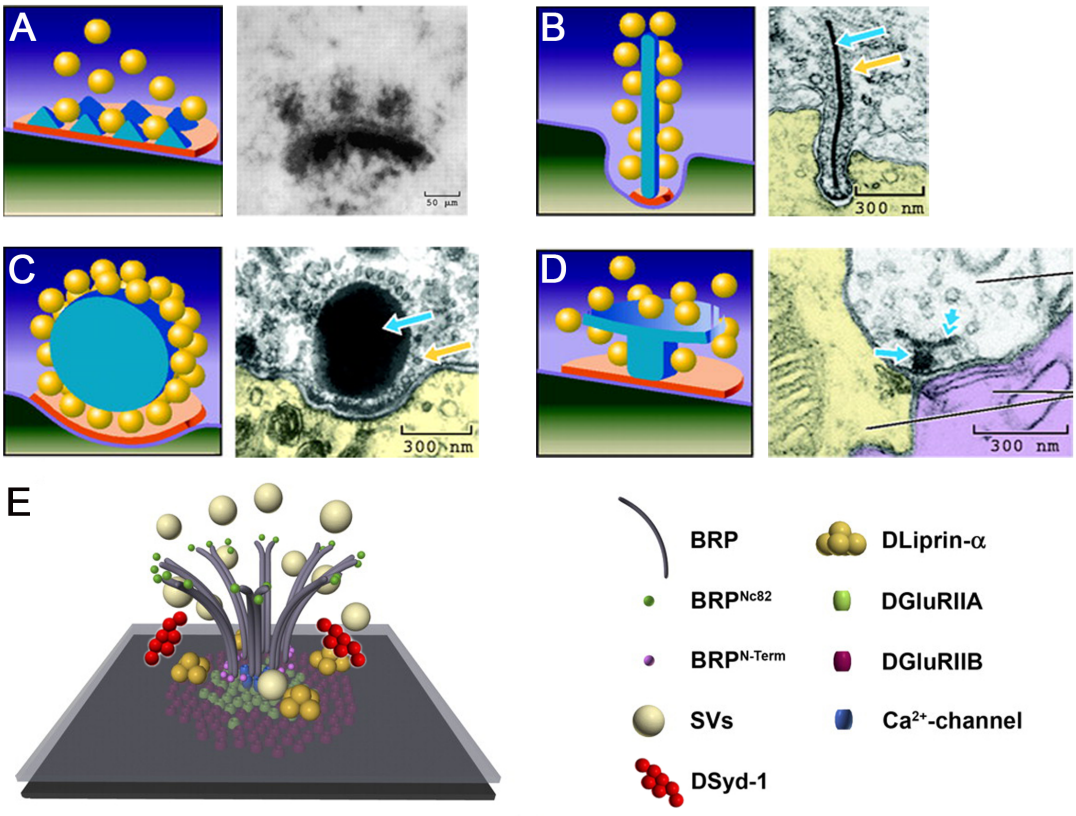


Fig. 2: Ultrastructure of the active zone.

**A-D:** Schematic representations and electron micrographs of (**A**) dense bodies at a mammalian CNS synapse, (**B**) an electroreceptor in skates, with a long ribbon-like dense projection (blue arrow), surrounded by SVs (yellow arrow), (**C**) a synaptic ribbon (blue arrow) of the frog inner ear hair cell surrounded by a halo of SVs (yellow arrow) and (**D**) a tetrad synapse between photoreceptor and laminar monopolar cells in *Drosophila*. The T-bar consists of a platform

(double arrow) and a pedestal (arrow).
**E:** Model of AZ organization at *Drosophila* NMJs.
**A-D:** Adapted and reprinted with permission, from Zhai & Bellen, 2004.
**E:** Adapted and reprinted with permission, from Fouquet et al., 2009.

### 2.2.1.1 Bruchpilot

The large scaffolding protein Bruchpilot (BRP) is an essential component of T-bars in *Drosophila*. Its N-terminal half encodes the *Drosophila* homologue of the mammalian protein ELKS (Kittel et al., 2006; Wagh et al., 2006). The BRP N-terminus clusters $Ca^{2+}$ channels and the C-terminus directly tethers SVs (Hallermann et al., 2010; Kittel et al., 2006). Moreover, the size of the readily-releasable pool of SVs is determined by the amount of BRP (Matkovic et al., 2013). As a consequence, in the absence of BRP, synapses lack T-bar dense bodies, $Ca^{2+}$ channels are unclustered and efficient neurotransmitter release is impaired (Kittel et al., 2006).

### 2.2.1.2 Syd-1

We identified Syd-1 in *Drosophila* as a BRP binding partner (Owald et al., 2010, Fig. 1), localizing to a subcompartment surrounding the AZ core (Owald et al., 2010, Fig. 3). It arrives early at nascent AZs during AZ formation (Owald et al., 2010, Fig. 9). Syd-1 is needed for the proper localization of BRP and liprin-α (Owald et al., 2010, Fig. 5, 6 and 10). Consequently, *syd-1* mutants form smaller presynaptic terminals (Owald et al., 2010, Fig. 4E) with fewer release sites (Owald et al., 2010, Fig. 4G), and they release less neurotransmitter (Owald et al., 2010, Fig. 4A). Remaining AZs are often large and misshapen and BRP forms ectopic accumulations distant from AZs (Owald et al., 2010, Fig. 5). Furthermore, Syd-1 organizes trans-synaptic signaling to control maturation of PSD composition (Owald et al., 2010, Fig. 7) via an interaction with the cell adhesion molecule Neurexin (Owald et al., 2012). Syd-1 was only recently identified to be present also at vertebrate synapses (mSYD1A; Wentzel et al. 2013), where it is involved in the tethering of SVs.

### 2.2.1.3 Liprin-α

Liprin-α is crucial for AZ formation as well as for SV clustering in *C. elegans* and *Drosophila* (Kaufmann et al., 2002; Miller et al., 2005; Dai et al., 2006; Patel et al., 2006). Such as Syd-1, Liprin-α arrives at the AZ very early in newly forming synapses and surrounds the AZ center (Fouquet et al., 2009). It binds to BRP, Syd-1 and RIM (Südhof,

2012). Moreover, Liprin-α is important for an appropriate CAZ morphology, as complex multi-T-bars form in *liprin-α* mutants (Kaufmann et al., 2002; Fouquet et al., 2009). In mammals liprin-α controls the SV pool size (Spangler et al., 2013).

### 2.2.2 The postsynapse

The postsynapse may reside in a neuron or in a muscle cell. In neurons the postsynapse is often located on the tip of membrane protuberances on dendrites called dendritic spines. The transmitter molecules released by the presynapse diffuse through the synaptic cleft and eventually bind to receptors in the postsynaptic membrane. The postsynaptic membrane exhibits an electron dense area called postsynaptic density (PSD), which spans about the same width as the AZ (reviewed by Sheng and Hoogenraad, 2007). In this sophisticated protein network receptors, scaffolds, adhesion proteins, kinases, phosphatases and cytoskeletal elements accumulate. It anchors the receptors and also supports and modulates their postsynaptic actions.

When a neurotransmitter binds to a receptor, this leads to a postsynaptic response. Whether the signal is transferred further along the postsynaptic neuron or whether the postsynaptic muscle cell contracts, depends, among other factors, on the strength of the incoming signal. Chemical synapses can be excitatory or inhibitory, depending on whether the postsynaptic cell is de- or hyperpolarized. An AP is generated when the incoming signal rises above a certain depolarization threshold.

Depending on the receptor, the response can be either the direct depolarization of the postsynaptic membrane or the activation of second messenger pathways. Ionotropic receptors are direct ligand-gated ion channels. Consequently, ligand binding rapidly leads to an influx of ions into the neuron, which allows for very quick transmission of the signal. The evoked postsynaptic currents are believed to last only a few milliseconds (Lüscher and Malenka, 2012). The highly sensitive metabotropic receptors, by contrast, are no ion channels. Following to ligand binding, intracellular signaling cascades are activated which may include second messenger production, activation of enzymes or activation of ion channels (Wicher, 2012). Many metabotropic receptors are G-protein coupled and activate G-proteins upon ligand binding. Processes at metabotropic receptors are slower than at ionotropic receptors but allow for stronger signal amplifications.

In insects, acetylcholine (ACh) is the major excitatory transmitter in the CNS (Gundelfinger and Hess, 1992). The postsynaptic response is mediated by nicotinic ACh receptors. Each ACh receptor comprises 5 subunits, and incorporates an ion channel. The ion channel transiently opens upon binding of ACh molecules, eventually triggering a postsynaptic response. Large families of ACh receptor subunits have been identified. The

subunit α7 can form homomeric subunits (Couturier et al., 1990; Grauso et al., 2002; Fayyazuddin et al., 2006). In *Drosophila* the subunit α7 (Dα7) was used for transgenesis. Fluorescently tagged it serves as a marker for ACh receptors(Leiss et al., 2009).

## 2.3 Synaptic plasticity

One important feature that defines the behavior of neural circuits is theability to change the pattern of synaptic weights that connect the individual neurons within the circuit.A presynaptic AP does not always trigger the same amount of neurotransmitter releaseand a certain quantity of released neurotransmitter does not always elicit the same postsynaptic response. The activity-dependent modulation of synaptic strength is termed synaptic plasticity (Konorski, 1948). Synaptic plasticity receives much attention in neurobiology: already Santiago Ramón y Cajal (Ramòn y Cajal, 1894) and, later, Donald Olding Hebb (Hebb, 1949) proposed that learning involves plastic changes of synaptic connections and that memory storage requires the stabilization of these changes.

### 2.3.1 Short-term plasticity

Short-term plasticity mechanisms last from milliseconds to several minutes (reviewed by Fioravante and Regehr, 2011). They are thought to be relevant for short-term adaptations to external stimuli, transient changes in behavior and short-term forms of memory. The changes in synaptic strength usually follow synaptic activity. The underlying mechanisms are in most cases located to the presynapse,often triggered by increased $Ca^{2+}$ concentrations.

Different short-term plasticity mechanisms have been observed, including facilitation, post-tetanic potentiation (PTP), presynaptic depression and postsynaptic desensitization (reviewed by Xu-Friedman and Regehr, 2004). Facilitation describes the increased postsynaptic response following the second of two APs that arrive in quick succession. PTP in contrast requires tens or hundreds of APs in a train. It can lead to a many-fold enhancement of postsynaptic strength and lasts from 5 milliseconds to several minutes. Both, facilitation and PTP are produced due to elevated $Ca^{2+}$ levels during synaptic activity in the presynaptic terminal. The first AP leads to $Ca^{2+}$ influx. When a second AP arrives causing $Ca^{2+}$ influx as long as the intracellular $Ca^{2+}$ levels are still elevated, the probability of neurotransmitter release is increased. Other synapses in contrast may be depressed by elevated synaptic activity. When a large fraction of primed

SVs has fused to the presynaptic membrane due to an AP, only few SVs are left and can release their content when a second AP arrives. Consequently, the postsynaptic response is smaller. This process is termed presynaptic depression. Postsynapses with ionotropic receptors that enter a non-conducting state after activation are subject to postsynaptic desensitization. The time course of postsynaptic depression depends on the receptor type

## 2.3.2 Long-term plasticity

Long-lasting activity-induced changes in the strength of synapses are thought to be the basis for memory formation (Mayford et al., 2012). These involve modifications in transmitter release, trans-synaptic signaling and postsynaptic receptor dynamics, to the point of gene expression within neurons (Ho et al., 2011). They can last for days or even weeks (Mayford et al., 2012).

Such changes can be caused by distinct patterns of synaptic activity: high frequency stimulation is followed by synaptic strengthening, conferred to as long-term potentiation (LTP), whereas low frequency stimulation weakens the postsynaptic response, termed long-term depression (LTD; reviewed by Lüscher and Malenka, 2012). LTP and LTD are the most prominent forms of long-term synaptic plasticity; they are commonly investigated in the mammalian hippocampus. Their underlying mechanisms vary depending on the neurons and circuits in which they function (Malenka and Bear, 2004).

Usually, LTP and LTD require the activation of ionotropic N-methyl-D-aspartate (NMDA)-type glutamate receptors. This allows for $Ca^{2+}$ influx, which, in turn, triggers the activation of intracellular signaling cascades. Both, LTP and LTD rely on increased $Ca^{2+}$ levels. Modest increases in $Ca^{2+}$ levels are needed to trigger LTD and much larger increases in $Ca^{2+}$ levels are optimal to trigger LTP. Following, α-amino-3-hydroxy-5-methyl-4-isoxazole propionic acid (AMPA) type glutamate receptors are redistributed: they are added to the postsynaptic membrane for LTP or removed from the postsynaptic membrane for LTD. NMDA and AMPA receptors both are permeable for $Na^+$ and $K^+$. The $Na^+$ influx is much stronger than the $K^+$ efflux, thus, the net effect is the depolarization of the postsynaptic membrane. The depolarization via AMPA receptors typically proceeds quicker and stronger than via NMDA receptors. Hence, the more AMPA receptors are present on the postsynaptic membrane the stronger is the postsynaptic depolarization following an AP. AMPA receptors can be very mobile; they travel on vesicles and are added to and removed from the postsynaptic membrane via exocytosis and endocytosys. This process takes place in a perisynaptic region, from where AMPA receptors reach their destination via lateral diffusion. Proteins of the PSD regulate their mobility as well as their stabilization in the postsynaptic membrane.

The second-messenger mechanisms underlying LTP involve the activation of the calcium/calmodulin-dependent kinase II (CaMKII). This in turn leads to the phosphorylation of a number of proteins and contributes to the exocytosis of AMPA receptors. However, as the induction and maintenance of LTP is a very complex process, a multitude of additional protein kinases have been suggested to contribute to LTP. LTD on the other hand is suggested to depend, among others, on the calcium/calmodulin-dependent protein phosphatase calcineurin and on the protein phosphatase 1 (PP1). They might, for example, regulate the phosphorylation state of AMPA receptors(Lüscher and Malenka, 2012).

Of note, long-term synaptic plasticity was recently observed also in GABAergic neurons (Kullmann and Lamsa, 2007). Furthermore, additional forms of synaptic plasticity include homeostatic plasticity and metaplasticity (reviewed by Citri and Malenka, 2008). Homeostatic plasticity describes, for example, synaptic scaling: the change in strength of all synapses of a neuron in response to prolonged changes in activity. Metaplasticity refers to the activity-induced changes in the capacity of synapses to express long-term plasticity.

In the long run, long-term synaptic changes may result in structural changes such as the reorganization of the actin cytoskeleton and consequental changes in dendritic spine morphology (Hotulainen and Hoogenraad, 2010) as well as in the length of the presynaptic membrane and in the number of presynaptic active zones(Zhao et al., 2012).

## 2.4 Transmitters

Chemical transmission is based on various types of substances, such as different kinds of neurotransmitters or neuropeptides. Both are small molecules that activate receptors on the postsynaptic neuron and can thereby elicit a postsynaptic response.

### 2.4.1 Classical neurotransmitters

Classical transmitters are synthesized and stored in small SVs at the axon terminal. In insects, classical neurotransmitters include ACh, glutamate, γ-aminobutyric acid (GABA) and biogenic amines such as dopamine, serotonin, histamine, octopamine, and tyramine. In insects, ACh is the major excitatory transmitter in the CNS. Glutamate on the other hand is released as fast excitatory transmitter at neuromuscular junctions. In vertebrates instead, ACh is released by motoneurons and glutamate is the predominant

transmitter in the CNS (Venken et al., 2011). GABA and glycine are inhibitory neurotransmitters. Octopamine and tyramine are biogenic amines only found in invertebrates. Their vertebrate counterparts are noradrenaline and adrenaline (David and Coulon, 1985; Evans and Maqueira, 2005).

### 2.4.2 Neuropeptides

While only about ten classical neurotransmitters exist, there is a huge diversity of neuropeptides (Wegener and Gorbashov, 2008). Neuropeptides are the most structurally and functionally diverse signaling molecules and exist in all animals with a nervous system (reviewed by Nässel, 2009). They can act as neuromodulators or as neurohormones. As neuromodulators, neuropeptides are released within or outside of the synaptic cleft, mediating many different effects, typically by acting on G-protein coupled receptors. As neurohormones, they are released into the circulation and act on targets further away from the release site. Neuropeptides are packed in large dense-core vesicles and often colocalize with classical transmitters. Classical transmitters are often released in response to smaller changes in $Ca^{2+}$ levels, whereas peptides are released in response to much higher $Ca^{2+}$ levels. In this manner, different functional messages can be signaled to the target cell.

## 2.5 The nervous system of insects

The insect CNS consists of a dorsal brain and a ventral nerve cord. The brain of the fruit fly is composed of the supraesophageal ganglion and the subesophageal ganglion, separated by the esophagus. The supraesophageal ganglion comprises three fused units, called neuromeres: protocerebrum, deutocerebrum, and tritocerebrum. The most dorsal neuromere, the protocerebrum, does not receive any sensory modalities (Strausfeld and Bacon, 1983). The MBs and the central complex are part of it, as are neurosecretory cells, which secrete signaling molecules to the circulatory system. The deutocerebrum comprises, amongst others, the optic lobes (Strausfeld and Bacon, 1983) and the ALs (introduced in 2.6.2). Hence, it receives input from the antennae and the compound eyes and it processes the sensory information. The tritocerebrum contains neurons that connect to some mouthparts and to the anterior digestive tract; it is fused to the central subesophageal ganglion.

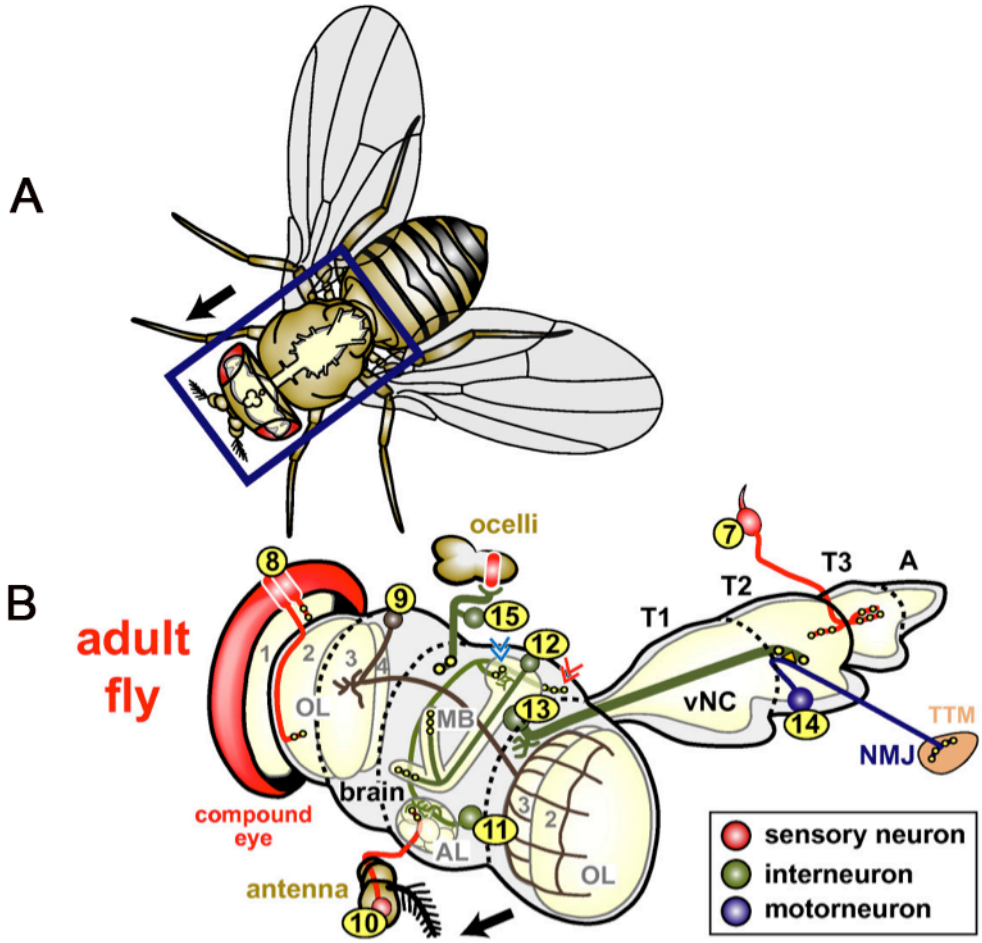


Fig. 3: Scheme of the central nervous system of *Drosophila melanogaster.*

**A:** Horizontal view of a *Drosophila* adult fly, illustrating the position of the CNS (cream) in relation to other body structures.
**B**: Three-dimensional extract from the area boxed in dark blue in **A**. The black arrow points to the anterior. Neuronal classes are explained in the box at the bottom right. Some model neurons are marked with numbers in yellow circles, and are explained below.
(7) Sensory neurons project into the ventral nerve cord (T1-3 and A indicate the three thoracic and fused abdominal segments). (8) Photoreceptor cells in the adult compound eye. (9) Representation of 20–30 dorsal cluster neurons, which are postsynaptic to photoreceptor neurons. ORNs in the antenna (10) terminate in specific glomeruli of the ALs. The main output from the ALs is constituted by projection neurons (11), which are postsynaptic to ORNs and innervate the lateral horn (red double chevron) and the calyx (blue double chevron), a dorsal structure of the MBs (Jefferis and Hummel, 2006). The MB neurons (12) project through calyx and peduncle, where many of them bifurcate to project into the vertical α/α'-and the horizontal β/β'/γ-lobes simultaneously. (13) The large giant fiber neuron connects the optic system via a large diameter axon to motoneurons in the second thoracic segment (14). (15) Ocellar photoreceptor neurons.
Reprinted with permission, from Sánchez-Soriano et al., 2007.

# 2.6 The olfactory circuit in *Drosophila*

## 2.6.1 Sensation of olfactory signals

The chemical sense smell is an ancient sensory modality. It is crucial for survival, as it guides food and mate selection and helps to avoid dangers. Insects possess a sensitive chemosensory system that detects and discriminates among a diverse array of chemicals. They detect odors with receptors in ORNs on their antenna and on the maxillary palp, both located on their head. 39 olfactory seven-transmembrane-domain receptors are known to be expressed in the adult (Vosshall et al., 2000), which are encoded by highly diverse gene families (Hallem and Carlson, 2006). In addition, Richard Benton and colleagues recently identified a novel class of olfactory receptors, unrelated to the odorant receptors characterized by Vosshall et al., 2000 (Benton et al., 2009). In total, 50-60 olfactory receptors are expressed in the antennae and maxillary palps of *Drosophila* (Wilson, 2013). In contrast to most animals including mammals, insect olfactory receptors possess ligand-activated ion channel activity (Benton, 2008; Wicher, 2012). After an olfactory molecule has activated the receptor, the ORN conveys information to the primary olfactory center, the AL (Stocker et al., 1983).

## 2.6.2 The antennal lobe

All ORNs that express the same odorant receptor, project to the same one or two glomeruli in an ALs; glomeruli are spatially delimited subunits of the ALs (Gao et al., 2000; Vosshall et al., 2000; Couto et al., 2005; Fishilevich and Vosshall, 2005). The ALs are sites of high synaptic complexity, implying that olfactory information from the ORNs is processed here. The major target neurons of the ORNs are projection neurons (PNs), which convey the olfactory information to secondary centers. A network of excitatory and inhibitory local neurons (LNs) interconnects the glomeruli and interacts with PNs, ORNs and other LNs (Stocker et al., 1990; Stocker, 1994; Ng et al., 2002; Wilson and Laurent, 2005; Shang et al., 2007). PN dendrites typically innervate a single glomerulus (Stocker et al., 1990). Each glomerulus is targeted by several PNs; they are called sister PNs and show similar activity patterns (Wilson, 2013). Of note, the PN dendrites can release neurotransmitter (Ng et al., 2002; Wilson et al., 2004). The PN axons converge on the antennocerebral tracts and target two separate bilateral neuropils, the lateral horns and the MBs (Strausfeld, 1976). The MBs receive olfactory input through the calyx. Olfactory information is conveyed to the calyx by PNs from the ALs via the inner antennocerebral tract (iACT; Fig. 5A).

## 2.6.3 The mushroom bodies

The MBs were first described by Félix Dujardin in 1850 (Dujardin, 1850), who called them *corps pédonculés*. MBs are prominent bilateral neuropil structures in the central arthropod brain. The MBs' intrinsic neurons, termed Kenyon cells (KCs; Kenyon, 1896), arborize extensively in the calyx, converge in the shape of a peduncle and form medial (β, β′, γ) and vertical (α, α′) lobes on their distal part (Tanaka et al., 2008). The KCs receive their olfactory input through the calyx. Here, their dendrites enwrap large presynaptic varicosities of PNs, conferred to as boutons (Schürmann, 1974; Yasuyama et al., 2002; Ramaekers et al., 2005). In the adult fruit fly, about 2500 KCs reside in each brain hemisphere (Technau, 1984). Furthermore, a large number of different non-MB cells, conferred to as MB extrinsic neurons, connects calyx, peduncle and lobes to other areas of the brain (Ito et al., 1998; Strausfeld et al., 2003).

To date, no common neurotransmitter could be discovered for the KCs. However, a large subset of neurons of the MBs was found to release the neuromodulator short neuropeptide F (Johard et al., 2008; Knapek et al., 2013). It is well possible that short Neuropeptide F is released by MB neurons as a co-transmitter.

The anatomical organization of the MBs as well as its connectivity to input and output neurons is not completely understood. However, a precise description of the connectivity of the MBs is a prerequisite for understanding the neuronal basis of MB-derived behaviors.

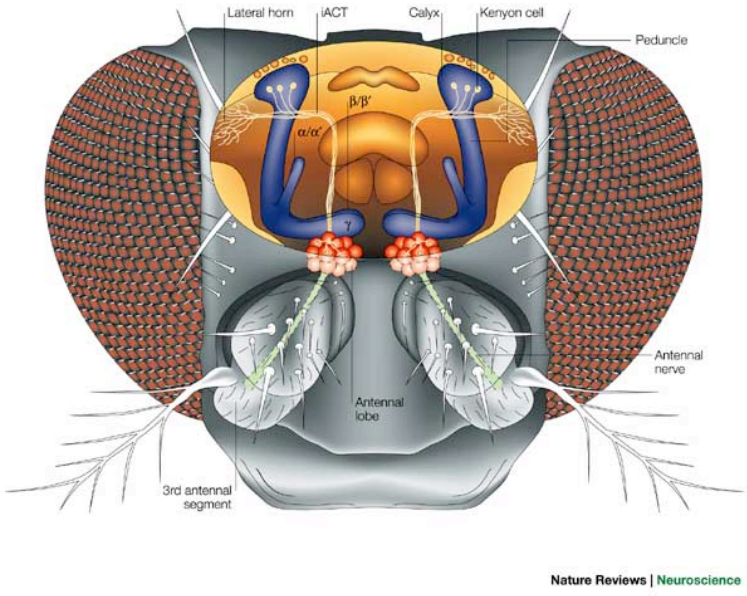

Fig. 4: Olfactory pathway

Odour information is carried from the antennae and maxillary palps (not shown) to the AL, where receptor fibrers are sorted according to their chemospecificities in about 50 glomeruli on each hemisphere. These represent the primary odour qualities, which are reported to two major target areas in the brain, the dorsolateral protocerebrum (lateral horn) and the calyx of the MB. The inner antennocerebral tract (iACT) connects individual glomeruli to both areas. α/α′, β/β′ and γ mark the three MB subsystems described by Crittenden et al., 1998.
From Heisenberg, 2003. Reprinted by permission of Macmillan Publishers Ltd: Nature Reviews Neuroscience.

## 2.6.4 Mushroom body related learning and memory in *Drosophila*

Félix Dujardin considered the MBs as the seat of intelligence, showing that advancing sociality was correlated with enlarged MBs (Dujardin, 1850). In fact, during the Flast decades, genetic modification in the fruit fly has provided strong evidence that the MBs play a major role in olfactory associative learning and memory (Heisenberg, 2003; Perisse et al., 2013). Moreover, the MBs are involved in other complex behavioral functions such as sleep/wake behavior, visual learning, courtship conditioning and decision-making (Liu et al., 1999; McBride et al., 1999; Joiner et al., 2006; Pitman et al., 2006; Yang et al., 2008; Miller et al., 2011). However, also MB extrinsic neurons are relevant for learning and memory: the two dorsal paired medial (DPM) neurons, the two anterior paired lateral (APL) neurons, and, in addition, different clusters of dopaminergic neurons (Davis, 2011; Chen et al., 2012). On each hemisphere of the fruit fly's brain reside one DPM and one APL neuron, which are electrically coupled with each other via gap junctions. The serotonergic DPM neuron bifurcates to innervate the vertical and the horizontal lobes of the MBs. The GABAergic APL neuron also bifurcates and separately innervates the calyces and the lobes (Yu et al., 2005; Liu and Davis, 2009). The dopaminergic protocerebral posterior lateral (PPL) neurons 1 cluster innervates the vertical lobes, whereas the dopaminergic PPL2ab neurons cluster projects to the calyx. A third cluster of dopaminergic cells, the protocerebral anterior medial (PAM) neurons cluster, innervates the horizontal lobes (Waddell, 2010; Davis, 2011). Furthermore, one dopaminergic dorsal anterior lateral (DAL) neuron in each hemisphere innervates calyx and lobes (Chen et al., 2012).

Incoming odor information leads to the activation of certain subsets of KCs (Dubnau and Chiang, 2013). In addition to the odor information, KCs receive inputs from several different neuromodulatory neurons (Busto et al., 2010). Amongst them are neurons that represent the unconditioned stimulus: the aversive or appetitive stimulus that, if coupled

to an odor, may induce olfactory associative learning. For instance, a specific set of dopaminergic neurons that innervates the MBs is activated, when a fruit fly is exposed to electric shocks (Busto et al., 2010; Riemensperger et al., 2005; Claridge-Chang et al., 2009; Aso et al., 2010). The three neuromodulators octopamine, serotonin and dopamine all shape the reinforcement system. Yet, the final MB-innervation is carried out by dopaminergic neurons for both, the representation of appetitive and aversive unconditioned stimuli (Perisse et al., 2013).

On a cellular level, the current model of MB based olfactory associative memory formation (reviewed by Heisenberg, 2003) is as follows: the activation of a KC by a PN (odor representation) leads to elevated $Ca^{2+}$ levels in KCs. On the other hand, the activation of KC receptors responsive to the cells that mediate the unconditioned stimulus (e.g. the dopamine receptor DopR), leads to G-protein coupled signaling. When a KC receives both inputs simultaneously, the G-protein coupled signaling and the $Ca^{2+}$ influx cause the activation of the $Ca^{2+}$/Calmodulin sensitive adenylyl cyclase *rutabaga* (Dubnau and Chiang, 2013). *rutabaga* activity, in turn, leads to increased synthesis of cyclic adenosine monophosphate (cAMP). Elevated cAMP levels activate Proteinkinase A (PKA), which might phosphorylate target proteins at KC presynapses (Heisenberg, 2003). Hence, this *rutbaga* dependent signaling can induce short-term plasticity. It can also stimulate the transcription factor CREB (cAMP response element binding protein), which leads to long-term plasticity and long-term memory (Dubnau and Chiang, 2013).

The anatomical subdivisions of the MBs correlate with functional differences in learning and memory. For example, the coincidence detection of odor and aversive unconditioned stimulus takes place in γ-type KCs (Qin et al., 2012). Following, communication between the different KC subtypes and MB extrinsic neurons is needed for the maintenance of memory. During the first few hours after coincidence detection, persistent activity in $\alpha'/\beta'$ KCs as well as in the APL and DPM neurons is needed. For LTM a second feedback loop is required, which involves the DAL neurons and $\alpha/\beta$ neurons (Dubnau and Chiang, 2013).

## 2.7 The connectivity in the mushroom body calyx

The calyx contains four major neuronal elements: axonal terminals of PNs, which are presumed to be predominantly cholinergic, projections of the GABAergic APL neurons,

projections of octopaminergic neurons and KC dendrites (Yasuyama et al., 2002; Sinakevitch and Strausfeld, 2005; Busch et al., 2009; Liu et al., 2009). Of note, few PNs might be GABAergic (Wilson and Laurent, 2005; Okada et al., 2009). In addition, also dopaminergic and serotonergic neurons provide innervation to the MB calyx(Aso et al., 2012; Pech et al., 2013). The present wiring diagram, based on electron microscopy and immunolabeling studies (Yasuyama et al., 2002; Butcher et al., 2012), suggests that the PNs form presynaptic boutons, providing input to KC dendrites and GABAergic fibers. GABAergic fibers, in turn, provide input to KCs and PNs (Fig. 5B-D). The PN boutons are termed microglomeruli. They are enwrapped by KC dendrites and possibly innervated by GABAergic fibers.

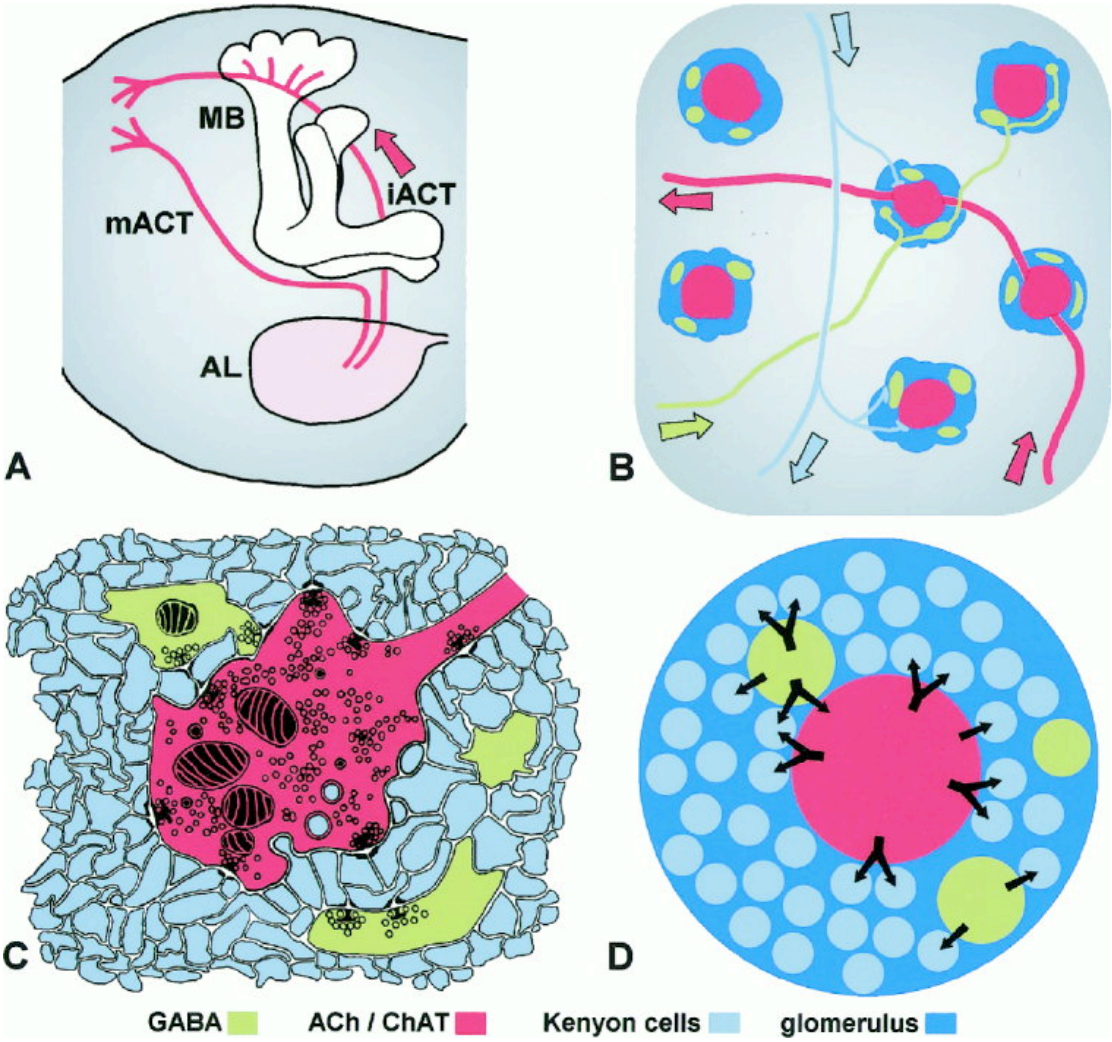


Fig. 5: Connectivity in the MB calyx

**A.** Scheme of a MB and PNs (red lines) within the inner antennocerebral tract (iACT) and the middle antennocerebral tract (mACT), which arise from the AL (in *Drosophila).*
**B:** Schematic diagram of the circuits in the calyx. Terminals of GABA immunoreactive neurons

(green) and choline acetyltransferase (ChAT) immunoreactive (presumed cholinergic) PNs (red) intersect at a repeated array of calycal glomeruli.
**C:** Representative diagram of the profiles in a single glomerulus, indicating typical synaptic organelles of the two types of presynaptic terminals.
**D:** Schematic view of the divergent synaptic connections of intrinsic and extrinsic fibers in the glomerulus.
From Yasuyama et al., 2002. Reprinted with permission of John Wiley and sons.

The assembly of the connections between PNs and KCs in the calyx is stereotypic. KC dendrites segregate into special domains and PN axons form stereotyped branches and boutons (Strausfeld et al., 2003; Tanaka et al., 2004; Lin et al., 2007). This indicates that the topographic olfactory map of the first-order olfactory center might be retained in a modified form in second–order olfactory centers.

The intention of this thesis is to improve our understanding of the organization of the circuitry in the MB calyx. Therefore, the synaptic contacts between neurons in the calyx were examined morphologically and functionally.

## 2.8 Synaptic plasticity in the MB calyx

Another aspect this thesis aims at is to uncover whether PNs and KCs in the calyx are capable of experience-dependent plasticity. There is evidence that neurons involved in the calyx circuitry show morphological differences upon changes in the environment. Several studies demonstrated in different insects that the volume of the MB calyx changes in an experience-dependent manner. For example, the volume of the calyx is sensitive to rearing conditions and visual input (Withers et al., 1993; Durst et al., 1994; Groh et al., 2004; Seid et al., 2005; Groh et al., 2006; Ismail et al., 2006; Kuhn-Buhlmann and Wehner, 2006). Furthermore, *Drosophila* mutants impaired in olfactory associative learning are defective in experience-dependent volume expansion of the calyx (Barth and Heisenberg, 1997; Hitier et al., 1998). In addition, the morphology of the calyx is modified upon olfactory associative learning in cockroaches (Lent et al., 2007). Interestingly, microglomeruli in the calyx undergo adaptive changes in morphology: sensory deprived honeybees develop less microglomeruli with larger boutons compared to forager bees from a natural colony (Krofczik et al., 2008). Moreover, increased foraging experience is associated with an increase in complexity in Kenyon cell dendrites (Farris et

al., 2001). Age is yet another factor that affects microglomerulus size and number (Seid et al., 2005; Groh et al., 2006).

Though, other studies indicate that ablation of sensory input in the fruit fly has no effect on dendritic or axonal arborization of PNs (Wong et al., 2002; Tanaka et al., 2004; Berdnik et al., 2006) or of third-order-neurons (Tanaka et al., 2004).

However, the observed volumetric changes of calyx and microglomeruli might have occurred due to changes at synaptic connections. We were eager to investigate whether the synapses between PN and KC (PN::KC synapses) are subject to synaptic plasticity.

# 3. MATERIAL AND METHODS

## 3.1 Animals

### 3.1.1 Genotypes used in Christiansen et al., 2011

c305a-GAL4 (Krashes et al., 2007)

c739-GAL4 (O'Dell et al., 1995; Yang et al., 1995)

gh146-GAL4 (Stocker et al., 1997)

h24-GAL4 (Zars et al., 2000)

ok107-GAL4 (Connolly et al., 1996)

UAS-brp-RNAi (Wagh et al., 2006)

UAS-synapto-pHluorin (Ng et al., 2002)

UAS-da7$^{GFP}$ (Leiss et al., 2009)

UAS-brp-short$^{mCherry}$ (Schmid et al., 2008)

UAS-syt$^{GFP}$ (Zhang et al., 2002)

mb247::brp-short$^{GFP}$ (Christiansen et al., 2011)

mb247::da7$^{GFP}$ (Kremer et al., 2010)

w, hsFlp; UAS-mcd8$^{GFP}$; FRT82B tubGAL80 / TM3 Sb; ok107-GAL4 (Lee and Luo, 2001)

w$^{-}$; FRT82B (Lee and Luo, 2001 Germany)

## 3.1.2 Genotypes used in Kremer et al., 2010

mz19-GAL4 / CyO

UAS-brp-short$^{mCherry}$mb247::da7$^{GFP}$ / UAS-dork1.Δc, mz19-GAL4/ +

UAS-brp-short$^{mCherry}$ mb247::da7$^{GFP}$ / UAS-dork1.Δnc and mz19-GAL4 / + UAS-brp-short$^{mCherry}$ mb247::da7$^{GFP}$ / UAS-pi3k

Including the following drivers and reporters:

mz19-GAL4 (Jefferis et al., 2004)

UAS-dork1.Δc (Nitabach et al., 2002)

UAS-dork1.Δnc (Nitabach et al., 2002)

UAS-pi3k (Leevers et al., 1996)

## 3.1.3 Genotypes used in Owald et al., 2010

*w*$^{1118}$ (Hazelrigg et al., 1984)

*dsyd-1 (*Owald et al*., 2010)*

*UAS-da7*$^{GFP}$*/ +* (Leiss et al., 2009)

*ok107*-GAL4 / + (Connolly et al., 1996)

All fly-strains were reared under standard laboratory conditions (Sigrist et al., 2003) at 25°C.

## 3.2 Molecular cloning

We generated transgenic flies carrying the *eGFP*-tagged *brp-short* construct under direct control of the MB enhancer *mb247* (Schulz et al., 1996), *mb247::brp-short*$^{GFP}$. *brp-short* corresponds to amino acids 473-1226 of the 1740 amino acid BRP protein (Schmid et al., 2008). *brp-short*$^{GFP}$ was inserted in the pCaSpeR vector carrying the *mb247* enhancer in front of a minimal promoter from a heat shock gene (Schulz et al., 1996), using the StuI and the XbaI restriction sites of the vector and the SpeI and HpaI sites of the insert. Secondly, the *mb247::da7*$^{GFP}$ transgenic fly stock carrying the eGFP tagged Dα7 subunit of the nicotinic ACh receptor under direct control of the mushroom body enhancer *mb247* was generated. Therefore *dα7*$^{GFP}$ was inserted in the pCaSpeR vector carrying the *mb247* enhancer (Schulz et al., 1996) using the restriction sites NotI and XbaI.

## 3.3 Dissection and immunohistochemistry

Adult and larval brains were dissected in ice-cold hemolymph-like saline (HL3) solution, fixed for 20min in 4% paraformaldehyde (Polyscience Inc, Warrington, PA) in phosphate buffered saline (PBS, pH 7.2) and then blocked for 20min in 10% normal goat serum (NGS) or, for activity modulation experiments, for 30 min in 10% fetal calf serum (FCS, Invitrogen, USA) in PBS with 0.3% Triton-X 100 (PBT). Adult and larval brains were incubated with primary antibodies together with 5% NGS overnight at room temperature and then washed in PBT for 3h, followed by overnight incubation with secondary antibodies at 4°C. The brains were then washed for 3h with 0.3 PBT and mounted in VectaShield (Vector laboratories, USA) on slides. Adult brains stained with Nc82 (BRP$^{Nc82}$; Whag et al., 2006) were preincubated with 1% PBT for 30min after fixation and were then incubated with the primary antibodies together with 5% NGS for 48h at room temperature. Afterwards the brains were washed for 5h with PBT.

## 3.4 Antibody concentrations

Mouse BRP$^{Nc82}$ 1:100, for activity modulation experiments 1:20; rabbit anti-DSyd-1 1:500 (Owald et al., 2010); rabbit anti-DsRed (Beckton Dickinson, USA) 1:500, for

activity modulation experiments (Rockland Immunochemicals, USA) 1:2000; rabbit anti-GFP (Molecular Probes, USA) 1:500; goat anti-mouse Alexa 488 (Invitrogen, Darmstadt, Germany, #A11001) 1:500; goat anti-rabbit Cy3 (Dianova, Hamburg, Germany, #111-167-003) 1:500; goat anti-mouse Cy5 (Dianova, Hamburg, Germany, #111-177-003) 1:500; goat anti-rabbit AlexaFluor 568 (Invitrogen, USA) 1:100.

## 3.5 Image acquisition

Conventional confocal images were acquired with a Leica TCS SP5 confocal microscope (Leica Microsystems) using a 63x, 1.4 N.A. oil objective for calyx scans and a 20x, 0.7 N.A. oil objective for whole brain overview scans. Voxel size was 71x71x200 nm for calyx imaging and 120x120x500 nm for whole brain imaging. Confocal stacks were processed using ImageJ software (http://rsbweb.nih.gov/ij/).

BRP-short can form agglomerations within the somata of the cells it is expressed in. As the KC somata are located very close to the calyx neuropil, we manually removed them in maximum intensity projections (Christiansen et al., 2011, Fig. 7M-O) for clarity.

For the activity modulation experiments confocal images were recorded using an Olympus confocal microscope with 60x 1.4 oil-immersion 11 objective (Olympus Germany GmbH). Image acquisition settings were standard for all images (60x 1.4 oil-immersion objective, 3x zoom). For each calyx we scanned a series of 60 to 100 slices with a voxel size of 0.138 x 0.138 x 0.25 µm.

Figures were prepared with Photoshop and Illustrator CS4 (Adobe Systems Incorporated, San Jose, CA, USA).

## 3.6 Analysis of the activity modulation experiment

For this experiment we used 7-day-old flies. The PN AZ parameters were analysed using the Imaris x 64 v6.1.5 software, optimized for the purpose (Bitplane AG).For the analysis of the AZ of the relevant PNs, we developed a semi-automatic analysis with Imaris, which

was applied to signal intensities in 3D reconstructions of the calyx. We calculated the number of AZs and the total area of AZs of the silenced PNs in the calyx.

Statistics were conducted using GraphPad Prism (GraphPad software, La Jolla, USA). The data were tested for normal distribution and homogeneity of variance with the Kolmogorov-Smirnov test. As the data were not normally distributed, Mann-Whitney test or Kruskal-Wallis followed by Dunn`s post-hoc pair-wise test were performed. The significance level was set to 5 %. * $P < 0.05$; ** $P < 0.01$; *** $P < 0.001$. In whisker box-plots, the box extends from the 25th to 75th percentiles with a line at the median. Whiskers mark minimum and maximum data points.

## 3.7 Analysis of the RNAi experiment

Flies expressing UAS-brp-RNAi under the control of ok107-GAL4 as well as w1118 controls were raised in 68 ml standard vials with a constant 12h light/dark regimen. Adult female flies (2-5d after eclosion) as well as female 3rd instar larvae were dissected.

$BRP^{Nc82}$ and DSyd-1 signal intensities were quantified similarly as described above for the activity modulation experiment. Calyces were segmented using the Fiji (ImageJA v1.44) plugin Segmentation Editor (http://pacific.mpi-cbg.de/). The images were then analyzed in Bitplane Imaris x64 v6.23. The masks created in Fiji were used as a template for isolating the calyces in Imaris. Subsequently, the overall surface of the $BRP^{Nc82}$ and DSyd-1 channels within the calyx was determined. In addition, number and surface areas of the individual $BRP^{Nc82}$ and DSyd-1 spots were identified, as well as the respective intensities within each spot. For this the Imaris surface tool was employed, using seed detection and region growing algorithms. The data was further analyzed using Microsoft Office 2008 and StatSoft Statistica 9.1.

## 3.8 MARCM

Genotype of flies with mCD8-GFP and $D\alpha7^{mCherry}$ co-expressing clones:

w,hsFlp / w; UAS-mcd8-GFP / UAS-$D\alpha7^{mCherry}$; FRT82b, tubGAL80 / neoFRT82b; ok107-GAL4 / +

Genotype of flies with mCD8-GFP and BRP-$short^{mCherry}$ co-expressing clones:

w,hsFlp / w; UAS-mcd8-GFP / UAS-brp-short$^{mCherry}$; FRT82b, tubGAL80 / neoFRT82b; ok107-Gal4 / +

Vials containing female and male eggs, 1st, 2nd or 3rd instar larvae or pupae were transferred into a 37°C water bath for 30min. Altogether we scanned 89 calyces. The clones depicted belong to the α/β KC subpopulation. For the clone expressing Dα7 shown in Christiansen et al., 2011 Fig. 6I,J, the heat shock was applied 5 days before pupal eclosion. For the clone expressing BRP-short shown in Christiansen et al., 2011 Fig. 6K,L, the heat shock was applied 3 days before pupal eclosion.

## 3.9 Functional imaging

Flies were cooled on ice for several minutes and immobilized in a truncated 1 ml pipette tip. This preparation was glued to a plastic cover slip (Plano GmbH) with dental glue (Protemp II, 3M ESPE). Subsequently, a window was cut into the head of the fly using a splint of a razor blade and a blade holder. Trachea and fat bodies were carefully removed to expose the brain. The brain was covered with Ringer's solution (HEPES 5mM, NaCl 130mM, KCl 5mM, $MgCl_2$ 2mM, $CaCl_2$ 2mM) as a physiological medium. For eliciting neuronal depolarization KCl (final concentration of 100mM) was injected into the drop of Ringer's solution covering the brain. The imaging setup consisted of a fluorescence microscope (Axio Examiner D1, Zeiss), equipped with a xenon lamp (Lambda DG-4, Sutter Instrument), a 14-bit camera (Coolsnap HQ2, Photometrics) and a GFP filter set. Data acquisition was controlled by the software Metafluor (Visitron Systems). Images were acquired using a 40x water immersion objective at a frame rate of 5 Hz and an excitation wavelength of 488nm. Image sequences were analyzed by choosing a region of interest (ROI) covering the calycal region. Average emission intensities from Synapto-pHluorin were quantified for each image. Average intensities of a ROI outside the labeled structure was subtracted as background. The emission intensity (F) at the frame immediately before KCl application was determined as $F_0$, and $DF/F_0$ was calculated for each image. The software Origin v8.1 (OriginLab) was used for data evaluation. For illustrating the entire MB (Christiansen et al., 2011, Fig. 5B), images were acquired at 1µm steps in the Z-direction. A maximum intensity Z-projection was generated from the entire stack.

# 4. PRESYNAPSES IN KENYON CELL DENDRITES IN THE MUSHROOM BODY CALYX OF *DROSOPHILA*

Cellular/Molecular

# Presynapses in Kenyon Cell Dendrites in the Mushroom Body Calyx of *Drosophila*

**Frauke Christiansen,[1,4]* Christina Zube,[1]* Till F. M. Andlauer,[1,4,5,6] Carolin Wichmann,[1,4] Wernher Fouquet,[1,4] David Owald,[1,4] Sara Mertel,[1] Florian Leiss,[2] Gaia Tavosanis,[2] Abud J. Farca Luna,[3] Andre Fiala,[3] and Stephan J. Sigrist[1,4]**

[1]Department of Genetics, Institute for Biology, Freie Universität Berlin, 14195 Berlin, Germany, [2]Department of Molecular Neurobiology, Dendrite Differentiation Group, Max Planck Institute of Neurobiology, 82152 München-Martinsried, Germany, [3]Department of Molecular Neurobiology of Behavior, Georg-August-Universität Göttingen, 37077 Göttingen, Germany, [4]NeuroCure Cluster of Excellence, Charité Berlin, 10117 Berlin, Germany, [5]Rudolf Virchow Center/Deutsche Forschungsgemeinschaft Research Center for Experimental Biomedicine, Universität Würzburg, 97080 Würzburg, Germany, and [6]Max Planck Institute for Colloids and Interfaces, Science Park Golm, 14424 Potsdam, Germany

**Plastic changes at the presynaptic sites of the mushroom body (MB) principal neurons called Kenyon cells (KCs) are considered to represent a neuronal substrate underlying olfactory learning and memory. It is generally believed that presynaptic and postsynaptic sites of KCs are spatially segregated. In the MB calyx, KCs receive olfactory input from projection neurons (PNs) on their dendrites. Their presynaptic sites, however, are thought to be restricted to the axonal projections within the MB lobes. Here, we show that KCs also form presynapses along their calycal dendrites, by using novel transgenic tools for visualizing presynaptic active zones and postsynaptic densities. At these presynapses, vesicle release following stimulation could be observed. They reside at a distance from the PN input into the KC dendrites, suggesting that regions of presynaptic and postsynaptic differentiation are segregated along individual KC dendrites. KC presynapses are present in $\gamma$-type KCs that support short- and long-term memory in adult flies and larvae. They can also be observed in $\alpha/\beta$-type KCs, which are involved in memory retrieval, but not in $\alpha'/\beta'$-type KCs, which are implicated in memory acquisition and consolidation. We hypothesize that, as in mammals, recurrent activity loops might operate for memory retrieval in the fly olfactory system. The newly identified KC-derived presynapses in the calyx are, inter alia, candidate sites for the formation of memory traces during olfactory learning.**

## Introduction

Animals detect odors through olfactory sensory neurons. The odor information is processed by a primary olfactory center, constituted by the antennal lobe in insects (Stocker et al., 1983) or the olfactory bulb in vertebrates (Mombaerts, 2001). Subsequently, olfactory information is conveyed to secondary centers via olfactory projection neurons (PNs) in insects or mitral/tufted cells in vertebrates. The olfactory nervous systems of insects and mammals are comparable in their anatomical organization, suggesting that fundamentals of olfaction and olfactory learning might be similar (Davis, 2004). In the relatively simple *Drosophila* brain, PNs target two separate neuropils, the lateral horn and the mushroom body (MB) (Strausfeld, 1976). In the MB calyx, PNs connect to Kenyon cells (KCs) via large cholinergic boutons that contact claw-like endings of the KC dendrites (Schürmann, 1974; Yasuyama et al., 2002; Ramaekers et al., 2005). Several behavioral and genetic studies in different insect species have demonstrated that the MBs play an essential role in olfactory associative learning (for review, see Heisenberg, 1998, 2003; Roman and Davis, 2001; Waddell and Quinn, 2001a; Dubnau et al., 2003; Gerber et al., 2004; Davis, 2005; Keene and Waddell, 2007). Moreover, they are involved in other complex behavioral functions such as sleep/wake behavior, visual learning, courtship conditioning, and decision making (Liu et al., 1999; McBride et al., 1999; Joiner et al., 2006; Pitman et al., 2006; Yang et al., 2008; Miller et al., 2011). Not only KCs are involved in olfactory learning and memory, but also a number of MB-extrinsic neurons have been shown to play important roles (Hammer and Menzel, 1995, 1998; Waddell et al., 2000; Yu et al., 2004; Thum et al., 2007; Claridge-Chang et al., 2009; Krashes et al., 2009; Liu and Davis, 2009; Aso et al., 2010). The anatomical organization of the MB as well as its connectivity to input and output neurons are not completely understood. However, a precise description of the connectivity of the MB is a prerequisite for understanding the neuronal basis of MB-derived behaviors.

In this study, we investigated the organization of KC and PN synapses within the MB calyx. In contrast to previous assumptions, dendrites of certain subpopulations of KCs ($\gamma$ and $\alpha/\beta$ cells) formed presynaptic active zones (AZs). Presynaptic AZs are

Received Dec. 15, 2010; revised April 14, 2011; accepted April 28, 2011.

Author contributions: F.C. and S.J.S. designed research; F.C., C.Z., C.W., W.F., D.O., S.M., F.L., G.T., A.J.F.L., and A.F. performed research; A.F. and S.J.S. contributed unpublished reagents/analytic tools; F.C., C.Z., T.F.M.A., A.J.F.L., and A.F. analyzed data; F.C., C.Z., and S.J.S. wrote the paper.

This work was supported by Deutsche Forschungsgemeinschaft Grants SFB 554 and EXC 257. We thank E. Buchner for the Nc82 antibody, A. Thum for pCaSpeR::mb247, G. Miesenböck for *UAS-synapto-pHluorin*, M. Heisenberg for *h24*-GAL4, B. Mentzel and T. Raabe for the MARCM lines, and F. Zehe and C. Quentin for technical assistance. We are grateful to M. Heisenberg, R. Kittel, A. Thum, E. Buchner, H. Tanimoto, and O. Khorramshahi for fruitful discussions and valuable suggestions.

*F.C. and C.Z. contributed equally to this work.

Correspondence should be addressed to Stephan J. Sigrist, Department of Genetics, Institute for Biology, Freie Universität Berlin, 14195 Berlin, Germany. E-mail: stephan.sigrist@fu-berlin.de.

DOI:10.1523/JNEUROSCI.6542-10.2011

 0270-6474/11/319696-12$15.00/0

the regions of synaptic vesicle (SV) fusion. The distribution of these KC presynaptic sites in the calyx followed a defined pattern; they were spatially separated from the sites of cholinergic input onto KCs, provided by PNs. These KC-specific presynaptic sites could be stimulated to release SVs. Our study adds another degree of complexity to the olfactory circuit of *Drosophila*.

## Materials and Methods

*Animals.* The following fly stocks were used: *c305a*-GAL4 (Krashes et al., 2007), *c739*-GAL4 (O'Dell et al., 1995; Yang et al., 1995), *gh146*-GAL4 (Stocker et al., 1997), *h24*-GAL4 (Zars et al., 2000), *ok107*-GAL4 (Connolly et al., 1996), *UAS-brp-RNAi* (Wagh et al., 2006, recombination of B3 and C8), *UAS-synapto-pHluorin* (Ng et al., 2002), *UAS-Da7$^{GFP}$* (Leiss et al., 2009), *UAS-brp-short$^{mCherry}$* (Schmid et al., 2008), *UAS-syt$^{GFP}$* (Zhang et al., 2002), *mb247::brp-short$^{GFP}$*, *w,hsFlp,UAS-mCD8-GFP;FRT82B,tubGAL80/TM3,Sb;ok107*-GAL4 (L. Luo, Howard Hughes Medical Institute, Stanford University, Palo Alto, CA), *w$^{-}$;FRT82B* (Lee and Luo, 2001). All fly strains were reared under standard laboratory conditions (Sigrist et al., 2003) at 25°C.

*Molecular cloning.* We generated transgenic flies carrying the eGFP-tagged *brp-short* construct under direct control of the MB enhancer *mb247* (Schulz et al., 1996). *brp-short* corresponds to amino acids 473–1226 of the 1740 aa Bruchpilot (BRP) protein (Schmid et al., 2008). *brp-short$^{GFP}$* was inserted in the pCaSpeR vector carrying the *mb247* enhancer in front of a minimal promoter from a heat shock gene (Schulz et al., 1996), using the StuI and the XbaI restriction sites of the vector and the SpeI and HpaI sites of the insert.

*Dissection and immunohistochemistry.* Adult and larval brains were dissected in ice-cold hemolymph-like saline (HL3) solution, fixed for 20 min in 4% paraformaldehyde in PBS, pH 7.2, and then blocked in 10% normal goat serum (NGS) in PBS with 0.3% Triton X-100 (PBT) for 20 min. Adult and larval brains were incubated with primary antibodies together with 5% NGS overnight at room temperature and then washed in PBT for 3 h, followed by overnight incubation with secondary antibodies at 4°C. The brains were then washed for 3 h with 0.3 PBT and mounted in VectaShield (Vector Laboratories) on slides. Adult brains stained with Nc82 (BRP$^{Nc82}$) (Wagh et al., 2006) were incubated with 1% PBT for 30 min after fixation and were then incubated with the primary antibodies together with 5% NGS for 48 h at room temperature. Afterward, the brains were washed for 5 h with PBT.

*Antibody concentrations.* Antibody concentrations were as follows: mouse BRP$^{Nc82}$, 1:100; rabbit anti-DSyd-1, 1:500 (Owald et al., 2010); rabbit anti-DsRed (BD Biosciences), 1:500; rabbit anti-GFP (Invitrogen), 1:500; goat anti-mouse Alexa 488 (Invitrogen; A11001), 1:500; goat anti-rabbit Cy3 (Dianova; 111-167-003), 1:500; goat anti-mouse Cy5 (Dianova; 111-177-003), 1:500.

*Image acquisition.* Conventional confocal images were acquired with a Leica TCS SP5 confocal microscope (Leica Microsystems) using a 63×, 1.4 NA oil objective for calyx scans and a 20×, 0.7 NA oil objective for whole-brain overview scans. Voxel size was 71 × 71 × 200 nm for calyx imaging and 120 × 120 × 500 nm for whole-brain imaging. Confocal stacks were processed using ImageJ software (http://rsbweb.nih.gov/ij/).

BRP-short can form agglomerations within the somata of the cells it is expressed in. As the KC somata are located very close to the calyx neuropil, we manually removed them in maximum-intensity projections (see Fig. 7*M–O*) for clarity.

*Analysis of the RNAi experiment.* Flies expressing *UAS-brp-RNAi* under the control of *ok107*-GAL4 as well as *w1118* controls were raised in 68 ml standard vials with a constant 12 h light/dark regimen. Adult female flies (2–5 d after eclosion) as well as female third-instar larvae were dissected.

BRP$^{Nc82}$ and DSyd-1 signal intensities were quantified similarly as described by Kremer et al. (2010). Calyces were segmented using the Fiji (ImageJA, version 1.44) plug-in Segmentation Editor (http://pacific.mpi-cbg.de/). The images were then analyzed in Bitplane Imaris 64×, version 6.23. The masks created in Fiji were used as a template for isolating the calyces in Imaris. Subsequently, the overall surface of the BRP$^{Nc82}$ and DSyd-1 channels within the calyx was determined. In addition, number and surface areas of the individual BRP$^{Nc82}$ and DSyd-1 spots were identified, as well as the respective intensities within each spot. For this, the Imaris surface tool was used, using seed detection and region growing algorithms. The data were further analyzed using Microsoft Office 2008 and StatSoft Statistica 9.1.

*Mosaic analysis with a repressible cell marker.* Genotype of flies with mCD8-GFP and Dα7$^{mCherry}$ coexpressing clones was as follows: *w,hs-Flp/w$^{-}$; UAS-mcd8-GFP/UAS-Dα7$^{mCherry}$; FRT82b, tubGAL80/neoFRT82b; ok107*-GAL4/+. Genotype of flies with mCD8-GFP and *BRP-short$^{mCherry}$* coexpressing clones was as follows: *w,hsFlp/w$^{-}$; UAS-mcd8-GFP/UAS-brp-short$^{mCherry}$; FRT82b, tubGAL80/neoFRT82b; ok107*-Gal4/+.

Vials containing female and male eggs, first-, second-, or third-instar larvae or pupae were transferred into a 37°C water bath for 30 min. Together, we scanned 89 calyces. The clones depicted belong to the α/β KC subpopulation. For the clone expressing Dα7 shown in Figure 6, *I* and *J*, the heat shock was applied 5 d before pupal eclosion. For the clone expressing BRP-short shown in Figure 6, *K* and *L*, the heat shock was applied 3 d before pupal eclosion.

*Functional imaging.* Flies were cooled on ice for several minutes and immobilized in a truncated 1 ml pipette tip. This preparation was glued to a plastic coverslip (Plano) with dental glue (Protemp II; 3M ESPE). Subsequently, a window was cut into the head of the fly using a splint of a razor blade and a blade holder. Trachea and fat bodies were carefully removed to expose the brain. The brain was covered with Ringer's solution (5 mM HEPES, 130 mM NaCl, 5 mM KCl, 2 mM $MgCl_2$, 2 mM $CaCl_2$) as a physiological medium. For eliciting neuronal depolarization, KCl (final concentration of 100 mM) was injected into the drop of Ringer's solution covering the brain. The imaging setup consisted of a fluorescence microscope (Axio Examiner D1; Zeiss), equipped with a xenon lamp (Lambda DG-4; Sutter Instrument), a 14 bit camera (Coolsnap HQ2; Photometrics), and a GFP filter set. Data acquisition was controlled by the software Metafluor (Visitron Systems). Images were acquired using a 40× water-immersion objective at a frame rate of 5 Hz and an excitation wavelength of 488 nm. Image sequences were analyzed by choosing a region of interest (ROI) covering the calycal region. Average emission intensities from Synapto-pHluorin were quantified for each image. Average intensities of a ROI outside the labeled structure was subtracted as background. The emission intensity ($F$) at the frame immediately before KCl application was determined as $F_0$, and $\Delta F/F_0$ was calculated for each image. The software Origin, version 8.1 (OriginLab), was used for data evaluation. For illustrating the entire MB (see Fig. 5*B*), images were acquired at 1 μm steps in the $Z$ direction. A maximum-intensity $Z$ projection was generated from the entire stack.

## Results

### KC-derived presynapses within the MB calyx of *Drosophila* adults and larvae

We aimed at characterizing KC presynapses in the MB using a detailed molecular-anatomical approach. Presynapses are characterized by AZs containing discrete electron-dense specializations of roughly uniform size, called T-bars in *Drosophila* (Prokop and Meinertzhagen, 2006; Wichmann and Sigrist, 2010). The large scaffolding protein BRP is an essential component of T-bars (Kittel et al., 2006; Wagh et al., 2006). To label AZs of KCs, we expressed a fragment of BRP (BRP-short) fused to GFP (BRP-short$^{GFP}$) specifically in KCs. BRP-short$^{GFP}$ colocalizes clearly with endogenous BRP (Schmid et al., 2008) but is not detected by the monoclonal αBRP antibody Nc82 (BRP$^{Nc82}$), which binds to an epitope close to the BRP C terminus (Wagh et al., 2006). Notably, BRP-short$^{GFP}$ depends on endogenous BRP for AZ localization (S. J. Sigrist, unpublished observations). Therefore, BRP-short labels only preexisting AZs, characterized by the presence of endogenous full-length BRP, which is recognized by BRP$^{Nc82}$. In addition, a previous study showed that the number of BRP$^{Nc82}$-positive puncta is not modified upon expression of BRP-short (Kremer et al., 2010).

To specifically label KC-derived AZs, the KC-specific enhancer *mb247* (Schulz et al., 1996) was fused to the BRP-short$^{GFP}$ open reading frame. As expected, MB lobes of both larvae (Fig.

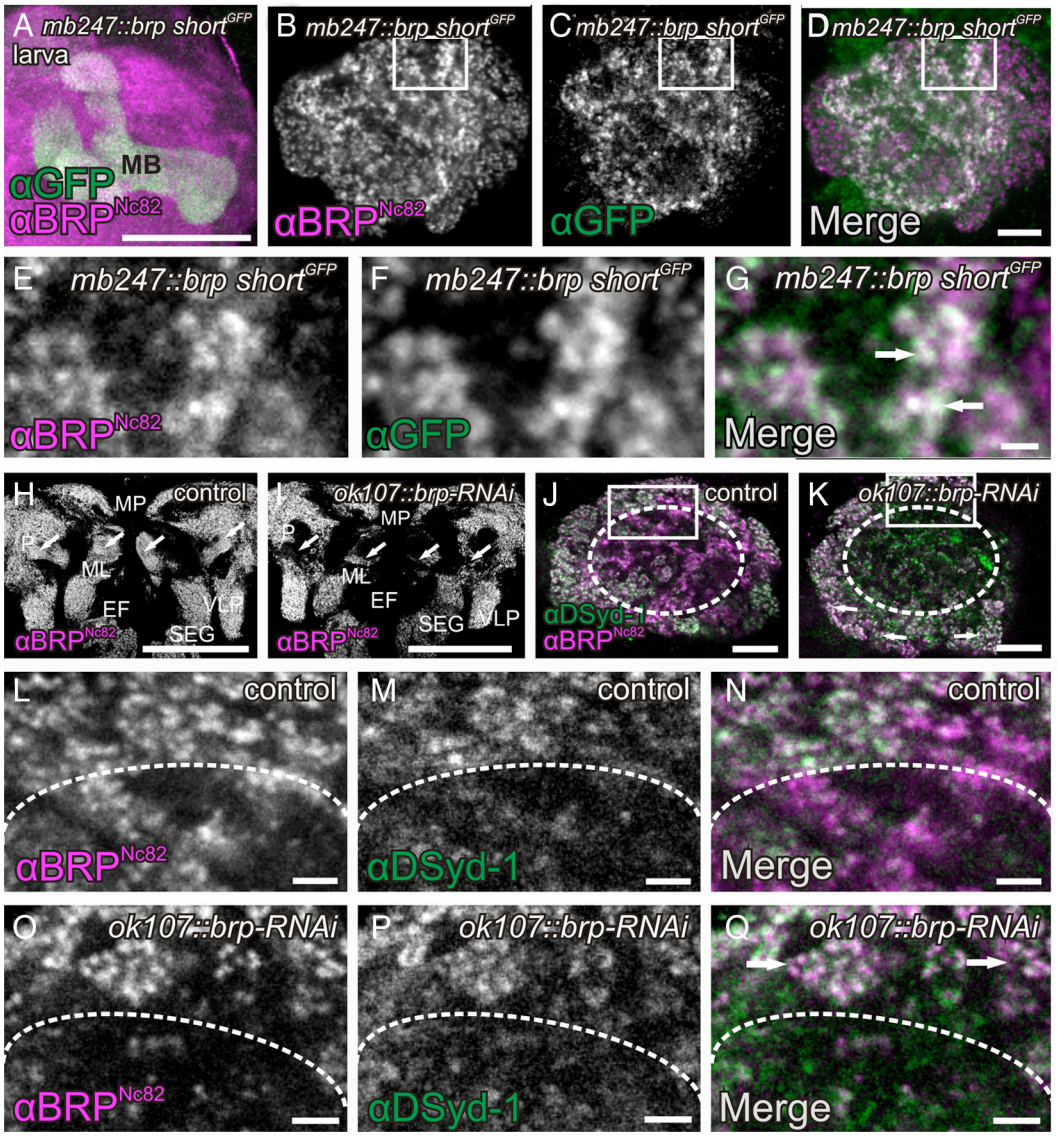


**Figure 1.** Evidence for KC-derived presynapses within the MB calyx of *Drosophila* larvae. ***A–G***, Expression of the BRP fragment BRP-short$^{GFP}$ under control of the KC enhancer *mb247* reveals a strong signal in the MB lobes (***A***, maximum-intensity projection) and the calyx of the larva (***C***, ***F***). Costaining with BRP$^{Nc82}$, an antibody against the presynaptic AZ protein BRP (***A***, mushroom body; ***B***, ***E***, calyx), showed a clear overlap with the KC-derived BRP-short$^{GFP}$ signal in the calyx (***D***, ***G***, arrows), suggesting the existence of a KC-derived population of AZs. ***E–G***, Cutout of the calyx shown in ***B–D*** in a higher magnification. ***H–Q***, *UAS-brp-RNAi* expressed in KCs (*ok107*-GAL4) provoked a strong reduction of the BRP$^{Nc82}$ label in both MB lobes and calyx. ***H***, ***I***, Larval brain overview. In the control brain stained with αBRP$^{Nc82}$, major neuropils are clearly visible, including the mushroom body lobes (***H***, arrows). *UAS-brp-RNAi* expressed in KCs resulted in a strong reduction of the MB lobe label (***I***, arrows). ***J***, ***K***, Colabeling of αBRP$^{Nc82}$ together with an antibody against the AZ protein DSyd1 showed a specific effect of the expression of *UAS-brp-RNAi* in KCs on the BRP label in the calyx. Reduction of BRP was confined to the regions in the center of the calyx (***K***, dotted circle) but did not occur in areas where KCs are postsynaptic to PN presynaptic terminals, the macroglomeruli (***K***, arrows). ***L–Q***, Higher magnification views of calycal regions shown in ***J*** and ***K***, marked in ***J*** and ***K*** by white rectangles. While the BRP label is clearly reduced (***O***, ***Q***, below the dotted line) compared with the control (***L***, ***N***), the DSyd1 label remains unaffected (***M***, ***P***). The macroglomeruli also show no reduction in BRP label (***Q***, arrows). ML, Medial lobe; P, peduncle; MP, medial protocerebrum; EF, esophageal foramen; VLP, ventrolateral protocerebrum; SEG, subesophageal ganglion; MB, mushroom body. All images show single optical slices, except when stated differently. Slice thickness, 200 nm. Scale bars: ***A***, ***H***, ***I***, 50 μm; ***B–D***, ***J***, ***K***, 10 μm; ***E–G***, 5 μm; ***L–Q***, 2 μm.

1*A*) and flies (Fig. 2*A*) were clearly labeled. Consistent with the expression previously reported for the mb247 enhancer (Riemensperger et al., 2005; Krashes et al., 2007), γ, α/β, and α′/β′ neurons were labeled by this construct (data not shown). In *mb247::brp-short$^{GFP}$* animals, BRP-short$^{GFP}$ was arranged in distinct puncta, which were also labeled by BRP$^{Nc82}$ (Figs. 1*A*, 2*A*). This indicates that endogenous BRP is present at these AZs. In our study, we used *mb247::brp-short$^{GFP}$* for the identification of KC-derived AZs.

To a minor degree, *mb247::brp-short$^{GFP}$* drives expression in MB-extrinsic neurons. It is therefore possible that the synapses we are looking at belong to MB-extrinsic neurons. To exclude this possibility, we confirmed our results by checking *UAS-brp-short$^{mCherry}$* expression in several different MB GAL4-lines [*ok107*-GAL4, *h24*-GAL4, *c739*-GAL4, *c305a*-GAL4 (see Fig. 7*A–O*) and *mb247*-GAL4, *201y*-GAL4, *d52 h*-GAL4, *1471y*-GAL4 (data not shown)].

Surprisingly, a clear BRP-short$^{GFP}$ label was also present in the calyces of both larvae (Fig. 2*C*,*D*,*F*,*G*) and adult flies (Fig. 1*C*,*D*,*F*,*G*). This label consisted of discrete puncta, typical for individual AZs, which were also labeled by BRP$^{Nc82}$ (Figs. 1*G*, arrows; 2*D*,*G*, arrows). We observed these puncta within calyces of both female and male animals, in second- and third-instar larvae, and throughout the life span from newly eclosed to 14-d-

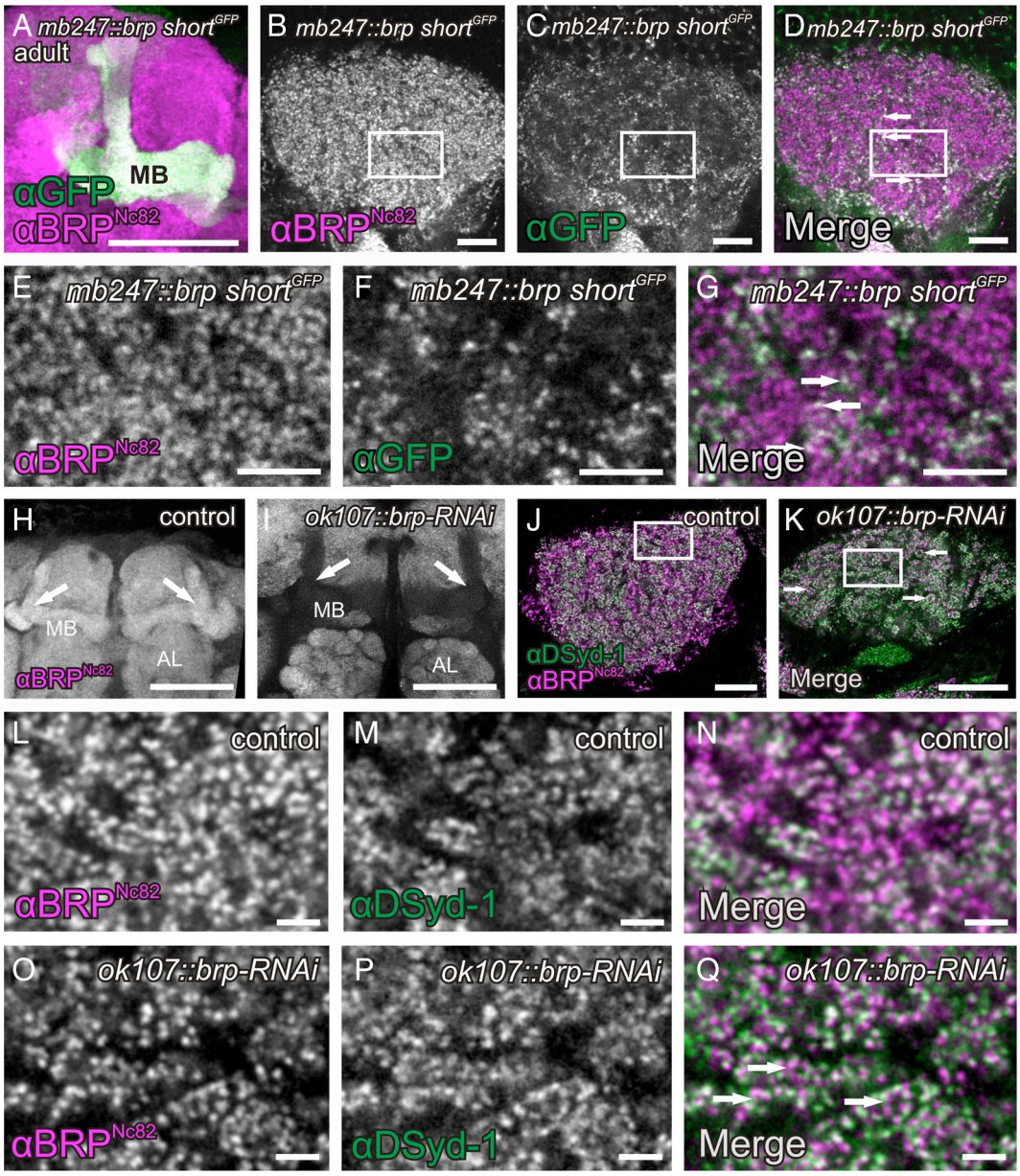


**Figure 2.** Evidence for KC-derived presynapses within the MB calyx of *Drosophila* adults. ***A–G***, Expression of the BRP fragment BRP-short$^{GFP}$ under control of the KC enhancer *mb247* reveals a strong signal in MB lobes (***A***, maximum-intensity projection) and calyces of adult flies (***C***; higher magnification in ***F***). The costaining of the presynaptic AZ protein BRP (***B***; high magnification in ***E***) showed a clear overlap with the KC-derived BRP-short$^{GFP}$ signal (***D***; higher magnification in ***G***; arrows), suggesting the existence of a KC-derived population of AZs. ***H–Q***, *UAS-brp-RNAi* expressed in KCs (*ok107*-GAL4) provoked a strong reduction of the BRP$^{Nc82}$ label in both MB lobes (***H***, ***I***, arrows) and calyces (***J***, ***K***, arrows; higher magnification in ***L*** and ***O***). In the calyx, the reduction of BRP was confined to the regions outside of microglomeruli (***K***, arrows). For a higher magnification, compare ***L–Q***. Since αDSyd-1 localization at AZs was shown to be independent of BRP (Owald et al., 2010), we used this marker as an independent reference. DSyd-1 labeling remained unaffected from the *brp-RNAi* expression in KCs (***M***, ***P***). MB, Mushroom body; AL, antennal lobe. All images show single optical slices, except when stated differently. Slice thickness, 200 nm. Scale bars: ***A***, ***H***, ***I***, 50 μm; ***B–D***, ***K***, 10 μm; ***E–G***, 5 μm; ***L–Q***, 2 μm.

old adult flies (data not shown). Furthermore, we confirmed these observations by expressing BRP-short$^{GFP}$ and BRP-short$^{mCherry}$ with several independent GAL4-KC drivers (see Fig. 7*A–O*) (data not shown). This result is surprising as KC dendrites were so far considered to be exclusively postsynaptic (Yasuyama et al., 2002).

It might be argued that the ectopic expression of BRP-short$^{GFP}$ could artificially cluster endogenous BRP and thereby mimic natural presynaptic AZs. To add further proof to the hypothesis that KCs express presynapses in the calyx and that BRP-short$^{GFP}$ highlights only already existing AZs, we attempted to reduce BRP levels by expressing *brp*-directed RNA interference constructs (*UAS-brp-RNAi*) specifically within KCs. We have demonstrated that this construct could be used to strongly reduce BRP levels in the eyes of adult flies as well as in larval motoneurons in a previous experiment (Wagh et al., 2006). For this RNAi experiment, we used an antibody against the presynaptic AZ protein DSyd-1 as an AZ marker independent of BRP. We characterized DSyd-1 in a previous study (Owald et al., 2010). DSyd-1 incorporation precedes BRP incorporation during AZ formation and also persists in *brp* mutants. *UAS-brp-RNAi* was expressed under control of the broad KC driver line *ok107*-GAL4. Expression of the RNAi clearly reduced BRP$^{Nc82}$ label in MB lobes and calyces of both adults (Fig. 1*H–Q*) and larvae (Fig. 2*H–Q*). We confirmed this observation by quantification (Fig. 3, Table 1). For this quantification, we used the 3D software Imaris to calcu-

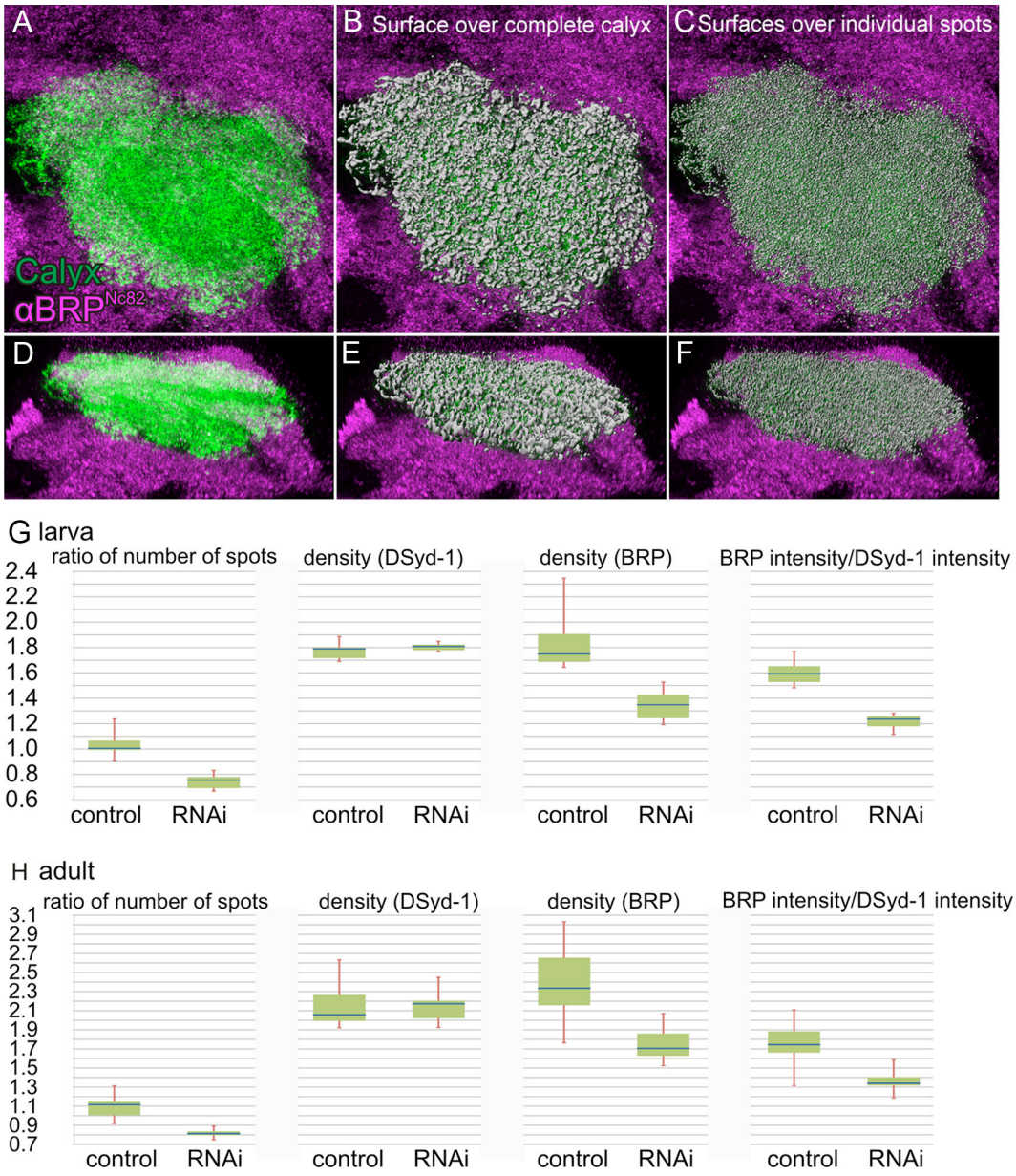


**Figure 3.** Segmentation and quantification of BRP$^{Nc82}$ signal within the calyx, with and without expression of *UAS-brp-RNAi* in KCs. ***A–F***, Visualization of the segmentation and 3D reconstruction of the calyx used for quantification. ***A–C***, Top view. ***D–F***, Side view. ***A***, ***D***, Segmented calyx (green) within the BRP$^{Nc82}$ staining labeling all neuropils (magenta). ***B***, ***E***, Computed 3D surface covering the complete BRP$^{Nc82}$-positive signal in the calyx (gray), superimposed on the staining shown in ***A*** and ***D***. ***C***, ***F***, Three-dimensional surfaces of individual BRP$^{Nc82}$-positive spots (gray), superimposed on the staining shown in ***A*** and ***D***. The surfaces used for the detection of the number of AZs. For additional detailed images of such a 3D reconstruction of the BRP$^{Nc82}$ signal, also see Kremer et al. (2010). ***G***, ***H***, Results of the quantification. Blue bar, Median; green box, interquartile range; red whiskers, min/max values. The Mann–Whitney *U* test was used to determine two-sided exact *p* values. ***G***, Larval calyces, $n = 6$ animals for both genotypes. Ratio of number of spots is the ratio of BRP$^{Nc82}$-positive spots versus DSyd-1-positive spots, $p = 0.002$. Density is the number of spots per calyx area. DSyd-1 density, $p = 0.485$; BRP$^{Nc82}$ density, $p = 0.002$. BRP intensity/DSyd-1 intensity is the ratio of the BRP$^{Nc82}$ signal intensity versus the DSyd-1 signal intensity within a surface covering the complete calyx, $p = 0.002$. ***H***, Adult calyces, $n = 10$ animals for *brp-RNAi* and $n = 9$ for controls. Ratio of number of spots, $p < 0.001$. DSyd-1 density, $p = 0.968$; BRP$^{Nc82}$ density, $p = 0.001$. Ratio of signal intensity, $p = 0.002$.

**Table 1. Change in percentage of the indicated parameters between *brp-RNAi* and control animals**

| | Ratio of number of spots (BRP$^{Nc82}$/DSyd-1) | Spot density (BRP$^{Nc82}$) | Spot density (DSyd-1) | Ratio of intensity (BRP$^{Nc82}$/DSyd-1) |
|---|---|---|---|---|
| Adults | −27.2 | −26.9 | +5.6 | −23.1 |
| Larvae | −24.8 | −22.9 | +1.1 | −22.4 |

For additional details, see Figure 3, *G* and *H*, and Results.

late 3D surfaces of calyces, based on BRP$^{Nc82}$ and DSyd-1 signals (Fig. 3*A–F*). In this manner, we determined the number of spots positive for BRP$^{Nc82}$ as well as for the independent marker DSyd-1. Here, individual spots correspond to individual presynaptic AZs (Kremer et al., 2010). In addition, we calculated the average intensities of the staining of the two markers within the calyx as well as the overall surface areas of BRP$^{Nc82}$- and DSyd-1-positive signals in the calyx. From these data, we determined four parameters, summarized in Table 1 and Figure 3, *G* and *H*. The results show that the DSyd-1 signal remained unaffected upon expression of the *RNAi*, while BRP levels were reduced, in the number of spots as well as in the staining intensity. The finding that the DSyd-1 signal was not reduced is consistent with the observation that the localization of DSyd-1 at AZs is independent of BRP. In view of these data, we conclude that KCs form presynaptic AZs within the calyx. In the following, we name these KC-derived AZs in the calyx, short KCACs.

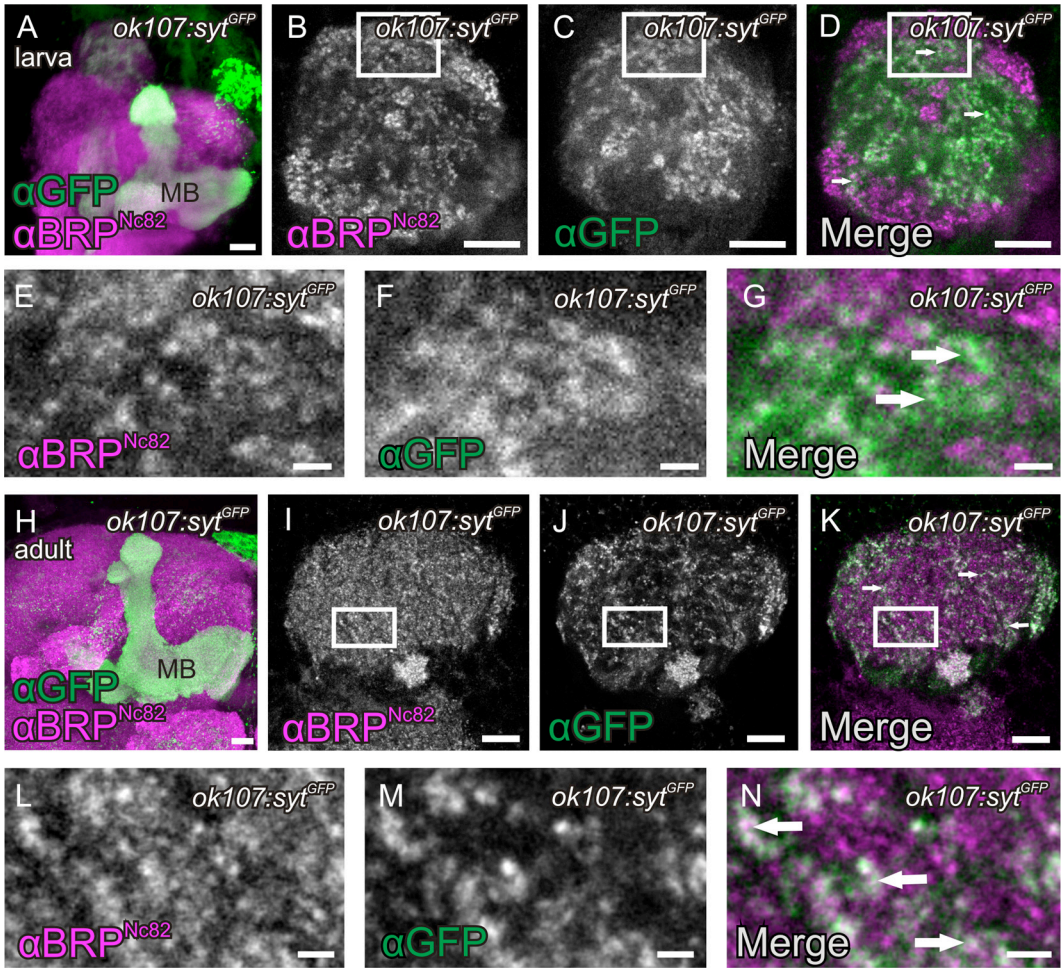


**Figure 4.** Presence of SVs in KCACs. ***A–H***, Expression of a GFP-fusion of the SV marker Synaptotagmin (syt $^{GFP}$) with the KC driver *ok107*-GAL4 in MB lobes and calyces of larvae (***A***, MB lobes, maximum-intensity projection; ***B–G***, calyx) and adult flies (***H***, MB lobes, maximum-intensity projection; ***I–N***, calyx). Costaining with BRP $^{Nc82}$ revealed that syt $^{GFP}$ expressed in KCs locates between microglomerular and macroglomerular complexes (***B–D***, arrows; ***I–K***, arrows). For a higher magnification in larvae, compare ***E–G*** (arrows), and for adults, ***L–N*** (arrows). All images show single optical slices, except when stated differently. Slice thickness, 200 nm. MB, Mushroom body. Scale bars: ***A***, ***B–D***, ***H–K***, 10 $\mu$m; ***E–G***, ***L–N***, 1 $\mu$m.

PNs contact KCs in structures called macroglomeruli (in larvae) (Ramaekers et al., 2005) or microglomeruli (in flies) (Schürmann, 1974; Yasuyama et al., 2002). Interestingly, only the BRP $^{Nc82}$ label outside microglomeruli or macroglomeruli was strongly reduced (Figs. 1*K*, dotted circle; *O*,*Q*, below dotted line; 2*K*,*O*,*Q*). The BRP $^{Nc82}$ immunoreactivity within microglomeruli or macroglomeruli, however, appeared unaffected (Figs. 1*K*,*O*,*Q*, arrows; 2*K*,*O*,*Q*, arrows). Notably, the quantification indicates a reduction of BRP levels in the calyx by >20% in both adult flies and larvae (Table 1). Therefore, we estimate that KC-derived AZs make up >20% of all AZs within the calyx.

### Activity-mediated vesicle cycling at KC-derived AZs in the calyx

So far, we assayed proteins specific and indicative for the AZ cytomatrix (BRP, DSyd-1) to demonstrate the existence of KC-derived presynaptic AZs. Next, we tested whether markers for SVs were associated with KCACs as well. To this end, we expressed a GFP-fusion to the presynaptic vesicle protein Synaptotagmin (*UAS-syt*$^{GFP}$) (Zhang et al., 2002) under control of the KC driver *ok107*-GAL4. Strong signals in both MB lobes (Fig. 4*A*,*H*) and calyx (Fig. 4*C*,*D*,*F*,*G*,*J*,*K*,*M*,*N*) were observed. While the Synaptotagmin label was less spatially confined than the AZ cytomatrix label (BRP $^{Nc82}$) (Fig. 4*B–G*,*I–N*), syt $^{GFP}$ expressed from KCs also clearly located in between macroglomeruli (data not shown) and microglomeruli (Fig. 4*K*,*N*, arrows).

To test whether the KCACs are capable of SV release, we made use of functional optical imaging of an *in vivo* preparation (Fig. 5*A*) to visualize Synapto-pHluorin (Ng et al., 2002) expressed in KCs by *ok107*-GAL4 (Fig. 5*B*). Synapto-pHluorin consists of the SV protein Synaptobrevin, fused at its lumenal C terminus to ecliptic pHluorin, a pH-sensitive mutant of GFP, which is non-fluorescent at a pH <6 upon excitation at 470 nm. After vesicle fusion with the AZ membrane, pHluorin is exposed to the higher pH value of the extracellular space, which enhances the fluorescence emission and yields a visible signal (Miesenböck et al., 1998). The calyx is spatially separated from the MB lobes region; therefore, Synapto-pHluorin expression can be selectively monitored in this neuropil. Fluorescence of Synapto-pHluorin could be observed in the calyx, again indicating the presence of KC-derived SVs within the calyx (Fig. 5*B*). Stimulation with KCl causes a general depolarization of the brain, which leads to SV release. While imaging this release, the measurable signal is superimposed on a general decrease of visible label due to photobleaching. Nonetheless, upon depolarization, a strong increase in fluorescence in the calyx was observed (Fig. 5*C*,*D*). Thus, the presynaptic AZs derived from KCs in the calyx can release SVs.

### KCACs cluster distant from PN::KC synapses

Endogenously present BRP$^{Nc82}$-positive spots in the MB lobes were, to a large extent, also targeted by BRP-short expressed in KCs. In the calyx, however, only a fraction of the BRP$^{Nc82}$-positive spots could be labeled by KC-expressed BRP-short (Figs. 1*B–D*, 2*B–D*). This is expected, since a dominant input to the calyx is delivered by PNs (Yasuyama et al., 2002), and according to our quantification, only ~20% of the calycal AZs are expected to correspond to KC-derived AZs (KCACs) (Table 1, Fig. 3). KCACs located in between macroglomeruli and microglomeruli. This suggests that KCACs remain segregated from the cholinergic PN::KC synapses. To explicitly examine this, we introduced additional molecular markers. First, we sought to label the postsynaptic densities (PSDs) of KCs at their cholinergic input synapses. To this end, we fused the KC-specific enhancer *mb247* to the gene encoding for the Dα7 acetylcholine (ACh) receptor subunit (Grauso et al., 2002; Fayyazuddin et al., 2006) (*mb247::dα7$^{GFP}$*), flanked by the *gfp* gene. We have already previously used Dα7$^{GFP}$ to label PSDs of cholinergic synapses (Leiss et al., 2009; Raghu et al., 2009; Kremer et al., 2010). The GFP signal of *mb247::dα7$^{GFP}$* was absent from the MB lobes of larvae and adults (data not shown), indicating that, as expected, ACh receptors of KCs are restricted to the calyx region. Within the MB calyx, *mb247::dα7$^{GFP}$* produced a strong staining in macroglomeruli (in larvae) (data not shown) and microglomeruli (in adults) (Fig. 6*A*). The GFP label was arranged in little patches corresponding to postsynaptic sites, which were juxtaposed to individual PN AZs (Kremer et al., 2010). To visualize PN-derived AZs, we expressed *UAS-brp-short$^{mCherry}$* under the control of a broad PN driver (*gh146*-GAL4) (Fig. 6*B*,*F*) together with *mb247::dα7$^{GFP}$* (Fig. 6*A*). As expected, we observed presynaptic AZs of PNs juxtaposed to the cholinergic PSDs of the KCs in the adult calyx (Fig. 6*C*,*D*, arrows). In contrast, when we expressed BRP-short in KCs (mb247::brp-short$^{GFP}$) (Fig. 6*E*) together with *UAS-brp-short$^{mCherry}$* under control of the PN driver (*gh146*-GAL4) (Fig. 6*F*), the KC-derived BRP-short signals grouped away from the PN AZ populations (Fig. 6*G*,*H*, arrows).

In summary, covisualization of KCACs together with presynaptic AZs of PNs in larvae (data not shown) and adult flies underlined that the PN-derived AZs are primarily restricted to the microglomerular domains, while the KCACs reside within the intermicroglomerular regions.

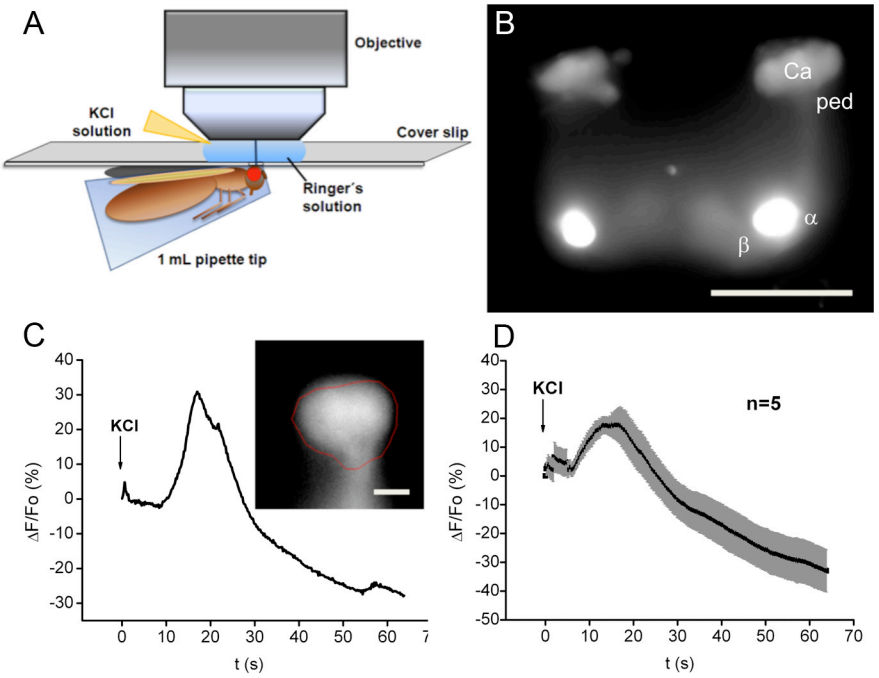


**Figure 5.** Evidence that KCACs are part of active synapses. Optical imaging of SV release at KCs analyzed using Synapto-pHluorin. ***A***, Experimental setup during functional imaging. ***B***, Expression of Synapto-pHluorin in KCs. Note that the calyx region can easily be distinguished from the lobe regions in the *in vivo* preparation. ***C***, Relative change in fluorescence emission after stimulation with KCl in the calycal region, indicated by the red line shown in the inserted image of the calyx. ***D***, Average of change in fluorescence in five flies. The trace indicates mean values; the gray shadows represent SEMs. The increase in fluorescence emission after stimulation with 100 mM KCl solution (superimposed on the decrease in emission caused by photobleaching) demonstrates that the KC dendrites in the calyx are capable of releasing SVs. Scale bars: ***B***, 100 μm; ***C***, 10 μm.

### Segregation of presynaptic and postsynaptic domains within KC dendrites

KCACs appeared clearly segregated from the cholinergic PN::KC synapses. Our analysis already suggested that both presynaptic and postsynaptic elements are formed by KC dendrites but are spatially segregated. For an analysis on the level of single neurons, we produced single KC clones using mosaic analysis with a repressible cell marker (MARCM) (Lee et al., 1999; Luo, 2007). While expression of mCD8::GFP allowed for visualizing the cell morphology, coexpression of BRP-short$^{mCherry}$ served as a label for presynapses and coexpression of Dα7$^{mCherry}$ served as a label for postsynapses. As expected (Yasuyama et al., 2002), Dα7$^{mCherry}$ signal mainly clustered at the terminal claw-like regions of KC dendrites (Fig. 6*I*,*J*, arrows). Also, BRP-short$^{mCherry}$ signal was observed in KC dendrites. However, we rarely found BRP-short$^{mCherry}$ clusters directly at claws but rather at more proximal parts of the dendrites (Fig. 6*K*,*L*).

It might be argued that axons running back from the lobe region into the calyx might be responsible for the KC-derived AZ label observed within the calyx. Yet in our single-cell analysis such axons were never observed. Instead, the physical segregation of presynaptic and postsynaptic specializations along KC dendrites could be further corroborated when we coexpressed BRP-short$^{mCherry}$ and Dα7$^{GFP}$ using the broad KC driver *ok107*-GAL4 (Fig. 7*A–C*). We found that the BRP-short$^{mCherry}$ signal was restricted to areas between the microglomeruli, visualized by Dα7$^{GFP}$ (Fig. 7*C*, arrows). Thus, markers for presynaptic and postsynaptic specializations arrange separately when coexpressed within KCs dendrites. It thus appears likely that KC dendrites are of mixed identity and form presynaptic and postsynaptic stretches in consecutive, but hardly overlapping segments. For a schematic interpretation of these results, see Figure 6*M*.

### The KC subtypes γ and α/β, but not α′/β′, form KCACs

Depending on their axonal elaboration within the MB lobes, KCs are subgrouped into several classes (α/β, α′/β′, γ) (Crittenden et al., 1998). To examine the contribution of specific KC subtypes to the calycal microcircuitry, KC subtype-specific GAL4 lines for γ neurons [*h24*-GAL4 (Zars et al., 2000; Akalal et al., 2006)], α/β

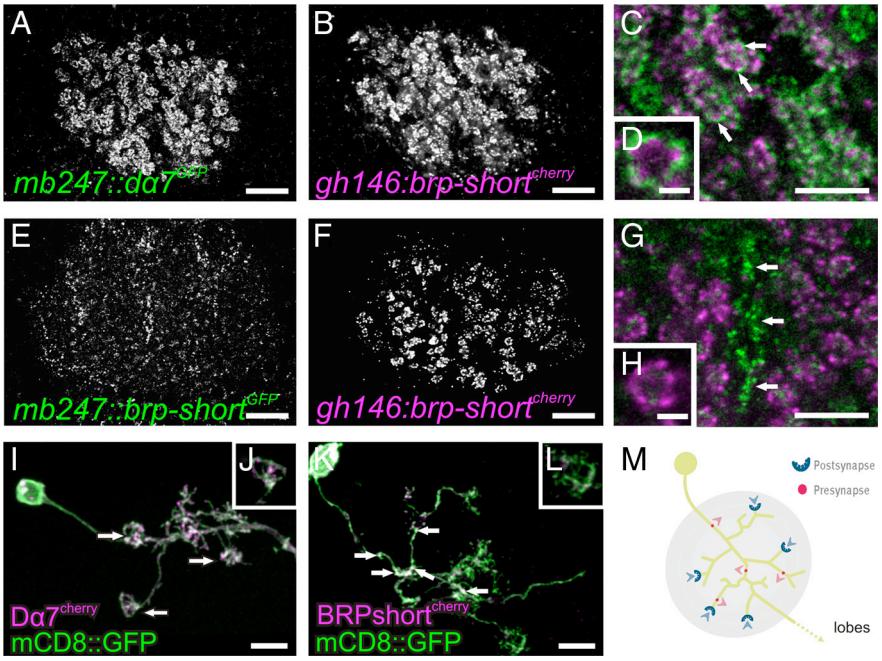


**Figure 6.** Presynaptic and postsynaptic domains segregate within KC calyx dendrites. ***A–H***, Analysis of synaptic elements in the calyx of adult flies. KCACs cluster distant from PN::KC synapses. ***A–D***, Visualization of cholinergic PSDs of KCs (*mb247-dα7*$^{GFP}$) (***A***) together with PN-derived AZs ( *gh146*-GAL4 driving *UAS-brp-short*$^{mCherry}$) (***B***). A higher magnification of both merged labels shows that PN AZs locate at the inner edge of the microglomeruli, juxtaposed to KC PSDs (***C***, arrows; single microglomerulus in ***D***). ***E–H***, In contrast, KC-expressed BRP-short (*mb247::brp-short*$^{GFP}$) (***E***) clustered distant from PN AZ populations (marked by *gh146::brp-short*$^{mCherry}$) (***F***), as the merge of both labels at a higher magnification demonstrates (***G***, arrows; ***H***, single microglomerulus). ***I–L***, Visualization of single KCs in the calyx using the MARCM technique. ***I***, ***J***, Single KC (maximum-intensity projection) expressing Dα7$^{mCherry}$ together with mCD8::GFP. A preferential localization of ACh receptors at the KC claw-like endings is visible (***I***, arrows; ***J***, single claw). ***K***, ***L***, Single KC (maximum-intensity projection) expressing BRP-short$^{mCherry}$ together with mCD8::GFP. BRP signal is distributed along the KC dendrites (***K***, arrows), mostly separated from the KC claw-like endings (***K***, arrows; ***L***, single claw). ***M***, Schematic drawing of synaptic input and output regions on a single KC within the calyx. All images show single optical slices, except when stated differently. Slice thickness, 200 nm. Scale bars: ***A***, ***B***, ***E***, ***F***, 10 μm; ***C***, ***G***, ***I***, ***K***, 5 μm; ***D***, ***H***, 1 μm.

neurons [*c739*-GAL4 (O'Dell et al., 1995; Yang et al., 1995; Aso et al., 2009)], and α′/β′ neurons [*c305a*-GAL4 (Krashes et al., 2007)] were used for coexpression of *UAS-dα7*$^{GFP}$ and *UAS-brp-short*$^{mCherry}$ (Fig. 7*D–L*).

While expression in α′/β′-type KCs produced a clear Dα7$^{GFP}$ signal within the calyx, no BRP-short signals could be observed in the calyx (Fig. 7*D–F*) but in only α′/β′ lobes (data not shown). The Dα7$^{GFP}$ expression was strongest in four lateral units, whereas only a weak expression was observed in the center of the calyx (data not shown).

In γ KCs, Dα7 but also BRP signals were observed in the calyx, with AZ and PSD signals being mainly segregated to distinct domains (Fig. 7*G–I*). The Dα7 receptor construct labeled microglomeruli all over the calyx (Fig. 7*G*) but showed its strongest expression in the center as well as weaker levels in lateral regions of the calyx (data not shown). BRP-short preferentially localized around the Dα7-positive regions (Fig. 7*I*, arrows).

Also when expressed in α/β KCs, strong Dα7 and BRP-short signals were observed (Fig. 7*J–L*). As in the case of γ KCs, AZs and PSDs derived from α/β KCs appeared segregated to mutually exclusive domains. The Dα7 signal reproducibly labeled four units, residing laterally in the calyx (Fig. 7*M–O*). Closer analysis of image stacks identified four fascicles running along the cortex of the calyx (Fig. 7*O*, asterisks). These fascicles contained BRP when entering into the calyx, but contained Dα7 toward the center of the neuropil, with a border visible between both regions. It thus appears likely that individual α/β KC dendrites consecutively first form a proximal presynaptic specialization (BRP-positive AZs) followed by a more distal postsynaptic zone (Dα7-positive PSDs).

Thus, only γ and α/β, but not α′/β′ KCs seem to form KCACs. In an attempt to put these KC subtype-specific staining patterns in the context of the complete calyx, horizontal image stacks of adult calyces were examined. Here, BRP-short$^{mCherry}$ was expressed under control of the PN driver *gh146*-GAL4 in addition to *mb247::dα7*$^{GFP}$ (to visualize the PN::KC synapses) and a BRP$^{Nc82}$ staining. We observed that the calyx appears subdivided into five subunits (Fig. 7*P*). Four of them were arranged in a pattern resembling a semicircle posterior to the inner antennocerebral tract (iACT), with the two lateral units terminating at the iACT. A fifth unit resided in between the semicycle. All five units harbored PN::KC synapses in their centers, which were surrounded by BRP$^{Nc82}$-stained presynapses. We also analyzed the structure of the calyx with the previously mentioned KC-subset drivers (data not shown). The four laterally positioned subunits are mainly composed of α/β and α′/β′ postsynapses, with α/β KCACs clustered at their outer edges. These four units, arranged in a closed semicircle, are responsible for the quadripartite appearance of the calyx, which has been described previously (Ito et al., 1997). The center of the fifth unit predominantly harbors the γ neurons; their presynapses surround this unit and advance as far as in between the other four units. We summarized these findings in a tentative model (Fig. 7*Q*).

## Discussion

In this study, we used several approaches to provide evidence that the KC dendrites within the calyx of larval and adult *Drosophila* are not exclusively postsynaptic. They also form presynaptic AZs, which we named KCACs. Our findings are supported by data from two previous studies (Rolls et al., 2007; Pauls et al., 2010), which reported the presence of a presynaptic vesicle protein, Synaptobrevin, in KCs within the calyx. Here, we show that KCACs are able to release SVs by a functional imaging approach. Furthermore, we examined which different KC subtypes form KCACs and provide a detailed description of the KCAC location within the calyx. The presence of these previously undescribed KC-intrinsic presynaptic elements adds a new layer of complexity to the MB microcircuitry.

### KCACs and calycal microcircuitry

Within KC dendrites, AZs and PSDs are clearly organized into discrete subdomains (Fig. 6*I–M*). Here, the question emerges whether a given KC dendrite is either exclusively presynaptic or postsynaptic, or whether both presynaptic and postsynaptic domains can be present within the same KC dendrite in a consecutive fashion. MARCM identified single KCs, which showed BRP puncta spatially segregated from claw-like regions that are

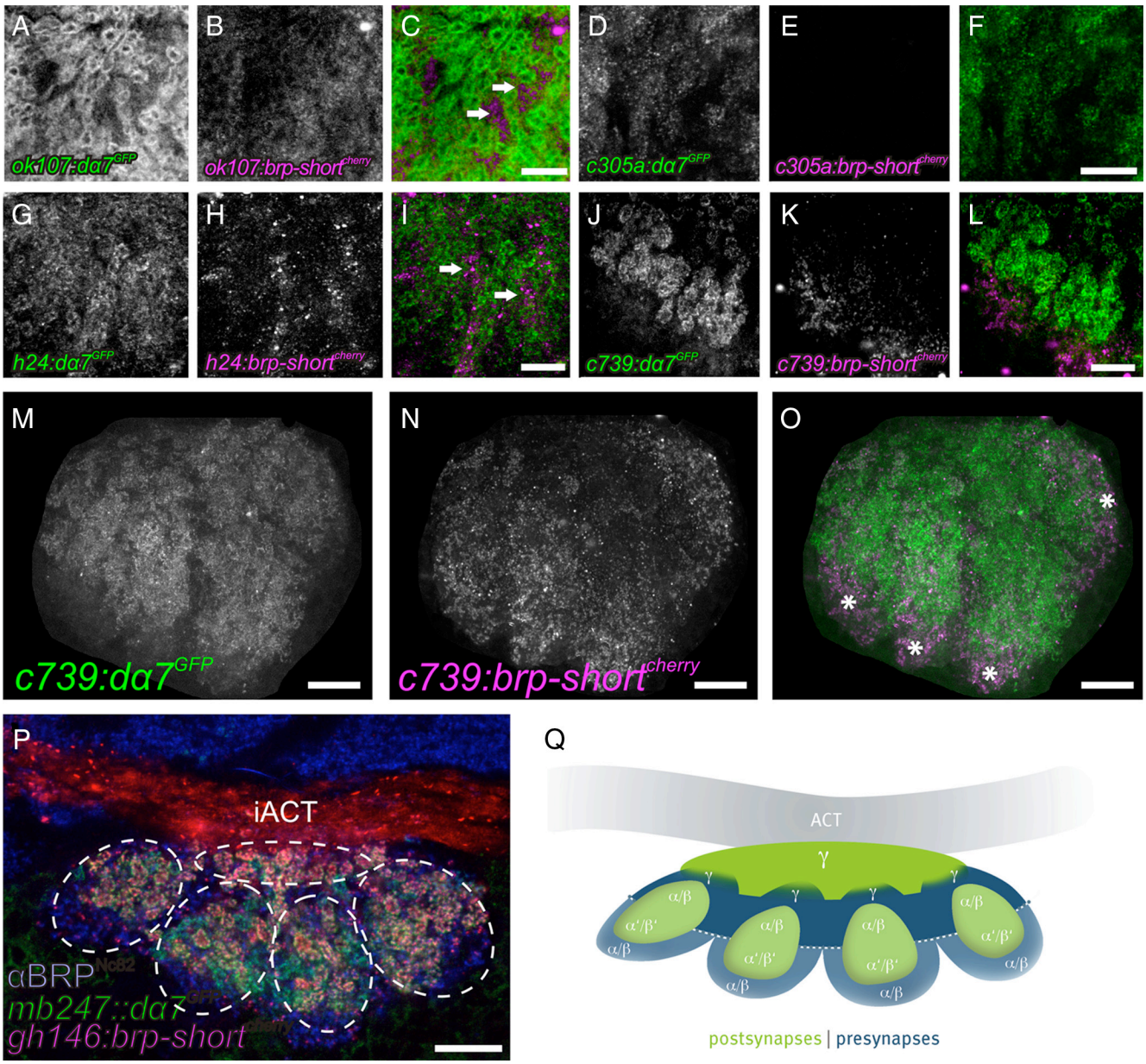


**Figure 7.** Coexpression of presynaptic (BRP-short) and postsynaptic (D$\alpha$7) markers identifies distinct regions within KC dendrites of adult calyces. ***A–L*** show cutouts of maximum-intensity projections of calyces. ***A–C***, *ok107*-GAL4 driving expression of both *UAS-dα7*$^{GFP}$ (***A***) and *UAS-brp-short*$^{mCherry}$ (***B***) within KC dendrites. The merged image shows that presynaptic and postsynaptic regions appeared largely segregated (***C***, arrows). ***D–F***, $\alpha'\beta'$ KCs (*c305a*-GAL4) expressing both *UAS-dα7*$^{GFP}$ (***D***) and *UAS-brp-short*$^{mCherry}$ (***E***). While a strong D$\alpha$7 signal was present (***D***), no BRP-short signal could be detected within the calyx (***E***, ***F***). ***G–I***, $\gamma$KC (*h24*-GAL4) expressing both *UAS-dα7*$^{GFP}$ (***G***) and *UAS-brp-short*$^{mCherry}$ (***H***). Both signals were present and clearly separated from each other (***I***). D$\alpha$7 was distributed in microglomerular structures, while the BRP-short signal localized in between (***I***, arrows). ***J–O***, $\alpha\beta$ KCs (*c739*-GAL4) expressing both *UAS-dα7*$^{GFP}$ (***J***, ***M***) and *UAS-brp-short*$^{mCherry}$ (***K***, ***N***). ***M–O*** show the whole calyx (maximum-intensity projection). The dendrites showed a similar segregation of presynaptic and postsynaptic regions (***L***, ***O***). Both signals were arranged into four distinct patches clearly separated from each other (***O***, asterisks). Here, BRP-short was located at the more peripheral part of the calyx (***K***, ***N***), whereas D$\alpha$7 showed a stronger signal toward the center of the neuropil (***J***, ***M***). ***P***, Horizontal section through the calyx of an adult fly. Visualization of calycal microglomeruli by *UAS-brp-short*$^{mCherry}$ expressed in PNs ( *gh146*-GAL4) and D$\alpha$7 expressed in KCs (*mb247::dα7*$^{GFP}$). A $\alpha$BRP$^{Nc82}$ label of all presynapses is shown in blue. The calyx is divided into five subunits, each harboring microglomeruli in the center, that are surrounded by other synapses. Four subunits protrude to the posterior part and one further subunit is located between them and the iACT. ***Q***, Schematic drawing of the distribution of presynaptic and postsynaptic regions of the different KC subtypes within the MB calyx. Postsynapses are shown in green, and presynapses are shown in blue. All images show single optical slices, except when stated differently. Slice thickness, 200 nm. iACT, Inner antennocerebral tract. Scale bars: ***C***, ***F***, ***I***, ***L***, 5 $\mu$m; ***M–P***, 10 $\mu$m. BRP-short can form agglomerations within the somata of the cells it is expressed in. As the KC somata are located very close to the calyx neuropil, we manually removed the somata from images ***M–O*** for clarity.

thought to harbor the postsynaptic specializations of cholinergic PN::KC synapses. In parallel experiments, we showed that these claws in fact clustered the acetylcholine receptor D$\alpha$7, as was expected from our previous work (Kremer et al., 2010). Thus, it appears likely that presynaptic and postsynaptic domains can be present within the same KC dendrite.

Based on the BRP-RNAi analysis, we estimate that ~20–30% of all presynapses in the calyx are KCACs, in both adults and larvae. These synapses are apparently part of the general calyx microcircuitry. They might synapse onto PNs, KCs themselves, the anterior paired lateral (APL) neuron, modulatory neurons, or so-far-undescribed cells. From our analysis, it appears unlikely

that PN boutons are direct postsynaptic partners of the KCACs, as the KCACs appear to be clearly physically segregated from the PN boutons. KCACs might, however, project onto PN axons.

It appears well possible that KCACs project onto the GABAergic APL neuron (Liu and Davis, 2009), which arborizes in the whole calyx. Within the insect antennal lobe, reciprocal dendrodendritic connections between the PNs and the partially GABAergic local interneurons (LNs) have been described (Sun et al., 1997; Didier et al., 2001; Ng et al., 2002). The PN neurites and the LNs are both transmissive and receptive in the antennal lobe, suggesting a computation between them. KCACs might be involved into similar computations in the calyx. This would be in accordance with EM studies in crickets that suggest presynapses in KCs that connect to GABAergic fibers in the MB calyx (Schürmann et al., 2008).

KCACs might also mediate KC::KC communication. In fact, dendritic segments of KCs that harbor presynapses appear to run in a parallel fashion (data not shown). This arrangement could promote the communication between dendritic segments of KCs via dendrodendritic synapses. Such KC::KC synapses could therefore modulate signals originating from the distal segments of the arborizations, which carry odor-evoked signals. By these means, an effective computation between KCs could be accomplished before they transmit their input signals downstream.

Unfortunately, at the moment no general PSD markers are available in *Drosophila*. Moreover, the neurotransmitter used by KCs remains unknown. With a general postsynaptic marker or knowledge about the KC transmitter, we could have generated tools to identify the postsynaptic partners of KCACs. Yet currently, despite efforts, we can only speculate about the postsynaptic partners of KCs in the calyx.

### Potential roles of KCACs in learning and memory processes

Memory traces are typically thought to be manifested as plastic changes in neuronal anatomy and physiology that occur in specific brain regions. Several lines of evidence indicate that MBs are causally involved in associative learning of olfactory stimuli (for review, see Heisenberg, 1998, 2003; Roman and Davis, 2001; Waddell and Quinn, 2001b; Dubnau et al., 2003; Gerber et al., 2004; Davis, 2005; Keene and Waddell, 2007). Flies with chemically ablated KCs or mutants lacking the MBs are deficient in olfactory learning (Heisenberg et al., 1985; de Belle and Heisenberg, 1994). Learning was investigated in flies mutant for the adenylyl cyclase rutabaga (*rut*) (Livingstone et al., 1984), which is suggested to act as a coincidence detector between conditioned stimulus (odor) and unconditioned stimulus (e.g., electric shock) (Tomchik and Davis, 2009). Reexpression of a *rut* cDNA in a $rut^-$ background within a subpopulation of KCs sufficed to restore odor learning (Zars et al., 2000; McGuire et al., 2003). For appetitive learning, reexpression of *rut* in either PNs or KCs is sufficient to restore the mutant defect, whereas aversive learning is rescued only by *rut* reexpression in KCs (Thum et al., 2007). Reversible disruption of transmitter release in *Drosophila* KCs, using a temperature-sensitive dynamin transgene, $UAS\text{-}shibire^{ts1}$ (Kitamoto, 2001), was shown to block memory retrieval in $\alpha/\beta$ neurons (McGuire et al., 2001; Isabel et al., 2004; Keene and Waddell, 2007; Krashes et al., 2007) and acquisition and stabilization of memory in $\alpha'/\beta'$ neurons (Keene and Waddell, 2007; Krashes et al., 2007). Together, these data imply that MBs play a major role in learning and memory. To form, stabilize, and retrieve memory (for review, see Keene and Waddell, 2007), KCs use their presynapses (for review, see Heisenberg, 2003; Davis, 2005; Keene and Waddell, 2007). The KC presynapses are so far believed to reside in the lobes.

The biogenic amines octopamine and dopamine are thought to mediate the unconditioned stimulus signal for learning olfactory associations, with octopamine representing appetitive stimuli and dopamine representing aversive stimuli (Schwaerzel et al., 2003; Schroll et al., 2006). Hammer and Menzel (1998) could show that, in honeybees, sugar can be replaced by octopamine application to the calyx to trigger the conditioned proboscis-extension reflex. In the fruit fly, the amines octopamine and dopamine are released onto MB lobes and calyx (Sinakevitch and Strausfeld, 2006; Busch et al., 2009; Mao and Davis, 2009). This holds also true for the larva [octopamine (A. Thum, personal communication); dopamine (Selcho et al., 2009)]. Therefore, the KCACs might be involved in appetitive learning as well as in aversive learning in fly and larva.

Notably, we found that the KC subpopulations $\gamma$ and $\alpha/\beta$, but not $\alpha'/\beta'$, form KCACs (Fig. 7). This dichotomy correlates with functional differences in learning and memory that have been assigned to these KC classes in previous studies. For example, $\alpha'/\beta'$ KCs were reported to be required during and after training to acquire and stabilize olfactory memory (Keene and Waddell, 2007; Krashes et al., 2007), whereas output from $\alpha/\beta$ neurons was postulated to be required to retrieve memory (McGuire et al., 2001; Keene and Waddell, 2007; Krashes et al., 2007). It has been proposed that, during acquisition, olfactory information received from PNs is first processed in parallel by the $\alpha/\beta$ and $\alpha'/\beta'$ KCs (Keene and Waddell, 2007; Krashes et al., 2007). Notably, activity in $\alpha'/\beta'$ KCs (which do not form KCACs) is supposed to trigger a recurrent loop between $\alpha'/\beta'$ KCs and dorsal paired medial neurons, which project to the MB lobes (Yu et al., 2005; Keene et al., 2006; Keene and Waddell, 2007; Krashes et al., 2007). This loop, in turn, might be necessary for memory consolidation in $\alpha/\beta$ neurons. Subsequently, memories could be stored in $\alpha/\beta$ neurons, whose activity is required during recall (Keene and Waddell, 2007; Krashes et al., 2007). As $\alpha'/\beta'$ neurons are devoid of KCACs, KCACs cannot be involved in the circuit described above. Instead, it is likely that additional, similar recurrent loops exist, which are mediated via KCACs. However, it remains unresolved how exactly KC::KC communication is organized anatomically and functionally. Our study now proposes a newly discovered synapse population as candidate sites for KC::KC communication.

In the mammalian olfactory system, major feedback pathways exist, which project onto neurons one level lower in hierarchy (Haberly, 1998). A recent publication (Hu et al., 2010) showed that likewise in *Drosophila* activation of KCs induced a depolarization in cell bodies of PNs and LNs within the antennal lobes. The authors thus suggested that MB lobes provide feedback to the ALs. Moreover, an additional memory trace appears to exist in the antennal lobe (Hammer and Menzel, 1995, 1998; Faber et al., 1999; Yu et al., 2004)/in the PNs (Thum et al., 2007). It may therefore well be the case that KCs project onto PNs or onto feedback neurons via their KCACs.

An urgent question of the field concerns the identification of the postsynaptic partner cells of KC presynapses, which harbor memory traces during olfactory conditioning. It is generally assumed that MB-extrinsic downstream neurons involved in behavioral execution of learned behavior serve as postsynaptic partners here. Our findings raise the possibility that microcircuits inside the MB could be places for further modulation and computation of olfactory processing and/or memory formation and modulation. As a consequence, not only the communication to

downstream neurons but also the representation of sensory information within the MB circuitry might be changed by experience. Future analysis using optophysiological tools at the KCACs, together with further anatomical work, should provide answers to these questions.

## References


Akalal DB, Wilson CF, Zong L, Tanaka NK, Ito K, Davis RL (2006) Roles for *Drosophila* mushroom body neurons in olfactory learning and memory. Learn Mem 13:659–668.

Aso Y, Grübel K, Busch S, Friedrich AB, Siwanowicz I, Tanimoto H (2009) The mushroom body of adult *Drosophila* characterized by GAL4 drivers. J Neurogenet 23:156–172.

Aso Y, Siwanowicz I, Bräcker L, Ito K, Kitamoto T, Tanimoto H (2010) Specific dopaminergic neurons for the formation of labile aversive memory. Curr Biol 20:1445–1451.

Busch S, Selcho M, Ito K, Tanimoto H (2009) A map of octopaminergic neurons in the *Drosophila* brain. J Comp Neurol 513:643–667.

Claridge-Chang A, Roorda RD, Vrontou E, Sjulson L, Li H, Hirsh J, Miesenböck G (2009) Writing memories with light-addressable reinforcement circuitry. Cell 139:405–415.

Connolly JB, Roberts IJ, Armstrong JD, Kaiser K, Forte M, Tully T, O'Kane CJ (1996) Associative learning disrupted by impaired Gs signaling in *Drosophila* mushroom bodies. Science 274:2104–2107.

Crittenden JR, Skoulakis EM, Han KA, Kalderon D, Davis RL (1998) Tripartite mushroom body architecture revealed by antigenic markers. Learn Mem 5:38–51.

Davis RL (2004) Olfactory learning. Neuron 44:31–48.

Davis RL (2005) Olfactory memory formation in *Drosophila*: from molecular to systems neuroscience. Annu Rev Neurosci 28:275–302.

de Belle JS, Heisenberg M (1994) Associative odor learning in *Drosophila* abolished by chemical ablation of mushroom bodies. Science 263:692–695.

Didier A, Carleton A, Bjaalie JG, Vincent JD, Ottersen OP, Storm-Mathisen J, Lledo PM (2001) A dendrodendritic reciprocal synapse provides a recurrent excitatory connection in the olfactory bulb. Proc Natl Acad Sci U S A 98:6441–6446.

Dubnau J, Chiang AS, Tully T (2003) Neural substrates of memory: from synapse to system. J Neurobiol 54:238–253.

Faber T, Joerges J, Menzel R (1999) Associative learning modifies neural representations of odors in the insect brain. Nat Neurosci 2:74–78.

Fayyazuddin A, Zaheer MA, Hiesinger PR, Bellen HJ (2006) The nicotinic acetylcholine receptor Dalpha7 is required for an escape behavior in *Drosophila*. PLoS Biol 4:e63.

Gerber B, Tanimoto H, Heisenberg M (2004) An engram found? Evaluating the evidence from fruit flies. Curr Opin Neurobiol 14:737–744.

Grauso M, Reenan RA, Culetto E, Sattelle DB (2002) Novel putative nicotinic acetylcholine receptor subunit genes, Dalpha5, Dalpha6 and Dalpha7, in *Drosophila melanogaster* identify a new and highly conserved target of adenosine deaminase acting on RNA-mediated A-to-I pre-mRNA editing. Genetics 160:1519–1533.

Haberly LB (1998) Olfactory cortex. In: The synaptic organization of the brain (Shepherd GM, ed), pp 317–345. New York: Oxford UP.

Hammer M, Menzel R (1995) Learning and memory in the honeybee. J Neurosci 15:1617–1630.

Hammer M, Menzel R (1998) Multiple sites of associative odor learning as revealed by local brain microinjections of octopamine in honeybees. Learn Mem 5:146–156.

Heisenberg M (1998) What do the mushroom bodies do for the insect brain? An introduction. Learn Mem 5:1–10.

Heisenberg M (2003) Mushroom body memoir: from maps to models. Nat Rev Neurosci 4:266–275.

Heisenberg M, Borst A, Wagner S, Byers D (1985) *Drosophila* mushroom body mutants are deficient in olfactory learning. J Neurogenet 2:1–30.

Hu A, Zhang W, Wang Z (2010) Functional feedback from mushroom bodies to antennal lobes in the *Drosophila* olfactory pathway. Proc Natl Acad Sci U S A 107:10262–10267.

Isabel G, Pascual A, Preat T (2004) Exclusive consolidated memory phases in *Drosophila*. Science 304:1024–1027.

Ito K, Awano W, Suzuki K, Hiromi Y, Yamamoto D (1997) The *Drosophila* mushroom body is a quadruple structure of clonal units each of which contains a virtually identical set of neurones and glial cells. Development 124:761–771.

Joiner WJ, Crocker A, White BH, Sehgal A (2006) Sleep in *Drosophila* is regulated by adult mushroom bodies. Nature 441:757–760.

Keene AC, Waddell S (2007) *Drosophila* olfactory memory: single genes to complex neural circuits. Nat Rev Neurosci 8:341–354.

Keene AC, Krashes MJ, Leung B, Bernard JA, Waddell S (2006) *Drosophila* dorsal paired medial neurons provide a general mechanism for memory consolidation. Curr Biol 16:1524–1530.

Kitamoto T (2001) Conditional modification of behavior in *Drosophila* by targeted expression of a temperature-sensitive *shibire* allele in defined neurons. J Neurobiol 47:81–92.

Kittel RJ, Wichmann C, Rasse TM, Fouquet W, Schmidt M, Schmid A, Wagh DA, Pawlu C, Kellner RR, Willig KI, Hell SW, Buchner E, Heckmann M, Sigrist SJ (2006) Bruchpilot promotes active zone assembly, $Ca^{2+}$ channel clustering, and vesicle release. Science 312:1051–1054.

Krashes MJ, Keene AC, Leung B, Armstrong JD, Waddell S (2007) Sequential use of mushroom body neuron subsets during *Drosophila* odor memory processing. Neuron 53:103–115.

Krashes MJ, DasGupta S, Vreede A, White B, Armstrong JD, Waddell S (2009) A neural circuit mechanism integrating motivational state with memory expression in *Drosophila*. Cell 139:416–427.

Kremer MC, Christiansen F, Leiss F, Paehler M, Knapek S, Andlauer TF, Förstner F, Kloppenburg P, Sigrist SJ, Tavosanis G (2010) Structural long-term changes at mushroom body input synapses. Curr Biol 20:1938–1944.

Lee T, Luo L (2001) Mosaic analysis with a repressible cell marker (MARCM) for *Drosophila* neural development. Trends Neurosci 24:251–254.

Lee T, Lee A, Luo L (1999) Development of the *Drosophila* mushroom bodies: sequential generation of three distinct types of neurons from a neuroblast. Development 126:4065–4076.

Leiss F, Koper E, Hein I, Fouquet W, Lindner J, Sigrist S, Tavosanis G (2009) Characterization of dendritic spines in the *Drosophila* central nervous system. Dev Neurobiol 69:221–234.

Liu L, Wolf R, Ernst R, Heisenberg M (1999) Context generalization in *Drosophila* visual learning requires the mushroom bodies. Nature 400:753–756.

Liu X, Davis RL (2009) The GABAergic anterior paired lateral neuron suppresses and is suppressed by olfactory learning. Nat Neurosci 12:53–59.

Livingstone MS, Sziber PP, Quinn WG (1984) Loss of calcium/calmodulin responsiveness in adenylate cyclase of *rutabaga*, a *Drosophila* learning mutant. Cell 37:205–215.

Luo L (2007) Fly MARCM and mouse MADM: genetic methods of labeling and manipulating single neurons. Brain Res Rev 55:220–227.

Mao Z, Davis RL (2009) Eight different types of dopaminergic neurons innervate the *Drosophila* mushroom body neuropil: anatomical and physiological heterogeneity. Front Neural Circuits 3:5.

McBride SM, Giuliani G, Choi C, Krause P, Correale D, Watson K, Baker G, Siwicki KK (1999) Mushroom body ablation impairs short-term memory and long-term memory of courtship conditioning in *Drosophila melanogaster*. Neuron 24:967–977.

McGuire SE, Le PT, Davis RL (2001) The role of *Drosophila* mushroom body signaling in olfactory memory. Science 293:1330–1333.

McGuire SE, Le PT, Osborn AJ, Matsumoto K, Davis RL (2003) Spatiotemporal rescue of memory dysfunction in *Drosophila*. Science 302:1765–1768.

Miesenböck G, De Angelis DA, Rothman JE (1998) Visualizing secretion and synaptic transmission with pH-sensitive green fluorescent proteins. Nature 394:192–195.

Miller PM, Saltz JB, Cochrane VA, Marcinkowski CM, Mobin R, Turner TL (2011) Natural variation in decision-making behavior in *Drosophila melanogaster*. PLoS One 6:e16436.

Mombaerts P (2001) How smell develops. Nat Neurosci 4 [Suppl]:1192–1198.

Ng M, Roorda RD, Lima SQ, Zemelman BV, Morcillo P, Miesenböck G (2002) Transmission of olfactory information between three populations of neurons in the antennal lobe of the fly. Neuron 36:463–474.

O'Dell KM, Armstrong JD, Yang MY, Kaiser K (1995) Functional dissection of the *Drosophila* mushroom bodies by selective feminization of genetically defined subcompartments. Neuron 15:55–61.

Owald D, Fouquet W, Schmidt M, Wichmann C, Mertel S, Depner H, Chris-

tiansen F, Zube C, Quentin C, Körner J, Urlaub H, Mechtler K, Sigrist SJ (2010) A Syd-1 homologue regulates pre- and postsynaptic maturation in *Drosophila*. J Cell Biol 188:565–579.

Pauls D, Selcho M, Gendre N, Stocker RF, Thum AS (2010) *Drosophila* larvae establish appetitive olfactory memories via mushroom body neurons of embryonic origin. J Neurosci 30:10655–10666.

Pitman JL, McGill JJ, Keegan KP, Allada R (2006) A dynamic role for the mushroom bodies in promoting sleep in *Drosophila*. Nature 441:753–756.

Prokop A, Meinertzhagen IA (2006) Development and structure of synaptic contacts in *Drosophila*. Semin Cell Dev Biol 17:20–30.

Raghu SV, Joesch M, Sigrist SJ, Borst A, Reiff DF (2009) Synaptic organization of lobula plate tangential cells in *Drosophila*: Dalpha7 cholinergic receptors. J Neurogenet 23:200–209.

Ramaekers A, Magnenat E, Marin EC, Gendre N, Jefferis GS, Luo L, Stocker RF (2005) Glomerular maps without cellular redundancy at successive levels of the *Drosophila* larval olfactory circuit. Curr Biol 15:982–992.

Riemensperger T, Völler T, Stock P, Buchner E, Fiala A (2005) Punishment prediction by dopaminergic neurons in *Drosophila*. Curr Biol 15:1953–1960.

Rolls MM, Satoh D, Clyne PJ, Henner AL, Uemura T, Doe CQ (2007) Polarity and intracellular compartmentalization of *Drosophila* neurons. Neural Dev 2:7.

Roman G, Davis RL (2001) Molecular biology and anatomy of *Drosophila* olfactory associative learning. Bioessays 23:571–581.

Schmid A, Hallermann S, Kittel RJ, Khorramshahi O, Frölich AM, Quentin C, Rasse TM, Mertel S, Heckmann M, Sigrist SJ (2008) Activity-dependent site-specific changes of glutamate receptor composition in vivo. Nat Neurosci 11:659–666.

Schroll C, Riemensperger T, Bucher D, Ehmer J, Völler T, Erbguth K, Gerber B, Hendel T, Nagel G, Buchner E, Fiala A (2006) Light-induced activation of distinct modulatory neurons triggers appetitive or aversive learning in *Drosophila* larvae. Curr Biol 16:1741–1747.

Schulz RA, Chromey C, Lu MF, Zhao B, Olson EN (1996) Expression of the D-MEF2 transcription in the *Drosophila* brain suggests a role in neuronal cell differentiation. Oncogene 12:1827–1831.

Schürmann FW (1974) On the functional anatomy of the corpora pedunculata in insects (in German). Exp Brain Res 19:406–432.

Schürmann FW, Frambach I, Elekes K (2008) GABAergic synaptic connections in mushroom bodies of insect brains. Acta Biol Hung 59 [Suppl]:173–181.

Schwaerzel M, Monastirioti M, Scholz H, Friggi-Grelin F, Birman S, Heisenberg M (2003) Dopamine and octopamine differentiate between aversive and appetitive olfactory memories in *Drosophila*. J Neurosci 23:10495–10502.

Selcho M, Pauls D, Han KA, Stocker RF, Thum AS (2009) The role of dopamine in *Drosophila* larval classical olfactory conditioning. PLoS One 4:e5897.

Sigrist SJ, Reiff DF, Thiel PR, Steinert JR, Schuster CM (2003) Experience-dependent strengthening of *Drosophila* neuromuscular junctions. J Neurosci 23:6546–6556.

Sinakevitch I, Strausfeld NJ (2006) Comparison of octopamine-like immunoreactivity in the brains of the fruit fly and blow fly. J Comp Neurol 494:460–475.

Stocker RF, Singh RN, Schorderet M, Siddiqi O (1983) Projection patterns of different types of antennal sensilla in the antennal glomeruli of *Drosophila melanogaster*. Cell Tissue Res 232:237–248.

Stocker RF, Heimbeck G, Gendre N, de Belle JS (1997) Neuroblast ablation in *Drosophila* P[GAL4] lines reveals origins of olfactory interneurons. J Neurobiol 32:443–456.

Strausfeld NJ (1976) Atlas of the insect brain. Berlin: Springer.

Sun XJ, Tolbert LP, Hildebrand JG (1997) Synaptic organization of the uniglomerular projection neurons of the antennal lobe of the moth *Manduca sexta*: a laser scanning confocal and electron microscopic study. J Comp Neurol 379:2–20.

Thum AS, Jenett A, Ito K, Heisenberg M, Tanimoto H (2007) Multiple memory traces for olfactory reward learning in *Drosophila*. J Neurosci 27:11132–11138.

Tomchik SM, Davis RL (2009) Dynamics of learning-related cAMP signaling and stimulus integration in the *Drosophila* olfactory pathway. Neuron 64:510–521.

Waddell S, Quinn WG (2001a) Flies, genes, and learning. Annu Rev Neurosci 24:1283–1309.

Waddell S, Quinn WG (2001b) What can we teach *Drosophila*? What can they teach us? Trends Genet 17:719–726.

Waddell S, Armstrong JD, Kitamoto T, Kaiser K, Quinn WG (2000) The amnesiac gene product is expressed in two neurons in the *Drosophila* brain that are critical for memory. Cell 103:805–813.

Wagh DA, Rasse TM, Asan E, Hofbauer A, Schwenkert I, Dürrbeck H, Buchner S, Dabauvalle MC, Schmidt M, Qin G, Wichmann C, Kittel R, Sigrist SJ, Buchner E (2006) Bruchpilot, a protein with homology to ELKS/CAST, is required for structural integrity and function of synaptic active zones in *Drosophila*. Neuron 49:833–844.

Wichmann C, Sigrist SJ (2010) The active zone T-bar—a plasticity module? J Neurogenet 24:133–145.

Yang CH, Belawat P, Hafen E, Jan LY, Jan YN (2008) *Drosophila* egg-laying site selection as a system to study simple decision-making processes. Science 319:1679–1683.

Yang MY, Armstrong JD, Vilinsky I, Strausfeld NJ, Kaiser K (1995) Subdivision of the *Drosophila* mushroom bodies by enhancer-trap expression patterns. Neuron 15:45–54.

Yasuyama K, Meinertzhagen IA, Schürmann FW (2002) Synaptic organization of the mushroom body calyx in *Drosophila melanogaster*. J Comp Neurol 445:211–226.

Yu D, Ponomarev A, Davis RL (2004) Altered representation of the spatial code for odors after olfactory classical conditioning; memory trace formation by synaptic recruitment. Neuron 42:437–449.

Yu D, Keene AC, Srivatsan A, Waddell S, Davis RL (2005) *Drosophila* DPM neurons form a delayed and branch-specific memory trace after olfactory classical conditioning. Cell 123:945–957.

Zars T, Fischer M, Schulz R, Heisenberg M (2000) Localization of a short-term memory in *Drosophila*. Science 288:672–675.

Zhang YQ, Rodesch CK, Broadie K (2002) Living synaptic vesicle marker: synaptotagmin-GFP. Genesis 34:142–145.

# 5. STRUCTURAL LONG-TERM CHANGES AT MUSHROOM BODY INPUT SYNAPSES

Please cite this article in press as: Kremer et al., Structural Long-Term Changes at Mushroom Body Input Synapses, Current Biology (2010), doi:10.1016/j.cub.2010.09.060

Current Biology *20*, 1–7, November 9, 2010 ©2010 Elsevier Ltd All rights reserved DOI 10.1016/j.cub.2010.09.060

Report

# Structural Long-Term Changes at Mushroom Body Input Synapses

**Malte C. Kremer,[1,7] Frauke Christiansen,[3,4,7] Florian Leiss,[1,7] Moritz Paehler,[5] Stephan Knapek,[1] Till F.M. Andlauer,[3,4,6] Friedrich Förstner,[2] Peter Kloppenburg,[5] Stephan J. Sigrist,[3,4,*] and Gaia Tavosanis[1,*]**

[1]Department of Molecular Neurobiology, Dendrite Differentiation Group

[2]Department of Systems and Computational Neurobiology Max Planck Institute (MPI) of Neurobiology, Munich-Martinsried 82152, Germany

[3]Department of Genetics, Institute for Biology, Freie Universität Berlin, Berlin 14195, Germany

[4]Cluster of Excellence NeuroCure, Charite, 10117 Berlin, Germany

[5]Cologne Biocenter, Center for Molecular Medicine and Excellence Cluster on Cellular Stress Responses in Aging-Associated Diseases, University of Cologne, Cologne 50674, Germany

[6]Bio-Imaging Center at the Rudolf Virchow Center/Deutsche Forschungsgemeinschaft Research Center for Experimental Biomedicine, University of Würzburg, Würzburg 97080, Germany

## Summary

**How does the sensory environment shape circuit organization in higher brain centers? Here we have addressed the dependence on activity of a defined circuit within the mushroom body of adult *Drosophila*. This is a brain region receiving olfactory information and involved in long-term associative memory formation [1]. The main mushroom body input region, named the calyx, undergoes volumetric changes correlated with alterations of experience [2–5]. However, the underlying modifications at the cellular level remained unclear. Within the calyx, the clawed dendritic endings of mushroom body Kenyon cells form microglomeruli, distinct synaptic complexes with the presynaptic boutons of olfactory projection neurons [6, 7]. We developed tools for high-resolution imaging of pre- and postsynaptic compartments of defined calycal microglomeruli. Here we show that preventing firing of action potentials or synaptic transmission in a small, identified fraction of projection neurons causes alterations in the size, number, and active zone density of the microglomeruli formed by these neurons. These data provide clear evidence for activity-dependent organization of a circuit within the adult brain of the fly.**

## Results and Discussion

### Development of Tools to Identify and Quantify Calycal Microglomeruli

Odors encountered in the environment and detected by olfactory sensory neurons are initially processed in a first olfactory center, the antennal lobe in insects or the olfactory bulb in mammals. This olfactory information is then conveyed by insect antennal lobe projection neurons or mammalian mitral/tufted cells to secondary centers for odor recognition and the formation of olfactory memories [8]. These two functions appear to be accomplished by two regions in the fly brain, the lateral horn and the mushroom body, respectively [1, 9]. Changes in the olfactory environment are reflected by changes in activity at the mushroom body input synapses [10]. Furthermore, because projection neurons can house an appetitive memory trace, the mushroom body input synapses might be potentially involved in olfactory memory formation [11]. It is unknown, though, whether alterations of presynaptic activity or formation of memories induce structural changes in the mushroom body.

In the *Drosophila* brain, most antennal lobe projection neurons send axonal projections terminating with bulbous boutons into the mushroom body calyx [12]. Here they form specialized synaptic complexes, called microglomeruli (Figure 1A; [6, 7]), with the dendrites of mushroom body Kenyon cells, which are essential for the formation and retrieval of olfactory memories [1]. Within a microglomerulus, a projection neuron bouton is enwrapped by actin-rich, claw-like, dendritic endings of more than one Kenyon cell and forms multiple synapses with these Kenyon cells' claws, each including a presynaptic active zone and a postsynaptic density (Figure 1A; [7]). In social insects, the size and number of microglomeruli are modified in correlation with changes in the sensory environment [13, 14]. Here we ask directly whether silencing olfactory projection neuron presynaptic activity or blocking their synaptic transmission alters the organization of calycal microglomeruli of *Drosophila*.

To this end, we generated genetic tools to identify the microglomeruli and the sites of synaptic contact within them. Projection neurons are the only reported cholinergic input to the mushroom body calyx [15]. Therefore, we constructed a fusion of the *MB247* fragment of the *D-mef2* promoter [16], active in a large subset of Kenyon cells [17–19], and the D$\alpha$7 subunit of the acetylcholine receptor tagged with eGFP [20, 21] (*MB247-D$\alpha$7-GFP*) to visualize the postsynaptic rim formed by claw-like dendritic endings of multiple Kenyon cells around each projection neuron bouton [7] (Figure 1C). The localization of D$\alpha$7-GFP within the calyx appeared to be specific for the postsynaptic densities of the Kenyon cell claws (Figures 1A, 1C, 1D, and 1F; see also Figures S1A–S1F available online), and it closely matched the active zone labeling in the projection neuron boutons (see below; Figures 1C–1F and Figures S1G–S1M). Importantly, expressing this construct did not affect the active zone number in the calyx (Figures S1N–S1P).

We also sought to label the presynaptic active zones associated with postsynaptic densities. The active zone protein Bruchpilot (BRP) shapes the presynaptic active zone T bar and is essential for proper active zone function [22, 23]. A fluorescently tagged fragment of BRP, which depends on endogenous BRP for localization [24] (*UAS-brp-short$^{cherry}$*), represents a reliable marker for active zones. Upon specific expression of *UAS-brp-short$^{cherry}$* in projection neurons, discrete BRP-short$^{cherry}$ dots lined the inner rim of the Kenyon

*Correspondence: stephan.sigrist@fu-berlin.de (S.J.S.), gaia@neuro.mpg.de (G.T.)

[7]These authors contributed equally to this work

Please cite this article in press as: Kremer et al., Structural Long-Term Changes at Mushroom Body Input Synapses, Current Biology (2010), doi:10.1016/j.cub.2010.09.060



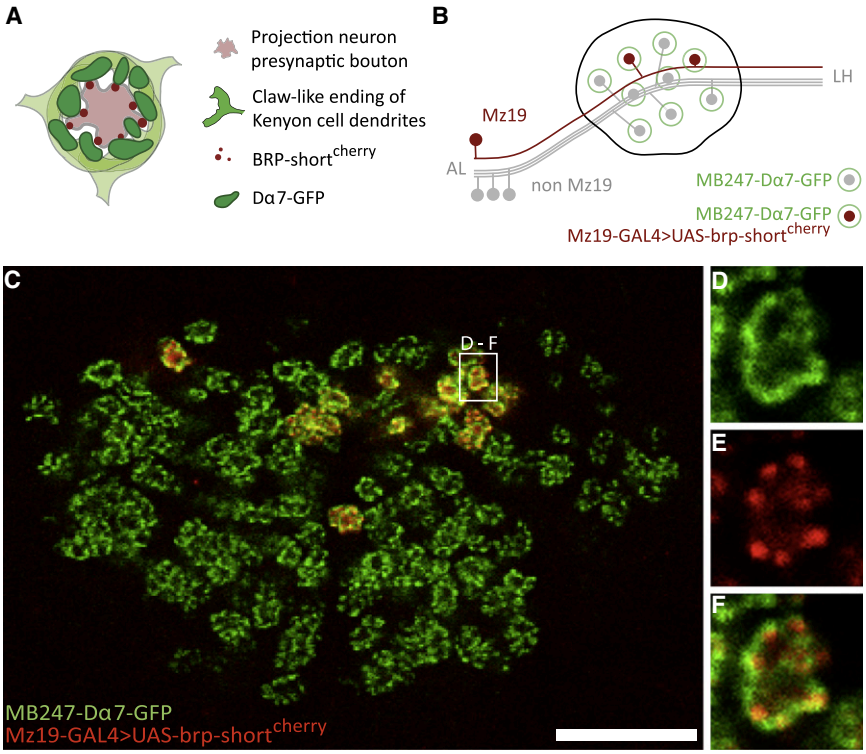


Figure 1. Pre- and Postsynaptic Labeling of Calycal Microglomeruli

(A) Schematic of a microglomerulus formed by the axonal bouton of a projection neuron and by the claw-like dendritic endings of multiple Kenyon cells. GFP-tagged Dα7 expressed in a large fraction of Kenyon cells marks the postsynaptic sites, whereas the fluorescently tagged Bruchpilot (BRP)-short protein, expressed within the Mz19-positive subset of projection neurons, labels presynaptic active zones. The lumen is defined as the area contained within the Dα7-GFP rim, the ring is defined as the surface occupied by the Dα7-GFP label, and the microglomerular size is defined as the sum of both.

(B) Schematic representation of the mushroom body calyx. A large fraction of microglomeruli in the calyx is labeled with MB247-Dα7-GFP (green rings). The Mz19-positive population of microglomeruli is labeled with MB247-Dα7-GFP and with fluorescently tagged BRP (BRP-short$^{cherry}$; red lumina).

(C) Example of one optical section demonstrating the Dα7-GFP labeling of a large fraction of microglomeruli (green) and the BRP-short$^{cherry}$ labeling of the Mz19-positive subpopulation (red).

(D–F) Higher magnifications of the boxed region in (C), split channels and merged, showing the close juxtaposition of the Dα7-GFP and BRP-short$^{cherry}$ labeling, presumably at sites of synaptic contact. Scale bar represents 10 μm.

cell claw, closely matching the Dα7-GFP signal at putative sites of synaptic contact (*Mz19-Gal4*; Figures 1A and 1C–1F). The number of active zones is not affected by the expression of *UAS-brp-short$^{cherry}$* (using *Mz19-Gal4*; Figures S1X–S1Z).

Previous data suggested that simple complete sensory deprivation experiments did not elicit detectable changes in the calyx (unpublished data; [25]). Therefore, we decided to generate a competitive situation in the calyx between silenced and nonsilenced projection neurons and among dendrite claws of the same Kenyon cell receiving normal or no presynaptic input. We thus manipulated and differentially labeled a defined subset of microglomeruli, highlighted by the *Mz19-Gal4* driver ([26]; Figure 1B). *Mz19-Gal4* is expressed after 18 hr after puparium formation [27] in 10–13 projection neurons whose dendrites are restricted to three glomeruli in the antennal lobe (DA1, VA1d, and DC3; [27]) and form boutons in a confined area of the calyx [7, 27, 28]. We used *Mz19-Gal4*-driven *UAS-brp-short$^{cherry}$* signal to identify the subset of microglomeruli formed by these projection neurons (Figures 1B and 1C–1F). Whereas calycal microglomeruli were highlighted with MB247-Dα7-GFP, the Mz19-positive subpopulation was identified by BRP-short$^{cherry}$ and MB247-Dα7-GFP (Figures 1B and 1C).

Within each calyx, we compared the Mz19-positive microglomeruli with those in which no *Mz19-Gal4*-driven expression of *brp-short$^{cherry}$* was observed. This experimental setup also allowed us to obviate the problems posed by the large variability of overall brain volume and calycal size among animals, independently of their genotype (in our experiments, approximately 10% of the calycal volume; see also [2]), and by potential differences in image acquisition and calycal labeling among animals. These factors could, in principle, hamper the detection of small morphological changes.

We reasoned that the structurally repetitive organization of the calyx, the introduction of a competitive situation within the calyx, and the specificity of the developed markers might facilitate revealing alterations induced by changes in presynaptic activity.

## Expression of a Leaky Potassium Channel Silences Projection Neurons

To address whether the size and number of microglomeruli and the active zone distribution in adult calyces depend on presynaptic activity, we sought to silence or at least drastically reduce firing of the Mz19-positive projection neuron population. Using the *Mz19-Gal4* driver, we expressed *UAS-dORK1.ΔC*, which functionally acts as a constitutively open $K^+$ selective pore or leak and should lead to hyperpolarization of the resting membrane potential; *UAS-dORK1.ΔNC*, a nonconducting version of the same channel, served as a control [29]. We performed whole-cell current-clamp recordings from the somata in an isolated, intact brain preparation to analyze the intrinsic firing properties of the projection neurons. Seven-day-old adult males were used, and the recorded neurons were labeled with biocytin to confirm their identity (Figures 2A and 2B). Mz19-positive projection neurons of both genotypes did not show spontaneous activity in the cell-attached configuration or in the whole-cell configuration. Control Mz19-positive projection neurons expressing *UAS-dORK1.ΔNC* had a resting membrane potential ($E_M$) of −59.3 ± 2.8 mV (n = 7) immediately after establishing the whole-cell configuration (Figure 2C). This is approximately 10 mV more hyperpolarized than the resting membrane potential reported by Gouwens and Wilson [30] for *Drosophila* projection neurons. Depolarizing current injection caused these neurons to fire action potentials at a threshold of 29.5 ± 7.3 mV measured at the soma (n = 7; Figure 2D). The action potentials had an amplitude of 6.6 ± 2.3 mV, possibly attenuated [30], an afterhyperpolarization of 2.6 ± 0.9 mV, and a width of 2.0 ± 0.7 ms at the half-maximal amplitude.

Please cite this article in press as: Kremer et al., Structural Long-Term Changes at Mushroom Body Input Synapses, Current Biology (2010), doi:10.1016/j.cub.2010.09.060



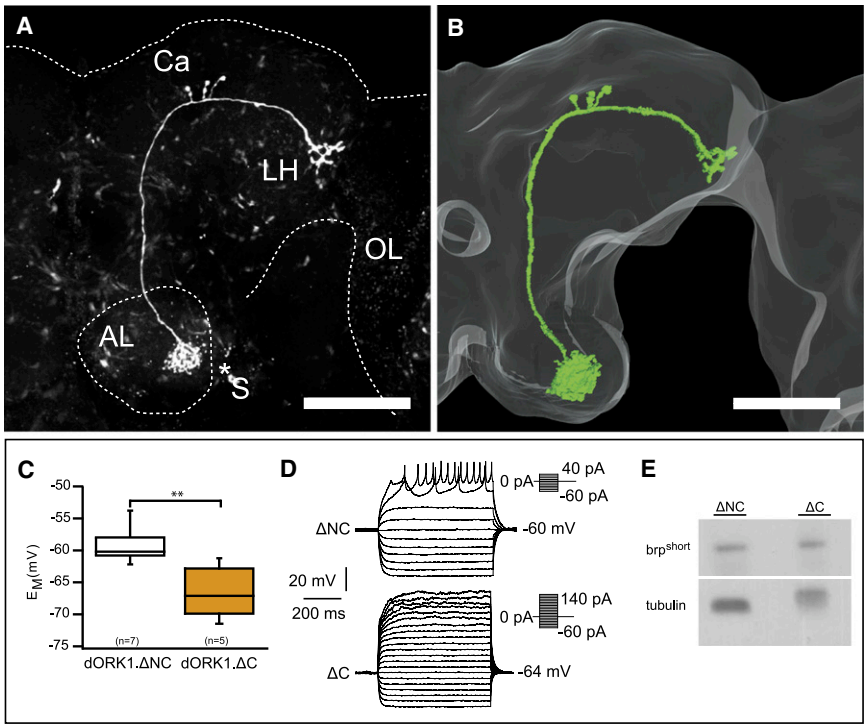


Figure 2. Expression of the Leaky Potassium Channel dORK1 Efficiently Silences Projection Neurons

(A and B) Morphology of an Mz19-positive projection neuron revealed by biocytin staining via the patch pipette (70 μm image stack). Maximum intensity projection (A) and 3D reconstruction (B) are shown. The neuron innervated a single glomerulus and sent a single axon to the calyces of the ipsilateral mushroom body (Ca) and lateral horn (LH). The position of the soma (S), which was lost during processing, is marked (*). Scale bar represents 50 μm.

(C and D) Basic electrophysiological properties of Mz19-positive projection neurons of control and *dORK1.ΔC*-expressing projection neurons.

(C) In *dORK1.ΔC*-expressing projection neurons, the resting membrane potential was significantly hyperpolarized compared to control cells ($p < 0.01$; unpaired t test). Whisker box plots: the box extends from the 25th to 75th percentiles, line at the median. Whiskers mark minimum and maximum data points.

(D) Control *dORK1.ΔNC*-expressing projection neurons started to fire action potentials at membrane potentials more depolarized than −29.5 ± 7.3 mV, measured in the soma (n = 7). In *dORK1.ΔC*-expressing projection neurons, even large depolarizing currents did not induce action potentials (n = 5). Current was injected for 500 ms in 10 pA increments from −60 to 40 pA for control *dORK1.ΔNC*-expressing projection neurons and from −60 to 140 pA for *dORK1.ΔC*-expressing projection neurons. Values in the text are given as means ± standard deviation.

(E) The level of BRP-short$^{cherry}$ protein was not significantly altered upon silencing neuronal activity in Mz19-positive projection neurons. BRP-short$^{cherry}$ protein was detected in extracts of control brains (ΔNC, ratio BRP/loading control = 0.55) or in brains of flies expressing *dORK1.ΔC* in the Mz19-positive projection neurons (ΔC, ratio BRP/loading control = 0.58). Tubulin represents the loading control.

In Mz19-positive projection neurons expressing *UAS-dORK1.ΔC*, the resting membrane potential was −66.5 ± 3.8 mV (n = 5) shortly after break-in, which is significantly more hyperpolarized than in control Mz19-positive projection neurons ($p < 0.01$, t test; Figure 2C), confirming the functional effect of the constitutively open $K^+$ channel. This hyperpolarization alone should drastically reduce the firing probability of the projection neurons. In fact, in Mz19-positive projection neurons expressing *UAS-dORK1.ΔC*, no action potentials could be elicited (n = 5), even when the cells were depolarized well above the spike threshold of control projection neurons (Figure 2D). It is expected that the large $K^+$ leak conductance prevented voltage spread from the site of current injection (soma) to a local spike initiation zone (see also [30]). There is no evidence for a highly localized expression of the *UAS-dORK1.ΔC*. Therefore, it is likely that this leak conductance also severely hindered the summation of excitatory synaptic potentials and prevented synaptic potentials from reaching the firing threshold, thereby effectively silencing the neurons in vivo. This manipulation of the Mz19-positive projection neuron activity does not significantly modify the level of BRP-short$^{cherry}$ protein (Figure 2E).

## Presynaptic Activity-Dependent Structural Reorganization of Microglomeruli

We next addressed whether the microglomeruli formed by boutons of the silenced Mz19-positive projection neurons were altered.

For every experimental group, we analyzed the two calyces of at least six 7-day-old adult males and obtained 60–100 confocal optical sections per calyx. To obtain an unbiased identification of microglomeruli in high numbers of single optical sections, we developed software for the automated detection of microglomeruli (Figures 3A–3D and Figure S2; Supplemental Experimental Procedures). In every optical section, we identified microglomerular rings based on the intensity of the Dα7-GFP signal, the size and shape of the structure, and whether the Dα7-GFP-positive structure surrounded a darker lumen. A microglomerulus was defined as the sum of a Dα7-GFP-positive ring object and the lumen it contained. The software detected more than 30% of the manually identified microglomeruli, including only 3% false positives. Importantly, the overall size distribution of the microglomeruli was not significantly different between manual and software-based identification, suggesting that the software detection is unbiased (Supplemental Experimental Procedures; Figure S2K). Furthermore, by using this approach, we could detect alterations in the number of Mz19-positive microglomeruli obtained by overexpression of PI3K, a manipulation that induced bouton sprouting of ellipsoid body projection neurons [31] and served as a positive control (Figure S3A).

We thus silenced the Mz19-positive neurons by expressing *dORK1.ΔC*. We found that the fraction of Mz19-positive microglomeruli per calyx was significantly increased compared to the nonsilenced *dORK1.ΔNC* control ($p < 0.05$, analysis of variance [ANOVA] with Bonferroni's correction; Figure 3E). It should be noted that, in motorneurons, hyperactivation—and not suppression of activity—leads to bigger axonal elaborations [32].

Moreover, we observed that the relative size of the microglomeruli was increased ($p < 0.05$, ANOVA with Bonferroni's correction; Figure 3F). This general enlargement of

Please cite this article in press as: Kremer et al., Structural Long-Term Changes at Mushroom Body Input Synapses, Current Biology (2010), doi:10.1016/j.cub.2010.09.060



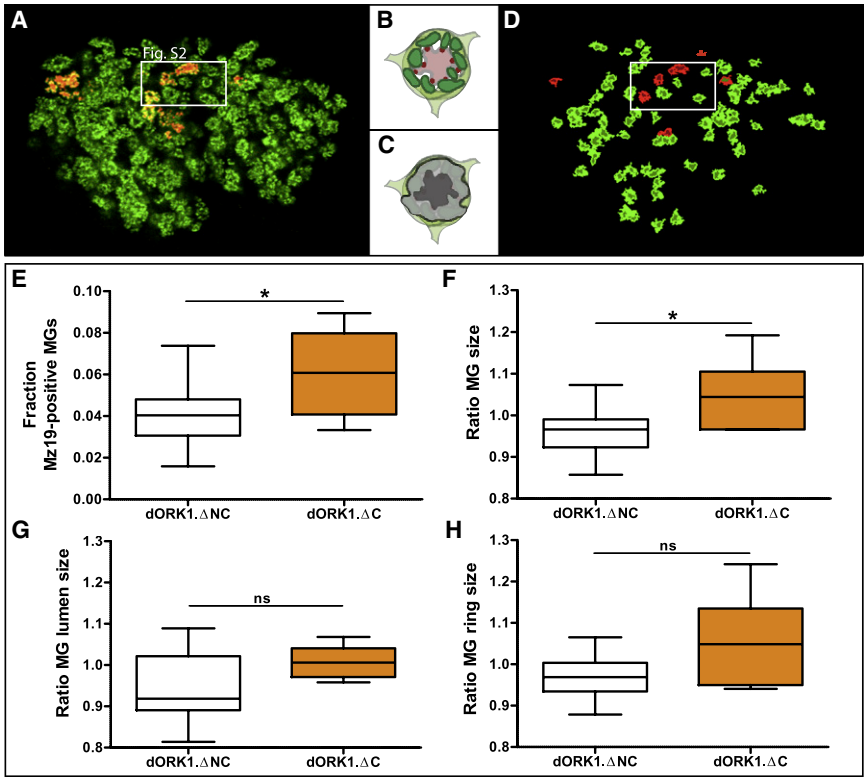


Figure 3. Silencing of Projection Neurons Modifies the Size and Number of Microglomeruli

(A and D) Microglomerular detection using automated image analysis (D) from the original image in (A).

(B and C) Schematic illustration of a microglomerulus (B; as in Figure 1A) and of its detection by the software (C). The light gray area in (C) represents the microglomerular ring, and the dark gray area represents the microglomerular lumen.

(D) In Mz19-negative microglomeruli, the ring is shown in bright green and the lumen is shown in dark green. In Mz19-positive microglomeruli, the ring is represented in bright red and the lumen in dark red. A detailed illustration of the automated detection is given in Figures S2A–S2J.

(E) The average percentage of Mz19-positive microglomeruli per calyx increased upon expression of the *dORK1.ΔC* construct in comparison to the control *dORK1.ΔNC*.

(F) Upon expression of *dORK1.ΔC* with *Mz19-Gal4*, the relative size of the Mz19-positive microglomeruli increased in comparison to control (*dORK1.ΔNC*). The relative size (ratio MG size) is the ratio between the average sizes of Mz19-positive and Mz19-negative microglomeruli per calyx.

(G) Upon expression of the *dORK1.ΔC* construct, the relative lumen size (ratio MG lumen size) was not significantly modified.

(H) In contrast, the relative ring size (ratio MG ring size) of the Mz19-positive microglomeruli increased in comparison to the control, although not to significant levels. Whisker box plots: the box extends from the 25th to 75th percentiles, line at the median. Whiskers mark minimum and maximum data points (*dORK1.ΔNC* n = 11; *dORK1.ΔC* n = 6 animals).

microglomerular size upon silencing correlated with an increase of the relative size of the Dα7-GFP-positive ring, which was, however, not significant (Figures 3G and 3H).

Hence, reducing the activity of the Mz19-positive projection neurons led to an increase in the number of the microglomeruli formed by those neurons. Additionally, the relative size of the microglomeruli increased.

Therefore, we next asked whether the number of individual presynaptic active zones per microglomerulus would increase as well or whether only size changes in the postsynaptic densities were taking place.

## Active Zone Density in Microglomeruli Depends on Presynaptic Activity

Individual synaptic release sites are characterized by a presynaptic active zone, identifiable by BRP [22, 33]. Thus, we analyzed the BRP-short$^{cherry}$ puncta in calyces of flies expressing *dORK1.ΔNC* or *dORK1.ΔC* and *brp-short$^{cherry}$* under the control of *Mz19-Gal4*. The BRP-short$^{cherry}$ puncta were counted using software for semiautomated detection (Figures 4A–4E; Supplemental Experimental Procedures) applied to 3D reconstructions of the whole calyx.

Strikingly, silencing the presynaptic neurons with *dORK1.ΔC* induced a clear increase in the number of BRP-short$^{cherry}$ puncta per calyx compared to the control ($p < 0.05$, Kruskal-Wallis test with Dunn's correction; Figures 4C and 4F). This increase could simply be due to the above-described higher number of Mz19-positive microglomeruli obtained upon silencing. We therefore determined the active zone density in the Mz19-positive terminals. Silencing those projection neurons resulted in a total increase in synaptic density in the Mz19-positive terminals ($p < 0.01$, Kruskal-Wallis test with Dunn's correction; Figure 4G; no significant increase in the total area of the presynaptic terminals, $p > 0.05$; Figures 4D and 4H). The size of single active zones was not modified in silenced projection neurons with respect to the control ($p > 0.05$, Kruskal-Wallis test with Dunn's correction; Figures 4E and 4I). Hence, silencing or strongly reducing the generation of action potentials in projection neurons induced increased active zone density.

In summary, the microglomeruli formed by silenced projection neurons were more numerous compared to the control. Additionally, the postsynaptic domain was larger and the density of presynaptic active zones was higher in the silenced rather than in the unaffected microglomeruli.

The overexpression of *dORK.1ΔC* in projection neurons led to hyperpolarization, decreased input resistance, and subsequent inhibition of action potential firing, and thus, presumably, suppression of action potential evoked synaptic transmission. To dissect the contribution of these components, we specifically suppressed synaptic vesicle fusion using tetanus toxin (*UAS-TNT*) under the control of *Mz19-Gal4* [34] (Figure S4). As a consequence, the relative size of the microglomeruli was significantly increased ($p < 0.001$, Student's t test with Welch's correction; Figure S4B). Because this result was similar to the effect of silencing the presynaptic neurons with *dORK1.ΔC* (Figures 3F–3H), increase of the synaptic complex size might be caused by the loss of synaptic transmission in both situations. In contrast to the effect caused by *dORK1.ΔC* expression, however, the fraction of

Please cite this article in press as: Kremer et al., Structural Long-Term Changes at Mushroom Body Input Synapses, Current Biology (2010), doi:10.1016/j.cub.2010.09.060



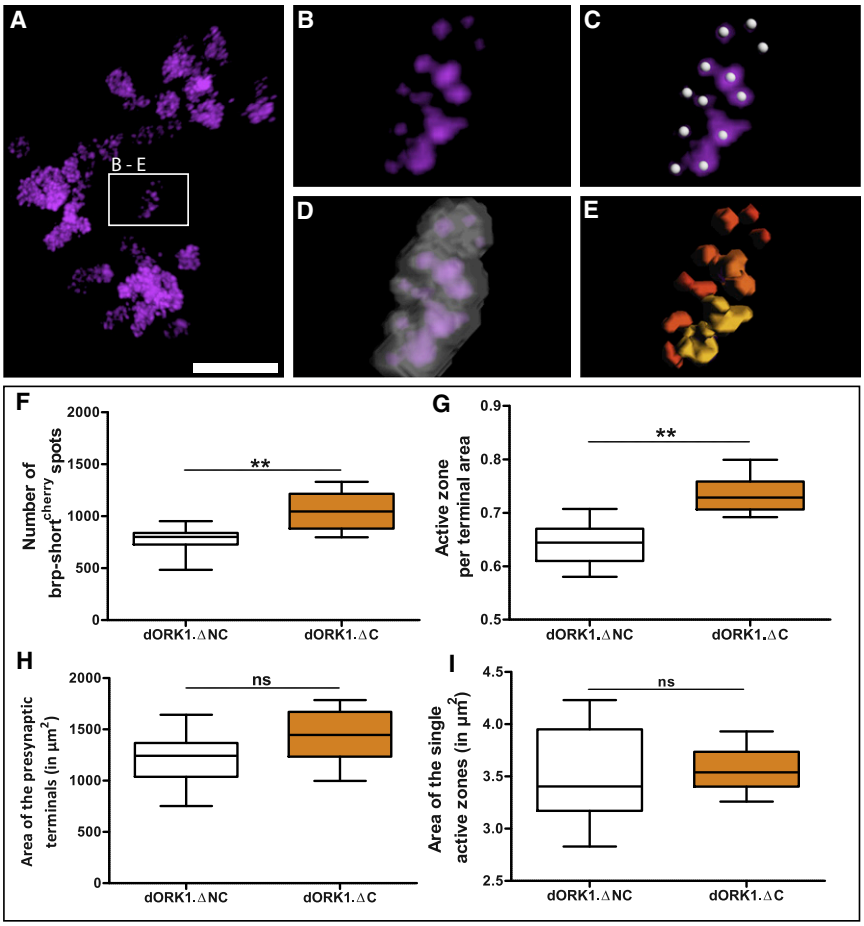


Figure 4. Silencing of Projection Neuron Activity Increases Their Active Zone Density in the Mushroom Body Calyx

(A) Maximum projection of an optical section series through a control mushroom body calyx expressing BRP-short$^{cherry}$ in all presynaptic terminals of the Mz19-positive projection neurons.

(B) 3D rendering of the raw data image of the region of the mushroom body calyx highlighted in (A).

(C) Identification of BRP-short$^{cherry}$-labeled active zones (Imaris surface seeds).

(D) 3D rendering of the surface model spanning over the total BRP-short$^{cherry}$ signal. This continuous surface represents the terminal area (Imaris surface tool applied to the BRP-short$^{cherry}$ signal). The total terminal area per calyx corresponds to the surface area of a 3D reconstruction of the complete Mz19-positive signal.

(E) Surface area rendering of individual 3D-modeled BRP-short$^{cherry}$ puncta. Surfaces were used to calculate the number and area of individual active zones (Imaris surface tool). Smaller objects are illustrated in red, and bigger objects are illustrated in yellow.

(F) Absolute number of BRP-short$^{cherry}$-labeled active zones identified, as represented in (C). This number was clearly increased upon silencing the Mz19-positive projection neurons.

(G) The active zone density is calculated as number of active zones per terminal area. A significant increase was obtained upon silencing.

(H and I) The total terminal area (H), as represented in (D), and the area of active zones (I), as represented in (E), were not modified upon silencing. Whisker box plots: the box extends from the 25th to 75th percentiles, line at the median. Whiskers mark minimum and maximum data points (*dORK1.ΔNC* n = 10; *dORK1.ΔC* n = 6 animals).

Mz19-positive microglomeruli was decreased upon expression of *TNT* ($p < 0.05$, t test; Figure S4A). Also, the number and density of active zones were clearly diminished upon *TNT* expression (number $p < 0.001$, t test; density $p < 0.001$, Mann-Whitney test; Figures S4E and S4F). Thus, the number of microglomeruli and the active zone density are distinctly regulated depending on the manipulation.

We suggest that antagonistic mechanistic components might confront each other here [35]. First, a mechanism seems to sense activity within projection neurons. If neuronal activity is suppressed, a coherent "compensatory" response is triggered, increasing bouton size and number, as well as the density of active zones at the affected terminals. In mammals, neuronal activity was found to effectively control neuronal gene transcription and translation [36]. Second, there appears to be a homeostatic compensation within the microglomerular microcircuit of the loss of synaptic transmission, leading to increased bouton and postsynaptic ring size. Finally, loss of transmission per se induces a reduction in the active zone density and in the number of microglomeruli. How these phenomena interact throughout physiological adaptations will be interesting to address in the future.

Here we have described changes in the number of calycal microglomeruli, as well as in their pre- and postsynaptic composition, that depend on the activity state of the presynaptic neuron and on transmission. Thus, we have revealed that the structural and synaptic organization of the adult mushroom body calyx of *Drosophila* requires appropriate presynaptic activity and synaptic transmission.

Microglomeruli are more ill defined in calyces of just-eclosed males (data not shown), suggesting a reorganization of the circuit during early adult life. In line with this hypothesis, the microglomerular circuit might be refined after eclosion in *Apis* [37]. It is thus possible that microglomeruli form normally but that projection neuron input is required during a hypothetical refinement phase. Alternatively, the initial formation of microglomeruli may be affected by the absence of appropriate presynaptic activity and/or synaptic transmission. In support of this second scenario, modification of synaptic input alters the dendritic differentiation of a motor neuron in fly embryos [38]. At this point, we cannot distinguish between these two possibilities.

Previous evidence indicated that, in the adult fly brain, the establishment of correct connectivity is largely independent of activity [25, 39–41]. Nonetheless, the activity-dependent component of circuit organization might be difficult to detect above interanimal variability. Thus, we propose that the type of approach described here, including internal controls, high-resolution imaging of pre- and postsynaptic elements, and software-based analysis, will be necessary to reveal similar phenomena in other regions of the fly brain. In the calyx, this analysis was facilitated by the organization in microglomeruli, recognizable repetitive structural elements.

In addition, we reckon that the effect of activity on circuit organization might be best revealed by unbalancing the circuit as we did by silencing only a defined fraction of olfactory projection neurons. As an example, monocular deprivation experiments, rather than binocular elimination of visual input,

were instrumental to the understanding of the role of activity in shaping the visual circuit in mammals [42].

Projection neuron activity delivers a representation of the olfactory environment to the calyx [10]. The effect of our manipulations of projection neuron activity suggests that olfactory experience modulates the calycal circuit. In line with this hypothesis, sensory experience modifies properties of microglomeruli in the honeybee and ant [13, 43]. The functional outcome of these adaptations remains to be investigated. Importantly, in *Drosophila*, alterations of olfactory experience determine volumetric changes of adult antennal lobes [44, 45]. Furthermore, because projection neurons can house an appetitive memory trace, the mushroom body input synapses might be potentially involved in olfactory memory formation [11]. Given the high resolution of the system we have established, we envisage that the next challenge will be to address directly whether the structure of defined microglomeruli can be modulated upon the establishment of long-term appetitive memories [46, 47].

## Experimental Procedures

### Fly Strains

The following genotypes were used: *Mz19-Gal4/CyO; UAS-brp-short$^{cherry}$ MB247-Dα7-GFP/UAS-dORK.ΔC*, *Mz19-Gal4/+; UAS-brp-short$^{cherry}$ MB247-Dα7-GFP/UAS-dORK.ΔNC*, *Mz19-Gal4/UAS-LacZ; UAS-brp-short$^{cherry}$ MB247-Dα7-GFP/+*, *Mz19-Gal4/UAS-TNTe; UAS-brp-short$^{cherry}$ MB247-Dα7-GFP/+*, and *Mz19-Gal4/+; UAS-brp-short$^{cherry}$ MB247-Dα7-GFP/UAS-PI3K*, including the following drivers and reporters: *Mz19-Gal4* (kindly provided by T. Hummel, Universität Münster, Germany), *UAS-LacZ* (T. Suzuki, MPI of Neurobiology, Munich, Germany), *UAS-TNTe* (H. Tanimoto, MPI of Neurobiology), *OK107-Gal4*, *UAS-dORK1.ΔC*, *UAS-dORK1.ΔNC* [29], and *UAS-PI3K*, obtained from the Bloomington Drosophila Stock Center. The *brp* fragment included in the *brp-short$^{cherry}$* construct was previously described [24] and includes the amino acids 473–1226 of the 1740 amino acid full-length BRP protein. The electrophysiology experiments were performed with flies expressing *mCD8-GFP* and either *dORK.ΔC* or *dORK.ΔNC* under the control of *Mz19-Gal4*. The flies were reared on standard *Drosophila* medium at 25°C.

### Molecular Cloning

For gene expression independent of the Gal4/UAS system, we generated transgenic flies carrying the eGFP-tagged Dα7 subunit of the nicotinic acetylcholine receptor under direct control of the mushroom body enhancer *MB247* [16]. *Dα7-eGFP* was inserted in the pCaSpeR vector carrying the *MB247* enhancer (kindly provided by A. Thum, Fribourg), using the NotI and XbaI sites to generate *MB247-Dα7-GFP*.

### Immunohistochemistry

For confocal microscopy, brains of 7-day-old male flies were dissected in cold phosphate-buffered saline (PBS) and fixed for 30 min in 4% paraformaldehyde (Polyscience) at room temperature. For immunostaining, brains were then blocked in 10% fetal calf serum (Invitrogen) in PBT (PBS with 0.3% Triton X-100) for 30 min, incubated with the primary antibodies nc82 (kind gift of E. Buchner; mouse, 1:20; [33]) and anti-DsRed (rabbit, 1:2000, Rockland Immunochemicals) and then with the secondary antibodies anti-mouse Cy3 (donkey, 1:100, Jackson Laboratories) and anti-rabbit AlexaFluor 568 (goat, 1:100, Invitrogen), mounted in VectaShield (Vector Laboratories), and imaged promptly.

### Electrophysiology and Single-Cell Labeling

We used an intact brain preparation by modifying preparations described previously [48–50]. See Supplemental Experimental Procedures for a detailed description.

### Western Blot

The heads of 7-day-old males of the appropriate genotypes were smashed with a micropestle in 2× Laemmli buffer, boiled, and spun, and the supernatant was loaded on 10% SDS-PAGE. After blotting, the membrane was probed with anti-RFP antibody (1: 2000; Rockland) and developed with ECL (Amersham).

### Optical Imaging

Confocal images for semiautomatic quantitative analysis were recorded using an Olympus confocal microscope with a 60× 1.4 oil-immersion objective. Image acquisition settings were standard for all images (60× 1.4 oil-immersion objective, 3× zoom). For each calyx, we scanned a series of 60 to 100 slices with a voxel size of 0.138 × 0.138 × 0.25 μm, except where otherwise stated.

### Image Analysis

For the analysis of postsynaptic Dα7-GFP rings, object-oriented image analysis was done using a customized algorithm developed with Definiens developer environment, and the automated analysis of images was performed with Definiens Developer XD 1.1 (see Supplemental Experimental Procedures for details). In the same set of images, projection neuron active zone parameters were analyzed using the Imaris × 64 version 6.1.5 software, optimized for the purpose (Bitplane AG) (see Supplemental Experimental Procedures for details). Figures were prepared with Photoshop and Illustrator CS4 (Adobe Systems).

### Data Analysis

Statistics were conducted using Microsoft Excel and GraphPad Prism. Data were tested for normal distribution and homogeneity of variance with Kolmogorov-Smirnov test and Bartlett's test, respectively. If none of these assumptions were violated, parametric comparisons (unpaired Student's t test or one-way ANOVA followed by Bonferroni-corrected post hoc tests) were applied. If homogeneity of variance was violated, Welch's correction for t test was used. If data were not normally distributed, nonparametric tests (Mann-Whitney test or Kruskal-Wallis followed by Dunn's post hoc pairwise test) were performed. The significance level was set to 5%. *$p < 0.05$, **$p < 0.01$, ***$p < 0.001$. In whisker box plots, the box extends from the 25th to 75th percentiles, with a line at the median. Whiskers mark minimum and maximum data points.

### Supplemental Information

Supplemental Information includes Supplemental Experimental Procedures and four figures and can be found with this article online at doi:10.1016/j.cub.2010.09.060.

### Acknowledgments

We are grateful to E. Buchner, T. Hummel, and A. Thum for generously contributing reagents; A. Ferrus, B. Gerber, M. Heisenberg, and H. Tanimoto for helpful discussions during the course of these studies; and F. Bradke, M. Hübener, and H. Tanimoto for critically reading the manuscript. We thank H. Wratil, J. Lindner, and J. Wächter for excellent technical assistance and U. Gaul for generous support to M.C.K. We thank the Bloomington Stock Center for fly lines and Flybase. This work was supported by a fellowship of the Boehringer Ingelheim fonds to M.P. and grants of the Deutsche Forschungsgemeinschaft to P.K. (KL 762/2-2 and KL 762/4-1), S.J.S. (Exc 257 and SFB 554), and G.T. (Ta 265/2-2).

Received: February 3, 2010
Revised: August 31, 2010
Accepted: September 24, 2010
Published online: October 14, 2010

### References

1. Keene, A.C., and Waddell, S. (2007). Drosophila olfactory memory: Single genes to complex neural circuits. Nat. Rev. Neurosci. *8*, 341–354.
2. Heisenberg, M., Heusipp, M., and Wanke, C. (1995). Structural plasticity in the Drosophila brain. J. Neurosci. *15*, 1951–1960.
3. Barth, M., and Heisenberg, M. (1997). Vision affects mushroom bodies and central complex in Drosophila melanogaster. Learn. Mem. *4*, 219–229.
4. Withers, G.S., Fahrbach, S.E., and Robinson, G.E. (1993). Selective neuroanatomical plasticity and division of labour in the honeybee. Nature *364*, 238–240.
5. Durst, C., Eichmüller, S., and Menzel, R. (1994). Development and experience lead to increased volume of subcompartments of the honeybee mushroom body. Behav. Neural Biol. *62*, 259–263.

Please cite this article in press as: Kremer et al., Structural Long-Term Changes at Mushroom Body Input Synapses, Current Biology (2010), doi:10.1016/j.cub.2010.09.060



6. Yasuyama, K., Meinertzhagen, I.A., and Schürmann, F.W. (2002). Synaptic organization of the mushroom body calyx in Drosophila melanogaster. J. Comp. Neurol. *445*, 211–226.
7. Leiss, F., Groh, C., Butcher, N.J., Meinertzhagen, I.A., and Tavosanis, G. (2009). Synaptic organization in the adult Drosophila mushroom body calyx. J. Comp. Neurol. *517*, 808–824.
8. Su, C.Y., Menuz, K., and Carlson, J.R. (2009). Olfactory perception: Receptors, cells, and circuits. Cell *139*, 45–59.
9. Heimbeck, G., Bugnon, V., Gendre, N., Keller, A., and Stocker, R.F. (2001). A central neural circuit for experience-independent olfactory and courtship behavior in Drosophila melanogaster. Proc. Natl. Acad. Sci. USA *98*, 15336–15341.
10. Wilson, R.I., and Mainen, Z.F. (2006). Early events in olfactory processing. Annu. Rev. Neurosci. *29*, 163–201.
11. Thum, A.S., Jenett, A., Ito, K., Heisenberg, M., and Tanimoto, H. (2007). Multiple memory traces for olfactory reward learning in Drosophila. J. Neurosci. *27*, 11132–11138.
12. Stocker, R.F. (1994). The organization of the chemosensory system in Drosophila melanogaster: A review. Cell Tissue Res. *275*, 3–26.
13. Krofczik, S., Khojasteh, U., de Ibarra, N.H., and Menzel, R. (2008). Adaptation of microglomerular complexes in the honeybee mushroom body lip to manipulations of behavioral maturation and sensory experience. Dev. Neurobiol. *68*, 1007–1017.
14. Seid, M.A., Harris, K.M., and Traniello, J.F. (2005). Age-related changes in the number and structure of synapses in the lip region of the mushroom bodies in the ant Pheidole dentata. J. Comp. Neurol. *488*, 269–277.
15. Yasuyama, K., Kitamoto, T., and Salvaterra, P.M. (1995). Immunocytochemical study of choline acetyltransferase in Drosophila melanogaster: An analysis of cis-regulatory regions controlling expression in the brain of cDNA-transformed flies. J. Comp. Neurol. *361*, 25–37.
16. Schulz, R.A., Chromey, C., Lu, M.F., Zhao, B., and Olson, E.N. (1996). Expression of the D-MEF2 transcription in the Drosophila brain suggests a role in neuronal cell differentiation. Oncogene *12*, 1827–1831.
17. Schwaerzel, M., Heisenberg, M., and Zars, T. (2002). Extinction antagonizes olfactory memory at the subcellular level. Neuron *35*, 951–960.
18. Riemensperger, T., Völler, T., Stock, P., Buchner, E., and Fiala, A. (2005). Punishment prediction by dopaminergic neurons in Drosophila. Curr. Biol. *15*, 1953–1960.
19. Krashes, M.J., Keene, A.C., Leung, B., Armstrong, J.D., and Waddell, S. (2007). Sequential use of mushroom body neuron subsets during drosophila odor memory processing. Neuron *53*, 103–115.
20. Grauso, M., Reenan, R.A., Culetto, E., and Sattelle, D.B. (2002). Novel putative nicotinic acetylcholine receptor subunit genes, Dalpha5, Dalpha6 and Dalpha7, in Drosophila melanogaster identify a new and highly conserved target of adenosine deaminase acting on RNA-mediated A-to-I pre-mRNA editing. Genetics *160*, 1519–1533.
21. Leiss, F., Koper, E., Hein, I., Fouquet, W., Lindner, J., Sigrist, S., and Tavosanis, G. (2009). Characterization of dendritic spines in the Drosophila central nervous system. Dev. Neurobiol. *69*, 221–234.
22. Kittel, R.J., Wichmann, C., Rasse, T.M., Fouquet, W., Schmidt, M., Schmid, A., Wagh, D.A., Pawlu, C., Kellner, R.R., Willig, K.I., et al. (2006). Bruchpilot promotes active zone assembly, Ca2+ channel clustering, and vesicle release. Science *312*, 1051–1054.
23. Fouquet, W., Owald, D., Wichmann, C., Mertel, S., Depner, H., Dyba, M., Hallermann, S., Kittel, R.J., Eimer, S., and Sigrist, S.J. (2009). Maturation of active zone assembly by Drosophila Bruchpilot. J. Cell Biol. *186*, 129–145.
24. Schmid, A., Hallermann, S., Kittel, R.J., Khorramshahi, O., Frölich, A.M., Quentin, C., Rasse, T.M., Mertel, S., Heckmann, M., and Sigrist, S.J. (2008). Activity-dependent site-specific changes of glutamate receptor composition in vivo. Nat. Neurosci. *11*, 659–666.
25. Tanaka, N.K., Awasaki, T., Shimada, T., and Ito, K. (2004). Integration of chemosensory pathways in the Drosophila second-order olfactory centers. Curr. Biol. *14*, 449–457.
26. Ito, K., Suzuki, K., Estes, P., Ramaswami, M., Yamamoto, D., and Strausfeld, N.J. (1998). The organization of extrinsic neurons and their implications in the functional roles of the mushroom bodies in Drosophila melanogaster Meigen. Learn. Mem. *5*, 52–77.
27. Jefferis, G.S., Vyas, R.M., Berdnik, D., Ramaekers, A., Stocker, R.F., Tanaka, N.K., Ito, K., and Luo, L. (2004). Developmental origin of wiring specificity in the olfactory system of Drosophila. Development *131*, 117–130.
28. Lin, H.H., Lai, J.S., Chin, A.L., Chen, Y.C., and Chiang, A.S. (2007). A map of olfactory representation in the Drosophila mushroom body. Cell *128*, 1205–1217.
29. Nitabach, M.N., Blau, J., and Holmes, T.C. (2002). Electrical silencing of Drosophila pacemaker neurons stops the free-running circadian clock. Cell *109*, 485–495.
30. Gouwens, N.W., and Wilson, R.I. (2009). Signal propagation in Drosophila central neurons. J. Neurosci. *29*, 6239–6249.
31. Martín-Peña, A., Acebes, A., Rodríguez, J.R., Sorribes, A., de Polavieja, G.G., Fernández-Fúnez, P., and Ferrús, A. (2006). Age-independent synaptogenesis by phosphoinositide 3 kinase. J. Neurosci. *26*, 10199–10208.
32. Budnik, V., Zhong, Y., and Wu, C.F. (1990). Morphological plasticity of motor axons in Drosophila mutants with altered excitability. J. Neurosci. *10*, 3754–3768.
33. Wagh, D.A., Rasse, T.M., Asan, E., Hofbauer, A., Schwenkert, I., Dürrbeck, H., Buchner, S., Dabauvalle, M.C., Schmidt, M., Qin, G., et al. (2006). Bruchpilot, a protein with homology to ELKS/CAST, is required for structural integrity and function of synaptic active zones in Drosophila. Neuron *49*, 833–844.
34. Sweeney, S.T., Broadie, K., Keane, J., Niemann, H., and O'Kane, C.J. (1995). Targeted expression of tetanus toxin light chain in Drosophila specifically eliminates synaptic transmission and causes behavioral defects. Neuron *14*, 341–351.
35. Bergquist, S., Dickman, D.K., and Davis, G.W. (2010). A hierarchy of cell intrinsic and target-derived homeostatic signaling. Neuron *66*, 220–234.
36. Loebrich, S., and Nedivi, E. (2009). The function of activity-regulated genes in the nervous system. Physiol. Rev. *89*, 1079–1103.
37. Ganeshina, O., Vorobyev, M., and Menzel, R. (2006). Synaptogenesis in the mushroom body calyx during metamorphosis in the honeybee Apis mellifera: An electron microscopic study. J. Comp. Neurol. *497*, 876–897.
38. Tripodi, M., Evers, J.F., Mauss, A., Bate, M., and Landgraf, M. (2008). Structural homeostasis: Compensatory adjustments of dendritic arbor geometry in response to variations of synaptic input. PLoS Biol. *6*, e260.
39. Hiesinger, P.R., Zhai, R.G., Zhou, Y., Koh, T.W., Mehta, S.Q., Schulze, K.L., Cao, Y., Verstreken, P., Clandinin, T.R., Fischbach, K.F., et al. (2006). Activity-independent prespecification of synaptic partners in the visual map of Drosophila. Curr. Biol. *16*, 1835–1843.
40. Scott, E.K., Reuter, J.E., and Luo, L. (2003). Dendritic development of Drosophila high order visual system neurons is independent of sensory experience. BMC Neurosci. *4*, 14.
41. Berdnik, D., Chihara, T., Couto, A., and Luo, L. (2006). Wiring stability of the adult Drosophila olfactory circuit after lesion. J. Neurosci. *26*, 3367–3376.
42. Wiesel, T.N. (1982). Postnatal development of the visual cortex and the influence of environment. Nature *299*, 583–591.
43. Stieb, S.M., Muenz, T.S., Wehner, R., and Rössler, W. (2010). Visual experience and age affect synaptic organization in the mushroom bodies of the desert ant Cataglyphis fortis. Dev. Neurobiol. *70*, 408–423.
44. Sachse, S., Rueckert, E., Keller, A., Okada, R., Tanaka, N.K., Ito, K., and Vosshall, L.B. (2007). Activity-dependent plasticity in an olfactory circuit. Neuron *56*, 838–850.
45. Devaud, J.M., Acebes, A., and Ferrús, A. (2001). Odor exposure causes central adaptation and morphological changes in selected olfactory glomeruli in Drosophila. J. Neurosci. *21*, 6274–6282.
46. Krashes, M.J., and Waddell, S. (2008). Rapid consolidation to a radish and protein synthesis-dependent long-term memory after single-session appetitive olfactory conditioning in Drosophila. J. Neurosci. *28*, 3103–3113.
47. Colomb, J., Kaiser, L., Chabaud, M.A., and Preat, T. (2009). Parametric and genetic analysis of Drosophila appetitive long-term memory and sugar motivation. Genes Brain Behav. *8*, 407–415.
48. Husch, A., Paehler, M., Fusca, D., Paeger, L., and Kloppenburg, P. (2009). Distinct electrophysiological properties in subtypes of nonspiking olfactory local interneurons correlate with their cell type-specific Ca2+ current profiles. J. Neurophysiol. *102*, 2834–2845.
49. Kloppenburg, P., Ferns, D., and Mercer, A.R. (1999). Serotonin enhances central olfactory neuron responses to female sex pheromone in the male sphinx moth manduca sexta. J. Neurosci. *19*, 8172–8181.
50. Kloppenburg, P., Kirchhof, B.S., and Mercer, A.R. (1999). Voltage-activated currents from adult honeybee (Apis mellifera) antennal motor neurons recorded in vitro and in situ. J. Neurophysiol. *81*, 39–48.

**Current Biology, Volume *20***

# Supplemental Information

# Structural Long-Term Changes

# at Mushroom Body Input Synapses

Malte C. Kremer, Frauke Christiansen, Florian Leiss, Moritz Paehler, Stephan Knapek, Till F.M. Andlauer, Friedrich Forstner, Peter Kloppenburg, Stephan J. Sigrist, and Gaia Tavosanis

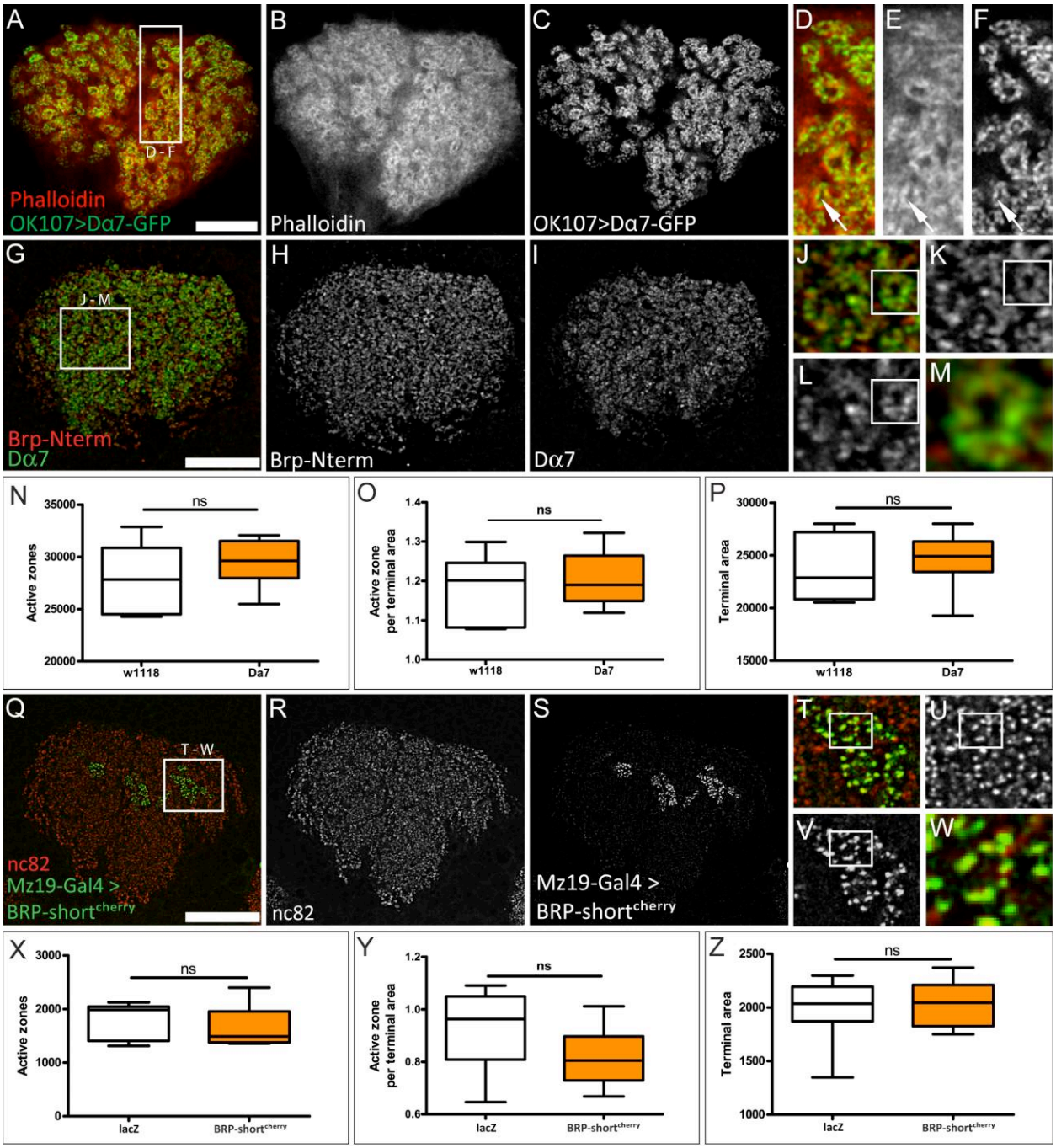


**Figure S1, Related to Figure 1. Specificity of Localization of the MB247-Dα7-GFP and BRP-short$^{cherry}$ Constructs in the Calyx**

(A- C) Dα7-GFP localizes at the actin-rich microglomeruli in the calyx.

(B) In the mushroom body calyx F-actin, detected with fluorescent phalloidin, is enriched in the microglomerular rings. These are formed by multiple Kenyon cell claws [1].

(C) Dα7-GFP nicely highlights the microglomeruli. Here, *UAS-Dα7-GFP* is expressed under the control of *OK107-Gal4*.

(A) Is the merge.

(D- F) Higher magnification of the region highlighted in A. In comparison to the localization of actin, the *Dα7-GFP* construct appears to have a more restricted localization, which is either patchy on the ring or more restricted to the inner rim of the actin-rich ring (arrow), suggesting that this construct is constrained to postsynaptic densities.
(G- I) Endogenous Dα7 closely matches a subset of active zones in the calyx
(H) Localisation of active zones in the calyx revealed by anti-Bruchpilot antibodies (BRP-Nterm, comparable to Nc82 labelling) that highlight all synaptic sites in the calyx, not only the ones within microglomeruli.
(I) Localization of endogenous Dα7 in the calyx.
(G) Is the merge.
(J- L) Higher magnification of the region highlighted in G. Endogenous Dα7 and BRP intermingle at the microglomeruli. This suggests that the localization of the MB247-Dα7-GFP construct closely reflects the localization of endogenous Dα7.
(M) Magnification of a single microglomerulus that is highlighted in J.
(N- P) Comparison of the number of active zones (N), active zone density (O) and terminal area (P) in the calyces of flies either carrying the *MB247-Dα7-GFP* construct (Dα7) or not (w1118). The analysis is based on the nc82 labelling. No alterations can be observed upon expression of *MB247-Dα7-GFP*. Thus, the expression of this construct does not alter the number or the density of active zones. (n= 6 animals per genotype).
(Q- S) Endogenous BRP and BRP-short$^{cherry}$ co- localize within the Mz19-positive boutons.
(R) Identification of active zones in the calyx using the Nc82 antibody to detect endogenous BRP. Note that this antibody does not detect BRP-short$^{cherry}$ .
(S) Localization of BRP-short$^{cherry}$ within Mz19-positive projection neuron boutons.
(Q) Merge.
(T- V) Higher magnification of the region highlighted in Q.
(W) Magnification of the microglomerular region that is highlighted in T.
(X- Z) Comparison of the number of Nc82-positive active zones (X), active zone density (Y) and terminal area (Z) when *UAS-brp-short$^{cherry}$* (brp) or a control construct (*UAS-lacZ*) were expressed under the control of *Mz19-Gal4*. The analysis is based on the Nc82 labelling. No alterations were observed upon expression of *UAS-brp-short$^{cherry}$*, signifying that this construct does not alter the number or density of active zones. (*lacZ n= 8; brp-short$^{cherry}$* n= 7 animals). Scale bar= 10 μm in all images.

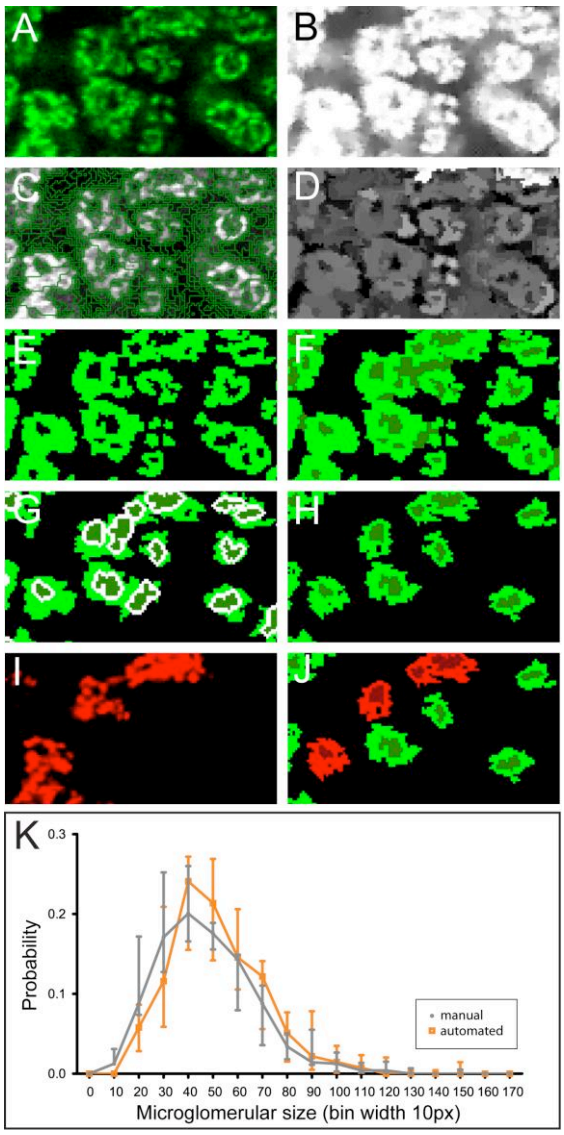


**Figure S2, Related to Figure 3. Detailed Illustration of the Automated Detection of Microglomeruli in Optical Sections of the Calyx**

(A) Example of one small area from a typical optical section used for the automated detection (section used corresponds to Fig. 3A, D, boxed region). Only the green channel was used for identification of the microglomeruli.

(B) The original image was filtered with an anisotropic filter and contrast was enhanced.

(C) Initial segmentation of the entire image was performed utilizing only the green channel image. Pixels were grouped into objects (outlined in green) including pixels with similar intensity values in both original and filtered images.

(D) The contrast of each object to adjacent objects was computed.

(E) A threshold was used to assign the brightest objects of this contrast map as candidate objects for microglomerular rings (dark green).

(F) A second threshold was used to assign the darkest objects as candidate objects lumen (light green). Objects of intermediate contrast were classified as calycal area, not included in microglomeruli (black).
(G) A number of criteria were used to exclude some of the candidate objects for both ring and lumen. These criteria included size and shape criteria as well as the constraint that lumen objects need to share a border with ring objects and vice versa, as described in the Supplemental Materials and Methods. The remaining lumen objects were enclosed by rings of two pixels width (white).
(H) The average brightness of each of these two pixels wide rings was determined and adjacent pixels were included into the ring as long as their brightness did not differ from the average brightness of the ring by more than 10%. This step thus allowed determining the outer border of microglomerular rings using local thresholds (light green rings). It is important to note that each of the lumina (dark green) and their surrounding rings (light green) were independent objects.
(I) In parallel, the BRP-short$^{cherry}$ signal was determined in the red channel image and objects representing active zones were created.
(J) Microglomeruli identified in the green channel image that colocalize with the independently generated objects in the red channel image are classified as Mz19-positive microglomeruli (light red/dark red). Parameters such as size, shape and number were determined utilizing the green channel image only.
(K) Comparison of the size distribution of microglomeruli detected manually (grey) or by the software (orange) in the same optical sections (n of calyces= 5). After detection, the measurement of the microglomerular size was done manually in both cases. Medians and interquartile range are presented. Comparison of the relative size distribution frequencies with Wilcoxon Matched Pairs Test revealed no significant difference between manual and automated microglomerular identification (mean $p > 0.5$).

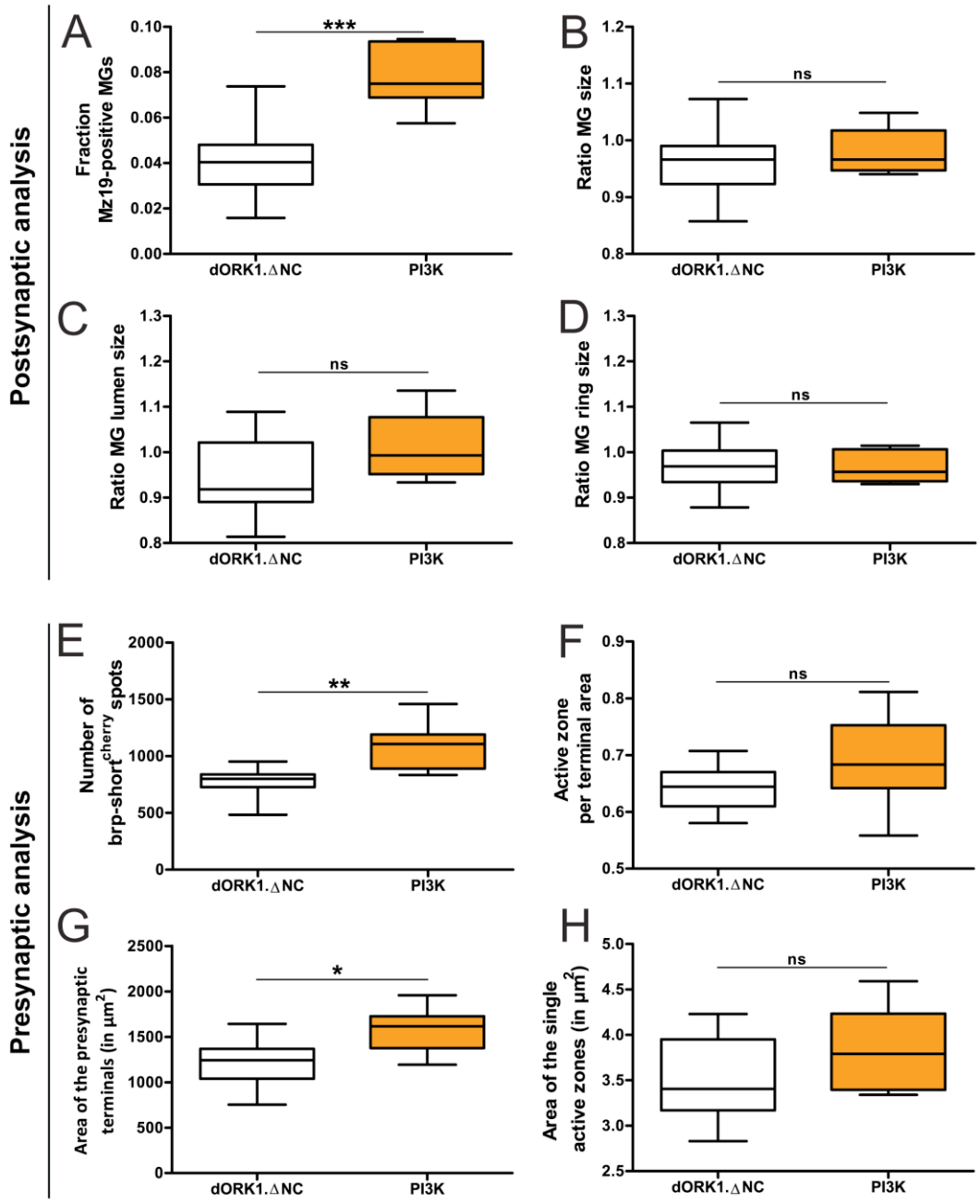


**Figure S3, Related to Figure 3. Overexpression of PI3K in the Mz19-Positive Projection Neurons Leads to Measurable Alterations of Microglomerular Number**

*PI3K* overexpression led to increased axonal diameter and number of boutons produced by ellipsoid body projection neurons [2]. We hypothesized that it might have a similar effect on olfactory projection neurons in the calyx. Thus, to test whether our approach allowed detecting alterations in structure or number of microglomeruli, we expressed wild-type *PI3K* under the control of *Mz19-Gal4*.

(A) We found that the fraction of Mz19-positive microglomeruli was clearly increased upon *PI3K* overexpression with *Mz19-Gal4* ($p < 0.001$, ANOVA with Bonferroni's correction). The average percentage of Mz19-positive microglomeruli per calyx is shown.
(B) However, *PI3K* overexpression did not cause significant changes in the relative size of the microglomeruli ($p > 0.05$, ANOVA with Bonferroni's correction). The relative size (ratio MG size) is the ratio between the average sizes of Mz19-positive and Mz19-negative microglomeruli per calyx.
(C- D) Overexpression of *PI3K* caused non-significant modifications of lumen and ring size. Statistics are described in the Materials and Methods and in the results. (n= 7-11 animals per genotype).
(E) The absolute number of BRP-short$^{cherry}$-labelled active zones identified as represented in Fig. 4C is clearly increased upon overexpression of *PI3K* ($p < 0.01$, Kruskal-Wallis test with Dunn's correction).
(F) Overexpression of *PI3K* did not alter the presynaptic active zone density ($p > 0.05$, Kruskal-Wallis test with Dunn's correction).
(G) The total terminal area is increased significantly upon *PI3K* overexpression.
(H) The area of active zones, as represented in Fig. 4E, is not significantly modified. Statistics are described in the Materials and Methods and in the results. (n= 9- 10 animals per genotype).
Taken together, we suggest that this manipulation mainly determines cell morphological changes in the olfactory projection neurons, namely an increase in the number of boutons. Thus, we could genetically induce detectable alterations in the number of Mz19-positive microglomeruli.

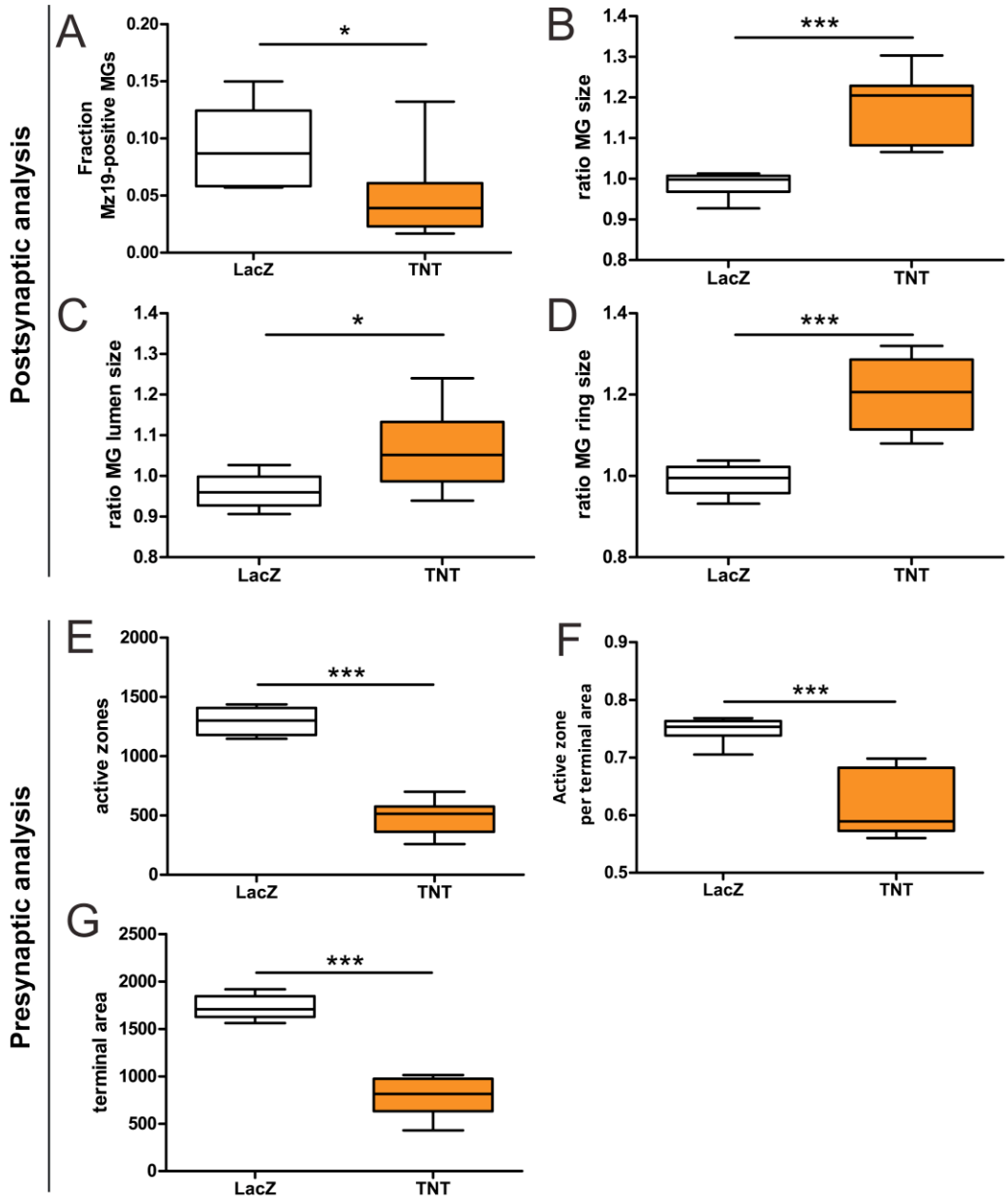


**Figure S4, Related to Figure 4. Size and Active Zone Density of Microglomeruli Depend on Synaptic Transmission**

Hyperpolarization, decreased input resistance and subsequent suppression of action potential firing should block action potential evoked synaptic transmission, but might also have additional effects. Hence, we asked whether a reduction in synaptic transmission was able to explain the effects observed after suppression of action potentials in projection neurons. Thus, we expressed tetanus toxin (*UAS-TNT*) that blocks vesicle fusion, under the control of *Mz19-Gal4* [3].

(A) In strong contrast to the effect caused by *dORK1.ΔC* expression the fraction of Mz19-positive microglomeruli was slightly, but significantly reduced upon expression of the *UAS-TNT* construct with *Mz19-Gal4* in comparison to the control construct *UAS-LacZ*. ($p < 0.05$, t-test).

(B- D) Upon expression of *TNT* with *Mz19-Gal4* the relative size ($p< 0.001$, t-test with Welch's correction) (B), the relative lumen size (C) and the relative ring size (D) of Mz19-positive microglomeruli increased in comparison to Mz19-positive microglomeruli expressing the control construct *UAS-LacZ*. Since this result was similar to the effect of silencing the presynaptic neurons with *dORK1.ΔC* (Fig. 3F-H), alterations of the synaptic complex size might be caused by the loss of synaptic transmission in both situations. (A- D n= 8-11 animals per genotype).
(E) The absolute number of BRP-short$^{cherry}$-labeled active zones identified as represented in Fig. 4 is clearly decreased upon expression of *TNT* ($p< 0.001$, t-test).
(F, G) A significant decrease of active zone density ($p< 0.001$, Mann-Whitney test) (F), as well as of the total terminal area (G) is obtained upon expression of *TNT*. (n= 7-9 animals per genotype). Statistics are described in the Materials and Methods.
To address the effect of manipulations of activity during adult life only, we expressed a temperature-sensitive allele of *shibire* (*shi*) or *dTRPA1* in the Mz19-positive projection neurons [4-5]. Nonetheless, *Mz19-Gal4* turned out to be unexpectedly lethal even at the permissive T ($18^0$C) in combination with various *shi$^{ts}$* insertions (with multiple insertions on X and 3$^{rd}$ from [4]; or with a single insertion on the 3$^{rd}$, T. Preat, unpublished). Furthermore, a protocol in which dTRPA1 was expressed in the Mz19-positive projection neurons and adult fly males were kept at $30^0$C during the first week after eclosion did not elicit modifications of microglomerular organization at day 7 post-eclosion. It remains unclear whether sustained modifications of projection neuron activity are elicited using this protocol. Taken together, future experiments will be required to address the effect of modulation of projection neuron activity selectively during adult life.

**Supplemental Experimental Procedures**

*Electrophysiology Detailed Methods*

We used an intact brain preparation by modifying preparations described previously [6-8]. Adult males, seven days post-eclosion, were cold-anesthetized and pinned dorsal side down in a Sylgard-coated (Dow Corning Corp., Midland, Michigan, USA) dish with cactus spines (*Opuntia chlorotica*). The proboscis, head capsule and the perineural sheath around the mushroom bodies were removed with fine forceps under 'normal extracellular saline' (see below). The intact brain was pinned in a Sylgard-coated recording chamber with fine cactus spines (*Opuntia microdasys*) through the perineural sheath around the optic lobes.

For the recordings, the somata of the projection neurons were visualized with a fixed stage upright microscope (BX51WI, Olympus, Hamburg, Germany) using a 60x water immersion objective (LUMplan FI/IR; 0.9 numerical aperture; 2 mm working distance; Olympus) with infrared-differential interference contrast (IR-DIC; [9]) and fluorescence optics. Projection neurons expressing *UAS-mCD8GFP* and *UAS-dORK.DC* or *UAS-dORK.DNC* under the control of *Mz19-Gal4* were identified by their GFP fluorescence that was visualized using a Chroma 41001 filter set (EX: HQ480/40x, BS: Q505LP, EM: HQ535/50m, Chroma, Rockingham, VT).

Whole-cell recordings were performed at 24 °C following the methods described by [10]. Electrodes with tip resistances between 7-9 MΩ were fashioned from borosilicate glass (0.86 mm inner diameter, 1.5 mm outer diameter, GB150-8P, Science Products, Hofheim, Germany) with a vertical pipette puller (PP-830; Narishige, London, UK). For current-clamp recordings the pipettes were filled with intracellular saline containing (in mM): 115 K-aspartate, 10 NaCl, 1 $CaCl_2$, 2 $MgCl_2$, 10 HEPES and 10 EGTA adjusted to pH 7.2 (with KOH), resulting in an osmolarity of approximately 265 mOsm. During the experiments the cells were superfused constantly with normal extracellular saline containing (in mM): 100 NaCl, 4 KCl, 6 $CaCl_2$, 2 $MgCl_2$, 10 HEPES, 35 glucose adjusted to pH 7.2 (with NaOH), resulting in an osmolarity of approximately 280 mOsm. Whole-cell current-clamp recordings were performed with an EPC9 patch-clamp amplifier (HEKA-Elektronik, Lambrecht, Germany) controlled by the program Pulse (version 8.63, HEKA-Elektronik) running under Windows. Electrophysiological data were sampled at intervals of 100 µs (10 kHz). The recordings were low pass filtered at 2 kHz with a 4-pole Bessel-Filter. Compensation of the offset potential and capacitive currents was performed using the 'automatic mode' of the EPC9 amplifier. The calculated liquid junction potential between intracellular and extracellular solution (14.6 mV) was also compensated. It was calculated with the Patcher's Power Tools plug-in (from http://www.mpibpc.gwdg.de/abteilungen/140/software/index.html) for Igor Pro (Wavemetrics, Portland, Oregon). Stimulus protocols used for each set of experiments are provided in Results. Action potential parameters were analyzed using the NeuroMatic plug-in for Igor Pro (Jason Rothman, http://www.neuromatic.thinkrandom.com/index.html). General data analysis was performed with Igor Pro 6 (Wavemetrics) and Sigma Stat (version 3.1; Systat Software Inc., San Jose, CA, USA). Data are given as mean ± SD. To determine differences in

means between cells types unpaired Student's *t* tests were performed. A significance level of 0.05 was accepted for all tests.

To label single cells, 1% biocytin (B4261, Sigma) was added to the pipette solution. After the recordings, the brains were fixed in Roti-Histofix (P0873, Carl Roth, Karlsruhe, Germany) containing 0.1% Triton-X100 (Serva, Heidelberg, Germany) for 1-2 h at 4 °C and rinsed in 0.1 M Tris-HCl buffered solution (TBS, pH 7.2, 3 x 10 min, RT). The brains were incubated for at least 12 h in *Alexa Fluor 633* (Alexa 633) conjugated streptavidin (1:600, 4 °C, S21375, Molecular Probes, Eugene, OR) that was dissolved in TBS containing 1% normal goat serum (S-1000, Vector Labs, Burlingame, CA). Brains were rinsed in TBS (3 x 10 min, 4 °C) and mounted in 50% glycerol (A3092, AppliChem, Darmstadt, Germany). Images of the whole-mount preparation were captured with a confocal microscope (LSM 510, Carl Zeiss, Göttingen, Germany) equipped with a Plan-Apochromat 20x (0.75 NA) objective. Streptavidin-Alexa 633 was imaged with 633 nm excitation and emission was collected through a 650 nm LP filter. Scaling, contrast enhancement and z-projections were performed using ImageJ v1.42o with the WCIF plug-in bundle (www.uhnresearch.ca/facilities/wcif/). Single labelled neurons were reconstructed in Amira 4.1 (Mercury Computer Systems, San Diego, CA USA). The final figures were prepared with Photoshop and Illustrator CS4 (Adobe Systems Incorporated, San Jose, CA, USA).

All chemicals used for these experiments, were obtained from Applichem (Darmstadt, Germany) or Sigma-Aldrich (Taufkirchen, Germany) in 'pro analysis' purity grade, unless stated otherwise.

*Image Analysis*

*Microglomeruli Identification and Quantification*

ImageJ was used for pre-processing the images. The images were filtered using a custom macro including smoothing and contrast enhancement filters to enhance presynaptic puncta (BRP-short$^{cherry}$ channel) and with an anisotropic diffusion 2D filter to enhance ring-like structures (D$\alpha$7-GFP channel). Smoother D$\alpha$7-GFP rings were obtained including information from adjacent sections. Contrast was enhanced on both D$\alpha$7-GFP and BRP-short$^{cherry}$ channels. Filtered images were only used for object recognition; all actual measurements were done on the original images. Definiens image analysis software (Definiens, Germany) was used for all quantitative measurements (Fig. S2A- K). Images were imported as multilayered files containing original images and filtered images. The D$\alpha$7-GFP signal was used for object recognition, while the BRP-short$^{cherry}$ signal was solely used to distinguish between Mz19-positive and Mz19-negative microglomeruli. Candidate objects for microglomerular rings were generated through two steps: first, pixels with similar intensity properties were grouped into objects and, second, the objects were selected using the contrast to neighbour objects, their shape and size. Microglomerular lumen candidate objects were defined as darker objects included within a microglomerular ring. The following criteria were used to exclude lumen candidate objects from the analysis: Objects smaller than 0.38 $\mu m^2$ or larger than 1.7 $\mu m^2$, objects with a difference between the radius of the smallest enclosing and the largest enclosed ellipse of more than

0.025 $\mu m^2$ and objects with a relative border to ring objects of less than 60%. Ring candidate objects were excluded from the analysis if they were not in contact with a lumen object or had an average brightness in the GFP channel of less than 80. Microglomeruli were defined as the sum of microglomerular rings (contacting microglomerular lumina) and microglomerular lumina. To determine the exact shape of postsynaptic rings each microglomerular lumen was surrounded by a ring of two pixels width. The average intensity of the D$\alpha$7 signal was computed for each of these rings individually and adjacent candidate pixels were included only if their intensity was at least 90% of the ring's average intensity. Microglomerular structures were assigned as either mz19 positive or negative based on the presence or absence of colocalizing BRP-short$^{cherry}$ signal (Fig. 3A- D, Fig. S2A- J).

The performance of the software was tested by comparing manual and automated identification (Fig. S2K). Confocal stacks of five calyces from different animals were evaluated using ImageJ. The Mz19-positive microglomeruli in each calyx were manually counted and their sizes were measured using the ImageJ measurement tool. We then run the above described automated analysis on the same data set and manually compared in each optical section which microglomeruli were identified by hand and which ones by the software. We performed this comparison on different versions of the software. We finally decided to opt for software parameters that allowed the detection of more than 30% of all manually identified Mz19-posititve microglomeruli (Fig. S2K) and included only 3% false positives. We then tested whether the population of microglomeruli detected by the software with these stringent parameters would represent the overall population of Mz19-positive microglomeruli. We thus generated histogram plots of the size distribution of the manually- and software-detected microglomeruli (Fig. S2K). These showed that software-based identification of microglomeruli gives a good representation of the manually detected ones. In fact, there are no significant differences over the entire size distribution.

We note that the D$\alpha$7-GFP signal was patchier in brains of just eclosed males. For this reason the microglomerular rings were poorly defined at these early stages. Therefore, detection of microglomeruli in brains of just eclosed animals was not reliable both manually or using the software that we developed.

*Identification and Measurement of the Presynaptic Active Zones*

For the analysis of the presynaptic active zones of the relevant projection neurons only the BRP-short$^{cherry}$ channel was processed in the same set of images used for the above-described analysis. All scans were processed as 8 bit tiff stacks. The images were not filtered. Tiff stacks were then analyzed with Imaris x 64 v6.1.5 software (Bitplane AG, Zurich, CH). The segmentation of single BRP-short spots was conducted semi-automatically with optimized parameters of the "seed detection" and "region growing" algorithms. To calculate the surface area of the parts of the calyx innervated by Mz19-positive active zones, the "surface tool" was adjusted and applied to all calyces. The total terminal area is defined as the surface area of a 3D reconstruction of the complete Mz19-positive signal in all optical sections within one calyx. All tools used for our analysis are included in the "MeasurementsPro" extension of Imaris and the

analysis is based on manually adjusted intensity-thresholds. The number of spots and the surface area of each detected active zone were calculated in Imaris and transferred to GraphPad Prism 4 software for statistical analysis.

**Supplemental References**


1. Leiss, F., Groh, C., Butcher, N.J., Meinertzhagen, I.A., and Tavosanis, G. (2009). Synaptic organization in the adult Drosophila mushroom body calyx. J Comp Neurol *517*, 808-824.
2. Martin-Pena, A., Acebes, A., Rodriguez, J.R., Sorribes, A., de Polavieja, G.G., Fernandez-Funez, P., and Ferrus, A. (2006). Age-independent synaptogenesis by phosphoinositide 3 kinase. J Neurosci *26*, 10199-10208.
3. Sweeney, S.T., Broadie, K., Keane, J., Niemann, H., and O'Kane, C.J. (1995). Targeted expression of tetanus toxin light chain in Drosophila specifically eliminates synaptic transmission and causes behavioral defects. Neuron *14*, 341-351.
4. Kitamoto, T. (2001). Conditional modification of behavior in Drosophila by targeted expression of a temperature-sensitive shibire allele in defined neurons. J Neurobiol *47*, 81-92.
5. Hamada, F.N., Rosenzweig, M., Kang, K., Pulver, S.R., Ghezzi, A., Jegla, T.J., and Garrity, P.A. (2008). An internal thermal sensor controlling temperature preference in Drosophila. Nature *454*, 217-220.
6. Kloppenburg, P., Ferns, D., and Mercer, A.R. (1999). Serotonin enhances central olfactory neuron responses to female sex pheromone in the male sphinx moth manduca sexta. J Neurosci *19*, 8172-8181.
7. Kloppenburg, P., Kirchhof, B.S., and Mercer, A.R. (1999). Voltage-activated currents from adult honeybee (Apis mellifera) antennal motor neurons recorded in vitro and in situ. J Neurophysiol *81*, 39-48.
8. Husch, A., Paehler, M., Fusca, D., Paeger, L., and Kloppenburg, P. (2009). Distinct electrophysiological properties in subtypes of nonspiking olfactory local interneurons correlate with their cell type-specific Ca2+ current profiles. J Neurophysiol *102*, 2834-2845.
9. Dodt, H.U., and Zieglgansberger, W. (1990). Visualizing unstained neurons in living brain slices by infrared DIC-videomicroscopy. Brain Res *537*, 333-336.
10. Hamill, O.P., Marty, A., Neher, E., Sakmann, B., and Sigworth, F.J. (1981). Improved patch-clamp techniques for high-resolution current recording from cells and cell-free membrane patches. Pflugers Arch *391*, 85-100.

# 6. A SYD-1 HOMOLOGUE REGULATES PRE- AND POSTSYNAPTIC MATURATION IN *DROSOPHILA*

# 7. GENERAL DISCUSSION

The recent progress in understanding the neuronal network for learning and memory in *Drosophila* has been impressive: the identities of many neurons involved in learning and memory, and even in different subtypes of learning and memory, have been deciphered (Davis, 2011). The mushroom bodies (MBs), higher integration centers in the brain, play a major role in storing and retrieving memories (Heisenberg, 2003; Perisse et al., 2013). Also some non-MB cells (MB extrinsic cells) can mediate learning and memory (Thum et al., 2007; Neuser et al., 2008; Chen et al., 2012). The principal MB-intrinsic cells are called Kenyon cells (KCs). It has become clear that different types of KCs are important for different phases of memory (Dubnau and Chiang, 2013). However, synaptic connectivity in the MBs is still not understood sufficiently. Moreover, the molecular architecture of synapses in the MBs has not yet been described in detail. We addressed both of these questions in the MB calyx of *Drosophila melanogaster* by examination of synaptic connectivity, protein architecture at presynaptic active zones (AZs: sites of neurotransmitter release) and, in addition, the extent of activity-dependent modulation at MB input synapses. This work resulted in the identification of a novel synapse population and in the first description of synaptic plasticity at MB input synapses.

The MBs are anatomically distinct neuropils of great interest to neurobidogists: they are involved in several higher cognitive functions, such as olfactory learning, sleep/wake behavior, visual learning, courtship conditioning and decision-making (Perisse et al., 2013;Liu et al., 1999; McBride et al., 1999; Joiner et al., 2006; Pitman et al., 2006; Yang et al., 2008; Miller et al., 2011). First and foremost, MBs are a major component of the olfactory circuitry. In the olfactory circuitry, olfactory receptor neurons (ORNs) convey sensory information from antennae and maxillary palps to the primary olfactory relay, the antennal lobes (ALs; Stocker et al., 1983). From there, projection neurons (PNs) transmit the olfactory information further to secondary centers, such as the MBs. The MBs receive olfactory input in a substructure named calyx, where PNs contact the dendrites of KCs (Yasuyama et al., 2002; Ramaekers et al., 2005). At the level of KCs, connectivity seizes to be easy to follow. In insects, various neurons contacting the MBs have been identified (Tanaka et al., 2008; Liu and Davis, 2009; Burke et al., 2012); they modulate information processing in MBs and connect the MBs to other brain areas. The identity of these neurons is intensely discussed in the field. Both, the localization of PN axons (Jefferis et al., 2007) and of dendritic projections of KCs in the calyx, have been

described (Zhu et al., 2003; Tanaka et al., 2004; Lin et al., 2007). However, the exact connectivity patterns could not yet be determined reliably.

In particular, little attention has been paid to the protein architecture of presynaptic AZs in MBs, even though better knowledge of the protein composition at AZs could shed light on functional properties of this neuropil.

So far, synaptic plasticity had not been observed in the calyx, despite reports that this neuropil can show morphological differences upon changes in activity (reviewed by Groh and Meinertzhagen, 2010). We were eager to reconcile these findings and therefore investigated whether the morphological changes could, to some extent, be due to synaptic plasticity.

## 7.1 Evidence for the existence of KC-derived presynapses in the mushroom body calyx

Previously, KCs were believed to be exclusively presynaptic in the calyx, the input region for olfactory information to MBs (Yasuyama et al., 2002). Nevertheless, we observed presynapses of KCs in the MB calyx. We discovered these KC presynapses by using the AZ-marker Bruchpilot-short (BRP-short); this tool was created in our lab to enable us to study AZs and in order to assign AZs to particular neuron populations (Schmid et al., 2008). We verified this observation with several independent approaches: We employed different KC-specific GAL4 lines and several transgenic constructs of presynaptic markers (Christiansen et al., 2011, Fig. 7A-O). Only one of these GAL4 lines did not produce a presynaptic signal in the calyx: *c305*-GAL4, driving expression in the KC-subset of α′/β′ neurons (Christiansen et al., 2011, Fig. 7E,F). In addition, we could confirm the presence of KC presynapes in the calyx by RNA interference: expression of the construct *UAS-brp-RNAi*, directed against BRP (Wagh et al., 2006), in KCs reduced BRP-levels in the calyx by 20%-30% (Christiansen et al., 2011, Fig. 1H-G and 2H-Q; quantification Fig. 3 and Table 1). In view of these data, we concluded that KCs form presynaptic AZs within the calyx and named these presynapses KC-derived AZs in the calyx, or KCACs. Our findings are supported by data from two previous studies (Rolls et al., 2007; Pauls et al., 2010), which reported the presence of Synaptobrevin, a presynaptic vesicle protein, in KCs within the calyx.

Of note, the existence of KCACs changes the previous view on the calyx as simple relay neuropils, where information is merely passed on from PNs to KCs. The large number of

KCACs indicates that KCs not only receive sensory information and transport it further to other parts of the MB neuropil; by contrast, KCs are in fact a major component of the local calycal microcircuitry: KCACs enable them to give lateral input to other cells and thereby influence information processing. Feedback from KCs could help shaping responses to sensory information by either expanding or constricting signals. In this manner, responses to odors could be either generalized or specified.

## 7.2 Mixed neurite identities in insect neuropils

The existence of KCACs is not surprising *per se*, as insect neurons may contain neurites of mixed identity (Watson, 1988). For example, Bassem Hassan and colleagues made the observation that at least four independent neuron populations express presynapses within their dendrites and contact other dendrites of the same neuron population (Nicolai et al., 2010). However, all cells they examined were bilaterally symmetrical neurons that cross or end at the midline. The authors speculated that by these means commissural neurons might exchange synaptic information across the two brain hemispheres. Furthermore, anatomical studies have demonstrated that PNs contain pre- and postsynapses in the ALs (Malun, 1991; Sun et al., 1997). Electrophysiological studies revealed reciprocal connections between PNs and local neurons (LNs) in the ALs in *Drosophila* (Huang et al., 2010; Yaksi and Wilson, 2010). In addition, PNs appear to be interconnected most likely by mixed chemical and electrical synapses in *Drosophila* (Kazama and Wilson, 2009). Moreover, Yasuyama et al. 2002 described axons with presynaptic specializations onto PN boutons in the calyx of *Drosophila*; they assumed that these belong to GABAergic neurons, based on anti-GABA stainings (GABA-immunoreactivity). This implicates that PNs express postsynapses next to their numerous presynapses in the calyx. Taken together, many different types of neurons within the central nervous system of insects - also in the olfactory nervous system - express both, input and output snyapses on their dendrites and / or axons. KCs with KCACs on their dendrites do thus not make an exception.

## 7.3 Input and output regions within Kenyon cells

We have provided evidence that KC dendrites are organized into discrete subdomains, containing either AZs or PSDs (Christiansen et al., 2011, Fig. 6I-M). For this purpose, we used the MARCM technique [mosaic analysis with a repressible cell marker (Lee et al., 1999)]; this method allows for temporal and spatial restriction of GAL4-mediated expression of transgenes. We used this technique to express both, GFP and either a presynaptic (UAS-brp-short$^{cherry}$) or a postsynaptic marker (UAS-dα7$^{cherry}$) in single KCs to examine the arrangement of KC pre- or postsynapses, respectively. We observed a preferential localization of postsynapses within claw-like endings and in fine terminal branches of KCs (Christiansen et al., 2011, Fig. 6I,J). The presynapses, by contrast, were distributed primarily along the neurites, mostly separated from the KC terminals (Christiansen et al., 2011, Fig. 6K,L). Therefore, it appears likely that pre- and postsynaptic domains can be present within the same KC dendrite, but in spatially separated sections.

In the ALs of *Periplaneta americana*, pre- and postsynapses of PNs are concentrated in different regions of PN fibers (Malun, 1991). Most presynapses localize to the thick parts of PNs, close to the entrance into the glomeruli they innervate. The postsynapses accumulate in the region of fine terminal branches of PNs. Consistent with these findings in *P. americana*, input and output synapses of PNs in the ALs of *Manduca sexta* are clearly segregated in different regions of the neurites within a glomerulus (Sun et al., 1997). The branches with a larger diameter exhibit numerous output synapses, whereas the fine branches receive input. Our findings indicate that a similar scenariowas present at the KC neurites in the calyx of *Drosophila*. The presynapses primarily resided along the thicker proximal parts and the postsynapses accumulated on the distal terminal branches and claws of the KC neurites.

## 7.4 Different, not necessarily mutually exclusive connection scenarios

At this point, we wondered which cells might be postsynaptic to KCs in the calyx and what the purpose of these synapses is. After a detailed confocal analysis, we assumed that

the KCs contact a neuron or a neuron population that innervates the complete calyx. This is due to the high number and broad distribution of KCACs within the calyx. Therefore we speculate that PNs, KCs and GABAergic fibers are the potential candidates for being postsynaptic partners of KCACs. Projections of these three cell populations cover the whole calyx (Yasuyama et al., 2002). Of course it remains possible that KCACs contact other neurons, or, not unlikely, several different neuron types.

### 7.4.1 KCs as postsynaptic partners

Axodendritic KC::KC contacts in the calyx are well feasible. In the adult fly, KC dendrites run in a parallel fashion through the outer layer of the calyx (data not shown). We suppose this layer to be equivalent to the "fibrous outer layer" described in Yasuyama et al., 2002. KCACs accumulate here stronger than in other parts of the calyx (Christiansen et al., 2011, Fig. 2 C,D). Nonetheless, KCACs are also frequently present in the inner regions of the calyx. The inner part is described as the "glomerular region" in Yasuyama et al. and is densely innervated by KC neurites, as well. This physical proximity of KCs *per se* might enable numerous synaptic contacts between them.

KCs are third-order neurons in the hierarchy of the olfactory nervous system in insects. As mentioned, the architecture of the olfactory pathway in mammals and insects is remarkably similar (Fig. 1). Interestingly, the third-order neurons of the olfactory nervous system in mammals, the pyramidal cells, are interconnected. The majority of synapses in the neocortex are recurrent synapses between pyramidal neurons (Braitenberg and Schüz, 1998).

Recurrent KC::KC synapses in the calyx could strengthen or weaken additional olfactory input to the MBs by stimulating or inhibiting other KCs in the calyx. They would thereby influence the impact of olfactory input. A KC receives on average input from only 3-4 presynapses of one bouton (Butcher et al., 2012) and the firing thresholds of KCs are high (Turner et al., 2008), which implies a need for input amplfication (Turner et al., 2008). If KCs were excitatory, they could shift the membrane potential of other KCs to a level transiently closer to the firing threshold and thereby make them more sensitive for incoming information via KCACs. However, KCACs could also help fine-tuning KCs: Glen Turner and colleagues suggest that all KCs of a subtype share physiological similarities. They found a trend for tuning widths to decrease from $\alpha'/\beta'$ to $\alpha/\beta$ to $\gamma$ KCs (Turner et al., 2008). Hence, KCs could be tuned within each subtype via KCACs. The third possibility is that KCACs inhibit other KCs laterally. Such inhibition might be required in order to prevent saturation of the responses of KCs, when a large amount of olfactory input arrives in the calyx. Moreover inhibition of other KCs could favor certain odors over others as a consequence of learning.

KC::KC synapses might also exist in other parts of the MBs, for example in the peduncle. However, this finding would not reduce the importance of KCACs. Neurons could, at the same time, be involved in different pathways in their different compartments (Laurent and Burrows, 1989).

### 7.4.2 PNs as postsynaptic partners

PNs synapse onto KCs in the calyx. If PNs were postsynaptic to KCACs, communication would take place bidirectionally between PNs and KCs. KC::PN connections would allow for feedback to the ALs, the neuropil downstream to the MBs. Jeff Hawkins postulates a "memory-prediction-framework" in his book *On Intelligence*. He claims that, in the mammalian cortex, not only lower brain areas project to higher brain areas, but that higher areas also feed information back to lower areas in the brain. While the information transferred upwards this hierarchy represents the perception of the environment, the information sent downwards would then represent a memory-derived prediction about the environment (Hawkins, 2004). Here, prediction is defined as the activity of sensory neurons before they are actually activated by an exterior stimulus. In this model, each stimulus is compared to the prediction about the stimulus. The animal compares novel situations to similar experiences from the past and can thus make predictions about the future. Hawkins proposes that what is perceived is a combination of what is sensed and what is predicted. He describes this procedure as the basis for intelligence because it enables the animal to make intelligent decisions. If such a downward-flow existed in insects, it would help also them to integrate memory with new stimuli.

However, if PNs were postsynaptic to KCACs, these synapses would not likely be formed at PN boutons. We found KCACs to reside in-between microglomeruli of the imago (Christiansen et al., 2011, Fig. 2B-G) and macroglomeruli of larvae (Christiansen et al., 2011, Fig. 1B-G), which suggests that KCACs localize separately from PN::KC synapses. PN postsynapses would thus have to be situated along the PN neurites.

### 7.4.3 GABAergic neurons as postsynaptic partners

A recent EM study also identified KC output synapses in the calyx (Butcher et al., 2012), and the authors assumed that KCs synapse onto neurons other than PNs and KCs. As GABAergic neurites are found in the whole calyx (Yasuyama et al., 2002), it is well possible that they are here postsynaptic to KCACs.

So far, the only identified GABAergic neuron in the calyx is the anterior paired lateral neuron (APL, Liu and Davis, 2009); its arborizations cover the whole calyx. The APL neuron is therefore potentially able to physically meet the numerous KCACs and to provide feedback to other cells in the calyx.

Given that one PN innervates several KCs (on average 6.4 claws per KC; Butcher et al., 2012), the APL neuron could, when activated by KCACs, hinder spiking in other KCs. Thereby, multiple representations of one odor in different groups of KCs could be prevented. If KCs were inhibitory instead of excitatory in the calyx, they could inhibit GABAergic neurites to prevent them from inhibiting other cells.

Of note, odor conditioning is concentration invariant in a certain range of odor concentration (Masek and Heisenberg, 2008). This instance is necessary, because the animal has to be able to keep track of the odor, as it approaches or avoids it. Hence, inhibition and disinhibition through GABAergic profiles, triggered by KCACs, could help to keep KCs or PN boutons in an optimal range, irrespective of the odor concentration.

Interestingly, the APL neuron innervates not only the calyx but the entire MB neuropil (Liu and Davis, 2009). Liu and Davis found APL neuron presynaptic specializations on the level of the MB lobes. Hence, the APL neuron might, depending on whether KCs are excitatory or inhibitory, directly inhibit or disinhibit KC output in the lobes, following its stimulation by KCACs.

Obviously, many connectivity scenarios are possible. However, not only the identity of the cells postsynaptic to KCACs is to be uncovered. Also the neurotransmitter of KCs is unknown and it is unclear, whether the KCACs form excitatory or inhibitory synapses. Therefore, a functional interpretation of the KCACs remains highly speculative.

## 7.5 Different synapse types within the calyx

A very exciting finding is that levels of presynaptic AZ proteins at KCACs differ from those at surrounding synapses. We used an antibody against the protein Syd-1 (*Drosophila* Syd-1: DSyd-1) as an AZ marker independent of BRP. DSyd-1 is a presynaptic AZ protein, which is expressed in the brain (Owald et al., 2010, Fig. 2B-D) and at NMJs (Owald et al., 2010, Fig. 3A,B) of *Drosophila*. It precedes BRP incorporation during AZ formation (Owald et al., 2010, Fig. 9A, arrowheads) and also persists in *brp* mutants (Owald et al., 2010, Fig. 10F). A $BRP^{Nc82}$ and αDSyd-1 co-staining in wildtype brains revealed that synapses in the calyx express different levels of the two proteins

(Christiansen et al., 2011, Fig. 1J,L-N and Fig. J,L-N). Notably, KCACs seem to express less DSyd-1 and more BRP than AZs of PNs [see microglomeruli in adult flies (Christiansen et al., 2011, Fig. 2J,L,M) and macroglomeruli in larvae (Christiansen et al., 2011, Fig. 1J,L-N; macroglomeruli are organized primarily outside the dotted line)]. Seemingly, AZs with little amounts of DSyd-1 can incorporate more BRP. In Owald et al., 2010 Fig. 5B,B',D, we show that DSyd-1 regulates BRP incorporation: in the complete absence of DSyd-1, T-bars are enlarged and malformed

The molecular diversity at synapses may contribute essentially to the functions of neurons and neuronal circuits and in particular to synaptic transmission and plasticity (Grant, 2007; O'Rourke et al., 2012). Of note, the expression levels of individual synaptic proteins explicitly influence the function of the synapse: the reduction of the expression of a single synaptic protein can lead to changes in synaptic physiology (Grant, 2007). At the presynaptic AZ a highly-ordered protein architecture forms an electron-dense structure called cytomatrix (cytomatrix at the AZ, CAZ). Both, BRP and DSyd-1 are part of the CAZ. The CAZ might control the spatio-temporal neurotransmitter release profile of a synapse by interacting with the vesicle fusion machinery (Sigrist and Sabatini, 2011). Differences in the assembly of the CAZ could be the basis for functional differences between synapse types: two studies suggest that AZs with larger dense bodies have a stronger output (Govind and Meiss, 1979; Govind et al., 2001). In *Drosophila*, dense bodies are called T-bars; BRP is an essential component of the T-bar (Fouquet et al., 2009). KCACs are enriched in BRP and might therefore have a strong output.

Differences in the composition of the CAZ could also point at differences in the persistence of the synapse. In the mammalian neocortex, microcircuits are continuously modified along with the interactions of animals with their environment (Fu and Zuo, 2011). The microcircuits may be rewired by the formation, elimination and modification of synaptic contacts. KCs are involved in olfactory learning and memory and in other complex behavioral functions, which require a high capacity for plasticity. It is easily imaginable that short-lived, quickly built synapses differ in their protein assembly from more stable, long-lasting synapses.

## 7.6 Synaptic plasticity in the calyx

PN::KC synapses form a large fraction of synapses in the calyx. They are organized in microglomeruli: large PN presynaptic boutons, which are surrounded by dendrites of different KCs, as well as by GABAergic neurites (Yasuyama et al., 2002; Butcher et al., 2012). Each microglomerulus contains several synapses. By disruption of the PN-KC

circuit, we could show that synapses of microglomeruli are subject to activity-dependent synaptic plasticity. Here, a small group of PNs was electrically silenced; subsequently, the synapses between them and postsynaptic KCs were examined for morphological changes. To this end, the open rectifier potassium channel *UAS-dork1.Δc* (Nitabach et al., 2002) was expressed under control of a PN subset driver. The targeted PNs were thus unable to generate action potentials (APs). In order to observe potential changes at the presynaptic AZs, we analyzed the signal intensities of labeled BRP. We found that the silenced PNs compensated their functional limitation by increasing the number of AZs per bouton (Kremer et al., 2010, Fig. 4F,G). Interestingly, we observed neither enlarged AZs (Kremer et al., 2010) nor enlarged boutons (Kremer et al., 2010, Fig. 4H). It was not completely surprising to find such activity-induced plasticity, as PNs are reported to be involved in olfactory associative learning (Thum et al., 2007). Certainly, learning is believed to involve changes at synapses (Mayford et al., 2012). Moreover, sizes and numbers of microglomeruli, as well as the complete volume of the calyx, are sensitive to external stimuli and age, and also to learning and memory processes (Groh and Meinertzhagen, 2010). The plasticity that we observed at PN boutons did not include changes of bouton volume. However, more microglomeruli were observed at silenced PNs than in control situations (Kremer et al., 2010, Fig. 3E) and, in addition, the size of these microglomeruli was increased (Kremer et al., 2010, Fig. 3F). Such adaptations might lead to the observed expansion of the volume of the calyx.

Synapses can undergo structural changes in response to external stimuli; this has been shown for a variety of species (Huntley et al., 2002; Holtmaat and Svoboda, 2009; Ho et al., 2011). Here, we provide the first demonstration of structural plasticity at synapses in the CNS of *Drosophila*. Earlier, in *Drosophila,* stimulus-induced morphological changes at synapses had only been shown at the neuromuscular junction (Sigrist et al., 2003). In the vertebrate CNS, by contrast, synaptic plasticity is a common feature(Ho et al., 2011). The hippocampus is a well-studied model system regarding synaptic plasticity. Granule cells from the dentate gyrus provide the main synaptic input to the hippocampus, where they form large so-called mossy fiber boutons (MFBs) with the dendrites of CA3 pyramidal neurons. MFBs exhibit various forms of synaptic plasticity (Nicoll and Schmitz, 2005). For instance, induced long term potentiation (LTP), a form of synaptic plasticity, leads to changes at MFBs: they exhibit more AZs, the length of the presynaptic membrane is increased and, in addition, dendritic spines form *de novo* (Zhao et al., 2012b). Our results indicate that similar processes may take place at *Drosophila* central synapses. PNs are involved in olfactory learning (Thum et al., 2007); however, whether the observed structural changes in microglomeruli are connected with learning and memory, remains to be investigated.

At first glance, it seems improbable that entire PN boutons and KC dendrites are quickly built or eliminated. The highly specialized anatomy of microglomeruli renders it unlikely

that they are subject to fast assembly and disassembly processes. Yet, in vertebrates, rapid morphological changes at complex synapses are described. Dendrites at MFBs, for instance, can grow or shrink within several minutes after a change in synaptic strength (Okamoto et al., 2009; Bosch and Hayashi, 2012). That is due to the fact that the actin cytoskeleton is highly dynamic (Hotulainen and Hoogenraad, 2010). Still, the rapid integration into or removal of new synapses from existing microglomeruli is more easily imaginable. A change in AZ density requires for quick protein assembly or disassembly at synapses. Electron microscopic work showed that T-bars of *Drosophila* photoreceptor neurons are subject to fast (minute-range) assembly and disassembly processes, when changes in function of the circuit occur (Rybak and Meinertzhagen, 1997; Prokop and Meinertzhagen, 2006). However, in our study, silencing of PNs was induced during the pupal stage and lasted during adulthood, as mediated by the driver *mz19*-GAL4 (Jefferis et al., 2004). The increase in the number of boutons in silenced PNs is thus probably due to the early onset of silencing. It remains to be proven that the observed changes can occur continuously in response to the changing environment.

# 8. APPENDIX

## 8.1 References

Aso Y, Siwanowicz I, Bracker L, Ito K, Kitamoto T, Tanimoto H (2010) Specific dopaminergic neurons for the formation of labile aversive memory. Curr Biol 20:1445-1451.

Aso Y, Herb A, Ogueta M, Siwanowicz I, Templier T, Friedrich AB, Ito K, Scholz H, Tanimoto H (2012) Three Dopamine Pathways induce Aversive Odor Memories with different Stability. PLoS Genet 8:e1002768

Barth M, Heisenberg M (1997) Vision affects mushroom bodies and central complex in *Drosophila melanogaster*. In: Learn Mem, pp 219-229.

Benton R (2008) Chemical sensing in *Drosophila*. In: Curr Opin Neurobiol, pp 357-363.

Benton R, Vannice K, Gomezdiaz C, Vosshall L (2009) Variant Ionotropic Glutamate Receptors as Chemosensory Receptors in *Drosophila*. In: Cell, pp 149-162.

Benzer S (1967) Behavioral mutants of *Drosophila* isolated by countercurrent distribution. Proc Natl Acad Sci USA 58:1112-1119.

Berdnik D, Chihara T, Couto A, Luo L (2006) Wiring stability of the adult *Drosophila* olfactory circuit after lesion. J Neurosci 26:3367-3376.

Bosch M, Hayashi Y (2012) Structural plasticity of dendritic spines. Curr Opin Neurobiol 22:383-388.

Braitenberg VS, Schüz A (1998) Cortex: Statistics and Geometry of Neuronal Connectivity, 2. Edition. Berlin, New York: Springer.

Brand AH, Perrimon N (1993) Targeted gene expression as a means of altering cell fates and generating dominant phenotypes. Development 118:401-415.

Brembs B, Christiansen F, Pflüger HJ, Duch C (2007) Flight initiation and maintenance deficits in flies with genetically altered biogenic amine levels. In: J Neurosci, pp 11122-11131.

Burke CJ, Huetteroth W, Owald D, Perisse E, Krashes MJ, Das G, Gohl D, Silies M, Certel S, Waddell S (2012) Layered reward signalling through octopamine and dopamine in *Drosophila*. Nature 492:433-437.

Busch S, Selcho M, Ito K, Tanimoto H (2009) A map of octopaminergic neurons in the *Drosophila* brain. In: J Comp Neurol, pp 643-667.

Busto GU, Cervantes-Sandoval I, Davis RL (2010) Olfactory learning in *Drosophila*. Physiology (Bethesda) 25:338-346.

Butcher NJ, Friedrich AB, Lu Z, Tanimoto H, Meinertzhagen IA (2012) Different classes of input and output neurons reveal new features in microglomeruli of the adult *Drosophila* mushroom body calyx. J Comp Neurol 520:2185-2201.

Chen CC, Wu JK, Lin HW, Pai TP, Fu TF, Wu CL, Tully T, Chiang AS (2012) Visualizing long-term memory formation in two neurons of the *Drosophila* brain. Science 335:678-685.

Christiansen F, Zube C, Andlauer TF, Wichmann C, Fouquet W, Owald D, Mertel S, Leiss F, Tavosanis G, Luna AJ, Fiala A, Sigrist SJ (2011) Presynapses in Kenyon cell dendrites in the mushroom body calyx of *Drosophila*. J Neurosci 31:9696-9707.

Citri A, Malenka RC (2008) Synaptic plasticity: multiple forms, functions, and mechanisms. Neuropsychopharmacology 33:18-41.

Claridge-Chang A, Roorda RD, Vrontou E, Sjulson L, Li H, Hirsh J, Miesenbock G (2009) Writing memories with light-addressable reinforcement circuitry. Cell 139:405-415.

Connolly JB, Roberts IJ, Armstrong JD, Kaiser K, Forte M, Tully T, O'Kane CJ (1996) Associative learning disrupted by impaired Gs signaling in *Drosophila* mushroom bodies. In: Science, pp 2104-2107.

Couteaux R, Pecot-Dechavassine M (1970) [Synaptic vesicles and pouches at the level of "active zones" of the neuromuscular junction]. C R Acad Sci Hebd Seances Acad Sci D 271:2346-2349.

Couto A, Alenius M, Dickson BJ (2005) Molecular, anatomical, and functional organization of the *Drosophila* olfactory system. Curr Biol 15:1535-1547.

Couturier S, Bertrand D, Matter JM, Hernandez MC, Bertrand S, Millar N, Valera S, Barkas T, Ballivet M (1990) A neuronal nicotinic acetylcholine receptor subunit (alpha 7) is developmentally regulated and forms a homo-oligomeric channel blocked by alpha-BTX. Neuron 5:847-856.

Dai Y, Taru H, Deken SL, Grill B, Ackley B, Nonet ML, Jin Y (2006) SYD-2 Liprin-alpha organizes presynaptic active zone formation through ELKS. In: Nat Neurosci, pp 1479-1487.

David JC, Coulon JF (1985) Octopamine in invertebrates and vertebrates. A review. Prog Neurobiol 24:141-185.

Davis RL (2011) Traces of *Drosophila* memory. Neuron 70:8-19.

Dubnau J, Chiang AS (2013) Systems memory consolidation in *Drosophila*. Curr Opin Neurobiol 23:84-91.

Dujardin F (1850) Mémoire sur le système nervaux des insectes. Ann Sci Nat Zool 14:195-206.

Durst C, Eichmuller S, Menzel R (1994) Development and experience lead to increased volume of subcompartments of the honeybee mushroom body. Behav Neural Biol 62:259-263.

Evans PD, Maqueira B (2005) Insect octopamine receptors: a new classification scheme based on studies of cloned *Drosophila* G-protein coupled receptors. Invert Neurosci 5:111-118.

Farris SM, Robinson GE, Fahrbach SE (2001) Experience- and age-related outgrowth of intrinsic neurons in the mushroom bodies of the adult worker honeybee. J Neurosci 21:6395-6404.

Fayyazuddin A, Zaheer MA, Hiesinger PR, Bellen HJ (2006) The nicotinic acetylcholine receptor Dalpha7 is required for an escape behavior in *Drosophila*. In: PLoS Biol, p e63.

Featherstone DE, Rushton E, Rohrbough J, Liebl F, Karr J, Sheng Q, Rodesch CK, Broadie K (2005) An essential *Drosophila* glutamate receptor subunit that functions in both central neuropil and neuromuscular junction. In: J Neurosci, pp 3199-3208.

Fioravante D, Regehr WG (2011) Short-term forms of presynaptic plasticity. Curr Opin Neurobiol 21:269-274.

Fishilevich E, Vosshall LB (2005) Genetic and functional subdivision of the *Drosophila* antennal lobe. Curr Biol 15:1548-1553.

Fouquet W, Owald D, Wichmann C, Mertel S, Depner H, Dyba M, Hallermann S, Kittel RJ, Eimer S, Sigrist SJ (2009) Maturation of active zone assembly by *Drosophila* Bruchpilot. J Cell Biol 186:129-145.

Fu M, Zuo Y (2011) Experience-dependent structural plasticity in the cortex. Trends Neurosci 34:177-187.

Gao Q, Yuan B, Chess A (2000) Convergent projections of*Drosophila* olfactory neurons to specific glomeruli in the antennal lobe. Nat Neurosci 3:780-785.

Govind CK, Meiss DE (1979) Quantitative comparison of low- and high-output neuromuscular synapses from a motoneuron of the lobster (Homarus americanus). Cell Tissue Res 198:455-463.

Govind CK, Quigley PA, Pearce J (2001) Synaptic differentiation between two phasic motoneurons to a crayfish fast muscle. Invert Neurosci 4:77-84.

Grant SG (2007) Toward a molecular catalogue of synapses. Brain Res Rev 55:445-449.

Grauso M, Reenan RA, Culetto E, Sattelle DB (2002) Novel putative nicotinic acetylcholine receptor subunit genes, Dalpha5, Dalpha6 and Dalpha7, in *Drosophila melanogaster* identify a new and highly conserved target of adenosine deaminase acting on RNA-mediated A-to-I pre-mRNA editing. In: Genetics, pp 1519-1533.

Groh C, Meinertzhagen IA (2010) Brain plasticity in Diptera and Hymenoptera. In: Front Biosci (Schol Ed), pp 268-288.

Groh C, Tautz J, Rossler W (2004) Synaptic organization in the adult honey bee brain is influenced by brood-temperature control during pupal development. Proc Natl Acad Sci U S A 101:4268-4273.

Groh C, Ahrens D, Rossler W (2006) Environment- and age-dependent plasticity of synaptic complexes in the mushroom bodies of honeybee queens. In: Brain Behav Evol, pp 1-14.

Gundelfinger ED, Hess N (1992) Nicotinic acetylcholine receptors of the central nervous system of*Drosophila*. Biochim Biophys Acta 1137:299-308.

Hallem EA, Carlson JR (2006) Coding of Odors by a Receptor Repertoire. Cell 125:143-160.

Hawkins J (2004) On Intelligence. New York: Henry Holt and Company.

Hazelrigg T, Levis R, Rubin GM (1984) Transformation of white locus DNA in *Drosophila*: dosage compensation, zeste interaction, and position effects. Cell 36:469-481.

Hebb DO (1949) The Organization of Behavior: A Neuropsychological Theory. New York: John Wiley & Sons.

Heisenberg M (2003) Mushroom body memoir: from maps to models. In: Nat Rev Neurosci, pp 266-275.

Heuser JE, Reese TS (1973) Evidence for recycling of synaptic vesicle membrane during transmitter release at the frog neuromuscular junction. J Cell Biol 57:315-344.

Hildebrand JG, Shepherd GM (1997) Mechanisms of olfactory discrimination: converging evidence for common principles across phyla. Annu Rev Neurosci 20:595-631.

Hitier R, Heisenberg M, Preat T (1998) Abnormal mushroom body plasticity in the *Drosophila* memory mutant amnesiac. Neuroreport 9:2717-2719.

Ho VM, Lee JA, Martin KC (2011) The cell biology of synaptic plasticity. Science 334:623-628.

Holtmaat A, Svoboda K (2009) Experience-dependent structural synaptic plasticity in the mammalian brain. Nat Rev Neurosci 10:647-658.

Hotulainen P, Hoogenraad CC (2010) Actin in dendritic spines: connecting dynamics to function. J Cell Biol 189:619-629.

Huang J, Zhang W, Qiao W, Hu A, Wang Z (2010) Functional connectivity and selective odor responses of excitatory local interneurons in *Drosophila* antennal lobe. Neuron 67:1021-1033.

Huntley GW, Benson DL, Colman DR (2002) Structural remodeling of the synapse in response to physiological activity. Cell 108:1-4.

Ismail N, Robinson GE, Fahrbach SE (2006) Stimulation of muscarinic receptors mimics experience-dependent plasticity in the honey bee brain. Proc Natl Acad Sci U S A 103:207-211.

Ito K, Suzuki K, Estes P, Ramaswami M, Yamamoto D, Strausfeld NJ (1998) The organization of extrinsic neurons and their implications in the functional roles of the mushroom bodies in *Drosophila melanogaster* Meigen. In: Learning & Memory, pp 52-77.

Ito M, Masuda N, Shinomiya K, Endo K, Ito K (2013) Systematic analysis of neural projections reveals clonal composition of the*Drosophila* brain. Curr Biol 23:644-655.

Jefferis GS, Hummel T (2006) Wiring specificity in the olfactory system. Semin Cell Dev Biol 17:50-65.

Jefferis GS, Marin EC, Stocker RF, Luo L (2001) Target neuron prespecification in the olfactory map of*Drosophila*. In: Nature, pp 204-208.

Jefferis GS, Potter CJ, Chan AM, Marin EC, Rohlfing T, Maurer CR, Jr., Luo L (2007) Comprehensive maps of *Drosophila* higher olfactory centers: spatially segregated fruit and pheromone representation. Cell 128:1187-1203.

Jefferis GS, Vyas RM, Berdnik D, Ramaekers A, Stocker RF, Tanaka NK, Ito K, Luo L (2004) Developmental origin of wiring specificity in the olfactory system of *Drosophila*. Development 131:117-130.

Johard HAD, Enell LE, Gustafsson E, Trifilieff P, Veenstra JA, Nässel DR (2008) Intrinsic neurons of *Drosophila* mushroom bodies express short neuropeptide F: relations to extrinsic neurons expressing different neurotransmitters. In: J Comp Neurol, pp 1479-1496.

Joiner WJ, Crocker A, White BH, Sehgal A (2006) Sleep in *Drosophila* is regulated by adult mushroom bodies. Nature 441:757-760.

Kaufmann N, DeProto J, Ranjan R, Wan H, Van Vactor D (2002) *Drosophila* liprin-alpha and the receptor phosphatase Dlar control synapse morphogenesis. Neuron 34:27-38.

Kazama H, Wilson RI (2009) Origins of correlated activity in an olfactory circuit. Nat Neurosci 12:1136-1144.

Kenyon FC (1896) The meaning and structure of the so-called "mushroom bodies" of the hexapod brain. American Naturalist 30:643-650.

Kittel RJ, Wichmann C, Rasse TM, Fouquet W, Schmidt M, Schmid A, Wagh DA, Pawlu C, Kellner RR, Willig KI, Hell SW, Buchner E, Heckmann M, Sigrist SJ (2006) Bruchpilot promotes active zone assembly, $Ca^{2+}$ channel clustering, and vesicle release. In: Science, pp 1051-1054.

Knapek S, Kahsai L, Winther AME, Tanimoto H, Nässel DR (2013) Short Neuropeptide F Acts as a Functional Neuromodulator for Olfactory Mmemory in Kenyon Cells of *Drosophila* Mushroom Bodies. J Neurosci 33:5340-5345

Konorski (1948) Conditional Reflexes and Neuron Organization. Cambridge: Cambridge Univ. Press.

Krashes MJ, Keene AC, Leung B, Armstrong JD, Waddell S (2007) Sequential use of mushroom body neuron subsets during *Drosophila* odor memory processing. In: Neuron, pp 103-115.

Kremer MC, Christiansen F, Leiss F, Paehler M, Knapek S, Andlauer TFM, Förstner F, Kloppenburg P, Sigrist SJ, Tavosanis G (2010) Structural Long-Term Changes at Mushroom Body Input Synapses. In: Curr Biol.

Krofczik S, Khojasteh U, De Ibarra NH, Menzel R (2008) Adaptation of microglomerular complexes in the honeybee mushroom body lip to manipulations of behavioral maturation and sensory experience. In: Dev Neurobiol, pp 1007-1017.

Kuhn-Buhlmann S, Wehner R (2006) Age-dependent and task-related volume changes in the mushroom bodies of visually guided desert ants, Cataglyphis bicolor. J Neurobiol 66:511-521.

Kullmann DM, Lamsa KP (2007) Long-term synaptic plasticity in hippocampal interneurons. In: Nat Rev Neurosci, pp 687-699.

Laissue PP, Reiter C, Hiesinger PR, Halter S, Fischbach KF, Stocker RF (1999) Three-dimensional reconstruction of the antennal lobe in *Drosophila melanogaster*. J Comp Neurol 405:543-552.

Laurent G, Burrows M (1989) Intersegmental interneurons can control the gain of reflexes in adjacent segments of the locust by their action on nonspiking local interneurons. J Neurosci 9:3030-3039.

Lee T, Luo L (2001) Mosaic analysis with a repressible cell marker (MARCM) for *Drosophila* neural development. In: Trends Neurosci, pp 251-254.

Lee T, Lee A, Luo L (1999) Development of the*Drosophila* mushroom bodies: sequential generation of three distinct types of neurons from a neuroblast. In: Development, pp 4065-4076.

Leevers SJ, Weinkove D, MacDougall LK, Hafen E, Waterfield MD (1996) The *Drosophila* phosphoinositide 3-kinase Dp110 promotes cell growth. EMBO J 15:6584-6594.

Leiss F, Koper E, Hein I, Fouquet W, Lindner J, Sigrist S, Tavosanis G (2009) Characterization of dendritic spines in the *Drosophila* central nervous system. Dev Neurobiol 69:221-234.

Lent DD, Pinter M, Strausfeld NJ (2007) Learning with half a brain. Dev Neurobiol 67:740-751.

Lin H-H, Lai JS-Y, Chin A-L, Chen Y-C, Chiang A-S (2007) A map of olfactory representation in the*Drosophila* mushroom body. In: Cell, pp 1205-1217.

Liu L, Wolf R, Ernst R, Heisenberg M (1999) Context generalization in *Drosophila* visual learning requires the mushroom bodies. Nature 400:753-756.

Liu X, Davis RL (2009) The GABAergic anterior paired lateral neuron suppresses and is suppressed by olfactory learning. Nat Neurosci 12:53-59.

Liu X, Buchanan ME, Han KA, Davis RL (2009) The GABAA receptor RDL suppresses the conditioned stimulus pathway for olfactory learning. J Neurosci29:1573-1579.

Lüscher C, Malenka RC (2012) NMDA receptor-dependent long-term potentiation and long-term depression (LTP/LTD). Cold Spring Harb Perspect Biol 4.

Malenka RC, Bear MF (2004) LTP and LTD: an embarrassment of riches. Neuron 44:5-21.

Malun D (1991) Inventory and distribution of synapses of identified uniglomerular projection neurons in the antennal lobe of Periplaneta americana. J Comp Neurol 305:348-360.

Mao Z, Davis RL (2009) Eight different types of dopaminergic neurons innervate the *Drosophila* mushroom body neuropil: anatomical and physiological heterogeneity. Front Neural Circuits 3:5.

Marin EC, Jefferis GS, Komiyama T, Zhu H, Luo L (2002) Representation of the glomerular olfactory map in the *Drosophila* brain. Cell 109:243-255.

Masek P, Heisenberg M (2008) Distinct memories of odor intensity and quality in *Drosophila*. Proc Natl Acad Sci U S A 105:15985-15990.

Matkovic T, Siebert M, Knoche E, Depner H, Mertel S, Owald D, Schmidt M, Thomas U, Sickmann A, Kamin D, Hell SW, Burger J, Hollmann C, Mielke T, Wichmann C, Sigrist SJ (2013) The Bruchpilot cytomatrix determines the size of the readily releasable pool of synaptic vesicles. J Cell Biol 202:667-683.

Mayford M, Siegelbaum SA, Kandel ER (2012) Synapses and memory storage. Cold Spring Harb Perspect Biol 4.

McBride SM, Giuliani G, Choi C, Krause P, Correale D, Watson K, Baker G, Siwicki KK (1999) Mushroom body ablation impairs short-term memory and long-term memory of courtship conditioning in *Drosophila melanogaster*. Neuron 24:967-977.

Miller KE, DeProto J, Kaufmann N, Patel BN, Duckworth A, Van Vactor D (2005) Direct observation demonstrates that Liprin-alpha is required for trafficking of synaptic vesicles. Curr Biol 15:684-689.

Miller PM, Saltz JB, Cochrane VA, Marcinkowski CM, Mobin R, Turner TL (2011) Natural Variation in Decision-Making Behavior in *Drosophila melanogaster*. PLoS One 6:e16436.

Mori K, Nagao H, Yoshihara Y (1999) The olfactory bulb: coding and processing of odor molecule information. Science 286:711-715.

Muller HJ (1927) Artificial transmutation of the gene. Science 66:84-87.

Nässel DR (2009) Neuropeptide signaling near and far: how localized and timed is the action of neuropeptides in brain circuits? Invert Neurosci 9:57-75.

Neuser K, Triphan T, Mronz M, Poeck B, Strauss R (2008) Analysis of a spatial orientation memory in *Drosophila*. In: Nature, p 5.

Ng M, Roorda RD, Lima SQ, Zemelman BV, Morcillo P, Miesenböck G (2002) Transmission of olfactory information between three populations of neurons in the antennal lobe of the fly. In: Neuron, pp 463-474.

Nicolai LJ, Ramaekers A, Raemaekers T, Drozdzecki A, Mauss AS, Yan J, Landgraf M, Annaert W, Hassan BA (2010) Genetically encoded dendritic marker sheds light on neuronal connectivity in *Drosophila*. Proc Natl Acad Sci U S A 107:20553-20558.

Nicoll RA, Schmitz D (2005) Synaptic plasticity at hippocampal mossy fibre synapses. Nat Rev Neurosci 6:863-876.

Nitabach MN, Blau J, Holmes TC (2002) Electrical silencing of *Drosophila* pacemaker neurons stops the free-running circadian clock. Cell 109:485-495.

O'Dell KM, Armstrong JD, Yang MY, Kaiser K (1995) Functional dissection of the *Drosophila* mushroom bodies by selective feminization of genetically defined subcompartments. In: Neuron, pp 55-61.

O'Rourke NA, Weiler NC, Micheva KD, Smith SJ (2012) Deep molecular diversity of mammalian synapses: why it matters and how to measure it. Nat Rev Neurosci 13:365-379.

Oh H-W, Campusano JM, Hilgenberg LGW, Sun X, Smith MA, O'Dowd DK (2008) Ultrastructural analysis of chemical synapses and gap junctions between *Drosophila* brain neurons in culture. In: Dev Neurobiol, pp 281-294.

Okada R, Awasaki T, Ito K (2009) Gamma-aminobutyric acid (GABA)-mediated neural connections in the *Drosophila* antennal lobe. J Comp Neurol 514:74-91.

Okamoto K, Bosch M, Hayashi Y (2009) The roles of CaMKII and F-actin in the structural plasticity of dendritic spines: a potential molecular identity of a synaptic tag? Physiology (Bethesda) 24:357-366.

Owald D, Fouquet W, Schmidt M, Wichmann C, Mertel S, Depner H, Christiansen F, Zube C, Quentin C, Korner J, Urlaub H, Mechtler K, Sigrist SJ (2010) A Syd-1 homologue regulates pre- and postsynaptic maturation in *Drosophila*. J Cell Biol 188:565-579.

Owald D, Khorramshahi O, Gupta VK, Banovic D, Depner H, Fouquet W, Wichmann C, Mertel S, Eimer S, Reynolds E, Holt M, Aberle H, Sigrist SJ (2012) Cooperation of Syd-1 with Neurexin synchronizes pre- with postsynaptic assembly. Nat Neurosci 15:1219-1226.

Patel MR, Lehrman EK, Poon VY, Crump JG, Zhen M, Bargmann CI, Shen K (2006) Hierarchical assembly of presynaptic components in defined C. elegans synapses. In: Nat Neurosci, pp 1488-1498.

Pauls D, Selcho M, Gendre N, Stocker RF, Thum AS (2010) *Drosophila* larvae establish appetitive olfactory memories via mushroom body neurons of embryonic origin. J Neurosci 30:10655-10666.

Pech U, Pooryasin A, Birman S, Fiala A (2013) Localization of the Contacts Between Kenyon Celss and Aminergic Neurons in the *Drosophila melanogaster* Brain using splitGFP Reconstitution. J Comp Neurol 521:3992-4026

Perisse E, Burke C, Huetteroth W, Waddell S (2013) Shocking revelations and saccharin sweetness in the study of *Drosophila* olfactory memory. Curr Biol 23:R752-763.

Pitman JL, McGill JJ, Keegan KP, Allada R (2006) A dynamic role for the mushroom bodies in promoting sleep in *Drosophila*. Nature 441:753-756.

Prokop A, Meinertzhagen I (2006) Development and structure of synaptic contacts in *Drosophila*. In: Seminars in Cell & Developmental Biology, pp 20-30.

Qin H, Cressy M, Li W, Coravos JS, Izzi SA, Dubnau J (2012) Gamma neurons mediate dopaminergic input during aversive olfactory memory formation in *Drosophila*. Curr Biol 22:608-614.

Ramaekers A, Magnenat E, Marin EC, Gendre N, Jefferis GS, Luo L, Stocker RF (2005) Glomerular maps without cellular redundancy at successive levels of the *Drosophila* larval olfactory circuit. Curr Biol 15:982-992.

Ramòn y Cajal S (1894) The Croonian Lecture: La fine structure des centres nerveux. Proc R Soc, London, B 55:444-461.

Riemensperger T, Voller T, Stock P, Buchner E, Fiala A (2005) Punishment prediction by dopaminergic neurons in *Drosophila*. Curr Biol 15:1953-1960.

Rizzoli SO, Betz WJ (2005) Synaptic vesicle pools. Nat Rev Neurosci 6:57-69.

Rolls MM, Satoh D, Clyne PJ, Henner AL, Uemura T, Doe CQ (2007) Polarity and intracellular compartmentalization of *Drosophila* neurons. In: Neural Dev, p 7.

Roy B, Singh AP, Shetty C, Chaudhary V, North A, Landgraf M, Vijayraghavan K, Rodrigues V (2007) Metamorphosis of an identified serotonergic neuron in the *Drosophila* olfactory system. Neural Dev 2:20.

Rubin GM, Spradling AC (1982) Genetic transformation of *Drosophila* with transposable element vectors. Science 218:348-353.

Rybak J, Meinertzhagen IA (1997) The effects of light reversals on photoreceptor synaptogenesis in the fly Musca domestica. Eur J Neurosci 9:319-333.

Sánchez-Soriano N, Tear G, Whitington P, Prokop A (2007) *Drosophila* as a genetic and cellular model for studies on axonal growth. In: Neural Dev, p 9.

Schmid A, Hallermann S, Kittel R, Khorramshahi O, Frölich A, Quentin C, Rasse T, Mertel S, Heckmann M, Sigrist S (2008) Activity-dependent site-specific changes of glutamate receptor composition in vivo. In: Nat Neurosci.

Schoch S, Gundelfinger ED (2006) Molecular organization of the presynaptic active zone. Cell Tissue Res 326:379-391.

Schulz RA, Chromey C, Lu MF, Zhao B, Olson EN (1996) Expression of the D-MEF2 transcription in the *Drosophila* brain suggests a role in neuronal cell differentiation. In: Oncogene, pp 1827-1831.

Schürmann FW (1974) [On the functional anatomy of the corpora pedunculata in insects (author's transl)]. Exp Brain Res 19:406-432.

Seid MA, Harris KM, Traniello JF (2005) Age-related changes in the number and structure of synapses in the lip region of the mushroom bodies in the ant Pheidole dentata. J Comp Neurol 488:269-277.

Shang Y, Claridge-Chang A, Sjulson L, Pypaert M, Miesenbock G (2007) Excitatory local circuits and their implications for olfactory processing in the fly antennal lobe. Cell 128:601-612.

Sheng M, Hoogenraad CC (2007) The postsynaptic architecture of excitatory synapses: a more quantitative view. Annu Rev Biochem 76:823-847.

Sigrist SJ, Sabatini BL (2011) Optical super-resolution microscopy in neurobiology. Curr Opin Neurobiol 22:86-93.

Sigrist SJ, Reiff DF, Thiel PR, Steinert JR, Schuster CM (2003) Experience-dependent strengthening of *Drosophila* neuromuscular junctions. J Neurosci 23:6546-6556.

Sinakevitch I, Strausfeld NJ (2005) Comparison of octopamine-like immunoreactivity in the brains of the fruit fly and blow fly. In: J Comp Neurol, pp 460-475.

Spangler SA, Schmitz SK, Kevenaar JT, de Graaff E, de Wit H, Demmers J, Toonen RF, Hoogenraad CC (2013) Liprin-alpha2 promotes the presynaptic recruitment and turnover of RIM1/CASK to facilitate synaptic transmission. J Cell Biol 201:915-928.

Squire LR, Kandel ER (1999) Memory : from mind to molecules, 2nd Edition. Greenwood Village, Colo.: Scientific American Library.

Stocker RF (1994) The organization of the chemosensory system in *Drosophila melanogaster*: a review. Cell Tissue Res 275:3-26.

Stocker RF, Singh RN, Schorderet M, Siddiqi O (1983) Projection patterns of different types of antennal sensilla in the antennal glomeruli of *Drosophila melanogaster*. Cell Tissue Res 232:237-248.

Stocker RF, Lienhard MC, Borst A, Fischbach KF (1990) Neuronal architecture of the antennal lobe in *Drosophila melanogaster*. Cell Tissue Res 262:9-34.

Stocker RF, Heimbeck G, Gendre N, de Belle JS (1997) Neuroblast ablation in *Drosophila* P[GAL4] lines reveals origins of olfactory interneurons. J Neurobiol 32:443-456.

Strausfeld NJ (1976) Atlas of the insect brain: Springer-Verlag.

Strausfeld NJ, Sinakevitch I, Vilinsky I (2003) The mushroom bodies of *Drosophila melanogaster*: an immunocytological and golgi study of Kenyon cell organization in the calyces and lobes. In: Microsc Res Tech, pp 151-169.

Strausfeld NJ, Bacon JP (1983) Multimodal convergence in the central nervous system of dipterous insects. Fortschritte der Zoologie 28:47-76.

Südhof TC (2012) The presynaptic active zone. Neuron 75:11-25.

Südhof TC, Rothman JE (2009) Membrane Fusion: Grappling with SNARE and SM Proteins. In: Science, pp 474-477.

Sun XJ, Tolbert LP, Hildebrand JG (1997) Synaptic organization of the uniglomerular projection neurons of the antennal lobe of the moth Manduca sexta: a laser scanning confocal and electron microscopic study. J Comp Neurol 379:2-20.

Tabuchi K, Sawamoto K, Suzuki E, Ozaki K, Sone M, Hama C, Tanifuji-Morimoto T, Yuasa Y, Yoshihara Y, Nose A, Okano H (2000) GAL4/UAS-WGA system as a powerful tool for tracing *Drosophila* transsynaptic neural pathways. In: J Neurosci Res, pp 94-99.

Tanaka NK, Tanimoto H, Ito K (2008) Neuronal assemblies of the *Drosophila* mushroom body. In: J Comp Neurol, pp 711-755.

Tanaka NK, Awasaki T, Shimada T, Ito K (2004) Integration of chemosensory pathways in the *Drosophila* second-order olfactory centers. In: Curr Biol, pp 449-457.

Technau GM (1984) Fiber number in the mushroom bodies of adult *Drosophila melanogaster* depends on age, sex and experience. J Neurogenet 1:113-126.

Thompson V (1977) Recombination and response to selection in *Drosophila melanogaster*. Genetics 85:125-140.

Thum AS, Jenett A, Ito K, Heisenberg M, Tanimoto H (2007) Multiple memory traces for olfactory reward learning in *Drosophila*. In: J Neurosci, pp 11132-11138.

Trujillo-Cenoz O, Melamed J (1973) The development of the retina-lamina complex in muscoid flies. J Ultrastruct Res 42:554-581.

Turner GC, Bazhenov M, Laurent G (2008) Olfactory representations by *Drosophila* mushroom body neurons. In: Journal of Neurophysiology, pp 734-746.

Venken KJ, Simpson JH, Bellen HJ (2011) Genetic manipulation of genes and cells in the nervous system of the fruit fly. Neuron 72:202-230.

Vosshall LB, Wong AM, Axel R (2000) An olfactory sensory map in the fly brain. In: Cell, pp 147-159.

Waddell S (2010) Dopamine reveals neural circuit mechanisms of fly memory. Trends Neurosci 33:457-464.

Wagh DA, Rasse TM, Asan E, Hofbauer A, Schwenkert I, Dürrbeck H, Buchner S, Dabauvalle M-C, Schmidt M, Qin G, Wichmann C, Kittel R, Sigrist SJ, Buchner E (2006) Bruchpilot, a protein with homology to ELKS/CAST, is required for structural integrity and function of synaptic active zones in *Drosophila*. In: Neuron, pp 833-844.

Watson AHD, M. Burrows (1988) The distribution and morphology of synapses on nonspiking local intemeurons in the thoracic nervous system of the locust. J Comp Neurol 272:605-616.

Wegener C, Gorbashov A (2008) Molecular evolution of neuropeptides in the genus *Drosophila*. Genome Biol 9:R131.

Wentzel C, Sommer JE, Nair R, Stiefvater A, Sibarita JB, Scheiffele P (2013) mSYD1A, a mammalian synapse-defective-1 protein, regulates synaptogenic signaling and vesicle docking. Neuron 78:1012-1023.

Wicher D (2012) Functional and evolutionary aspects of chemoreceptors. Front Cell Neurosci 6:48.

Wilson RI (2013) Early olfactory processing in *Drosophila*: mechanisms and principles. Annu Rev Neurosci 36:217-241.

Wilson RI, Laurent G (2005) Role of GABAergic inhibition in shaping odor-evoked spatiotemporal patterns in the *Drosophila* antennal lobe. In: J Neurosci, pp 9069-9079.

Wilson RI, Turner GC, Laurent G (2004) Transformation of olfactory representations in the *Drosophila* antennal lobe. In: Science, pp 366-370.

Withers GS, Fahrbach SE, Robinson GE (1993) Selective neuroanatomical plasticity and division of labour in the honeybee. Nature 364:238-240.

Wong AM, Wang JW, Axel R (2002) Spatial representation of the glomerular map in the *Drosophila* protocerebrum. Cell 109:229-241.

Xu-Friedman MA, Regehr WG (2004) Structural contributions to short-term synaptic plasticity. Physiol Rev 84:69-85.

Yaksi E, Wilson RI (2010) Electrical coupling between olfactory glomeruli. Neuron 67:1034-1047.

Yang CH, Belawat P, Hafen E, Jan LY, Jan YN (2008) *Drosophila* egg-laying site selection as a system to study simple decision-making processes. Science 319:1679-1683.

Yang MY, Armstrong JD, Vilinsky I, Strausfeld NJ, Kaiser K (1995) Subdivision of the *Drosophila* mushroom bodies by enhancer-trap expression patterns. In: Neuron, pp 45-54.

Yasuyama K, Meinertzhagen IA, Schürmann F-W (2002) Synaptic organization of the mushroom body calyx in *Drosophila melanogaster*. In: J Comp Neurol, pp 211-226.

Yu D, Keene AC, Srivatsan A, Waddell S, Davis RL (2005) *Drosophila* DPM neurons form a delayed and branch-specific memory trace after olfactory classical conditioning. In: Cell, pp 945-957.

Zars T, Fischer M, Schulz R, Heisenberg M (2000) Localization of a short-term memory in *Drosophila*. In: Science, pp 672-675.

Zhai RG, Bellen HJ (2004) The architecture of the active zone in the presynaptic nerve terminal. Physiology (Bethesda) 19:262-270.

Zhang X, Firestein S (2002) The olfactory receptor gene superfamily of the mouse. Nat Neurosci 5:124-133.

Zhang YQ, Rodesch CK, Broadie K (2002) Living synaptic vesicle marker: synaptotagmin-GFP. Genesis 34:142-145.

Zhao S, Studer D, Chai X, Graber W, Brose N, Nestel S, Young C, Rodriguez EP, Saetzler K, Frotscher M (2012b) Structural plasticity of hippocampal mossy fiber synapses as revealed by high-pressure freezing. J Comp Neurol 520:2340-2351.

Zhu S, Chiang A-S, Lee T (2003) Development of the *Drosophila* mushroom bodies: elaboration, remodeling and spatial organization of dendrites in the calyx. In: Development, pp 2603-2610.

# 8.2 Curriculum Vitae

# 8.3 List of Publications

Christiansen, F.*, Zube, C.*, Andlauer, T.F.M., Wichmann, C., Fouquet, W., Owald, D., Mertel, S., Leiss, F., Tavosanis, G., Farca Luna, A.J., Fiala, A., Sigrist ,S.J. (2011) Presynapses in Kenyon cell dendrites in the mushroom body calyx of *Drosophila*. J Neurosci 31:9696-9707.

*equal contribution

Kremer, M.C.*, Christiansen, F.*, Leiss, F.*, Paehler, M., Knapek, S., Andlauer, T.F.M., Förstner, F., Kloppenburg, P., Sigrist, S.J., Tavosanis, G. (2010) Structural Long-Term Changes at Mushroom Body Input Synapses. Curr Biol.20, 1938-44.

*equal contribution

Owald, D.*, Fouquet, W.*, Schmidt, M., Wichmann, C., Mertel, S., Depner, H., Christiansen, F., Zube, C., Quentin, C., Korner, J, Urlaub, H., Mechtler, K., and Sigrist, S.J. (2010). A Syd-1 homologue regulates pre- and postsynaptic maturation in *Drosophila*. J Cell Biol 188, 565-579.

*equal contribution

Brembs, B.*, Christiansen, F.*, Pflüger, H.J., Duch, C. (2007) Flight initiation and maintenance deficits in flies with genetically altered biogenic amine levels. J Neurosci 10, 11122-31.

*equal contribution

## 8.3.1 Published Abstracts at international Conferences

Christiansen F., Pflueger H. J., Duch C. & Brembs B. Profound flight performance deficit in *Drosophila* lacking octopamine. 5th forum of European Neuroscience, 8-12 July 2006, Vienna, Austria (Poster presented)

F. Christiansen, S.J. Sigrist. Kenyon cell Synapses and Olfactory Learning in *Drosophila melanogaster*. Molecular Dynamics of the Chemical Synapse, 20-23 August 2007, Westerburg, Germany (Poster presented)

Owald D., M. Schmidt, C. Wichmann, S. Mertel, W. Fouquet, F. Christiansen, K. Mechtler, M. Heckmann, S. J. Sigrist. The Bruchpilot Protein in Assembly of Active Zone Structure and Function. Molecular Dynamics of the Chemical Synapse, 20-23 August 2007, Westerburg, Germany

Owald D., M. Schmidt, C. Wichmann, S. Mertel, W. Fouquet, F. Christiansen, K. Mechtler, R. J. Kittel, M. Heckmann, S. J. Sigrist. The Bruchpilot Protein in Assembly of Active Zone Structure and Function. Neurobiology of *Drosophila*, 03-07 October 2007, Cold Spring Harbor, NY, USA

F. Christiansen, D. Owald, W. Fouquet, S. Mertel, S.J. Sigrist. Macromolecular active zone architecture in the mushroom body calyx of *Drosophila melanogaster*. Neurofly, 06-10 September 2008, Würzburg, Germany (Poster presented)

Journal of Neurogenetics, 2009, Vol. 23, No. s1, Pages S1-S102, DOI 10.1080/01677060902742364

Owald D., W. Fouquet, M. Schmidt, C. Wichmann, F. Christiansen, H. Depner, J. Körner, S. Mertel and S. J. Sigrist. Analysis of the Active Zone Protein DSyd-1. Neurofly, 06-10 September 2008, Würzburg, Germany

Journal of Neurogenetics, 2009, Vol. 23, No. s1, Pages S1-S102, DOI 10.1080/01677060902742364

F. Christiansen, D. Owald, W. Fouquet, S. Mertel, S.J. Sigrist. Macromolecular active zone architecture in the mushroom body calyx of *Drosophila melanogaster*. Axon Guidance, Synaptogenesis and Synaptic Plasticity, 10-14 September 2008, Cold Spring Harbor, NY, USA (Poster presented)

Owald D., W. Fouquet, M. Schmidt, C. Wichmann, F. Christiansen, H. Depner, S. Mertel and S. J. Sigrist. Spatio-Temporal Analysis of Active Zone Assembly in *Drosophila*. Axon Guidance, Synaptogenesis and Synaptic Plasticity, 10-14 September 2008, Cold Spring Harbor, NY, USA

# 8.4 Acknowledgements

Mein großer Dank gilt vor allem meinem Doktorvater Stephan Sigrist.

Ebenso möchte ich mich bei meinen weiteren Betreuern Erich Buchner und Martin Heisenberg herzlich bedanken.

Im Labor standen mir zur Seite: David Owald, Omid Khorramshahi,Carolin Wichmann, Harald Depner, Franziska Zehe, Christine Quentin, Christina Bochow, Wernher Fouquet, Sara Mertel und Peter Engerer. Hervorheben möchte ich Till Andlauer, dem ich für seine vielseitige Hilfe nicht genug danken kann.

Wegbereiter waren Robert Kittel, Hans-Joachim Pflüger, Björn Brembs und Carsten Duch. Außerdem begleiteten mich Florian Leiss und Gaia Tavosanis sowie Birgit Michels, Bertram Gerber und Hiromu Tanimoto.

Ich danke meinen Eltern Petra Christiansen und Dieter Wertheim sowie meiner Schwester Mira Christiansen. Besonderer Dank gilt meiner Tante Eva Wertheim.

Zuletzt danke ich von ganzem Herzen Rosalie und Minna sowie Tilmann Engelhardt, dem mein größter Dank gebührt.